12-2003

Investigation of Compound Micro Cantilever for Imaging and Identifying Micro/Nano Particulates

Ramanathan Narayanan
University of Tennessee - Knoxville

To the Graduate Council:

I am submitting herewith a thesis written by Ramanathan Narayanan entitled "Investigation of Compound Micro Cantilever for Imaging and Identifying Micro/Nano Particulates." I have examined the final electronic copy of this thesis for form and content and recommend that it be accepted in partial fulfillment of the requirements for the degree of Master of Science, with a major in Mechanical Engineering.

Dr .Don W. Dareing, Major Professor

We have read this thesis and recommend its acceptance:

Dr.J.A.M. Boulet, Dr.Arnold Lumsdaine, Dr.Thomas Thundat

Accepted for the Council:
Carolyn R. Hodges

Vice Provost and Dean of the Graduate School

(Original signatures are on file with official student records.)

To the Graduate Council:

I am submitting herewith a thesis written by Ramanathan Narayanan entitled "Investigation of Compound Micro Cantilever for Imaging and Identifying Micro/Nano Particulates". I have examined the final electronic copy of this thesis for form and content and recommend that it be accepted in partial fulfillment of the requirements for the degree of Master of Science, with a major in Mechanical Engineering.

Dr .Don W. Dareing

Major Professor

We have read this thesis
and recommend its acceptance:

Dr.J.A.M. Boulet

Dr.Arnold Lumsdaine

Dr.Thomas Thundat, ORNL

Accepted for the Council:

Anne Mayhew

Vice Provost and
Dean of Graduate Studies

(Original signatures are on file with official student records)

INVESTIGATION OF COMPOUND MICRO CANTILEVER FOR IMAGING AND IDENTIFYING MICRO/NANO PARTICULATES

A Thesis
Presented for the
Master of Science degree
The University of Tennessee, Knoxville

Ramanathan Narayanan
December 2003

Dedication

I would like to dedicate this thesis to my parents,

Mr.Narayanan Ramanathan

and

Mrs. Annapoorani Narayanan

who have given me two lives:

a physical life and a life in engineering.

This dedication is also for my uncle,

Mr. Vairavan Subramanian, Houston, Texas

who inspired me from my childhood to do master's degree.

I would also like to dedicate this thesis to my sister and all my friends who helped me in various stages in all possible ways.

Acknowledgements

The last two years has been an important phase in my life, and many things have occurred during this period. The process of earning a master's degree has transformed me into a new person. It is not only about knowledge gained and laboratory work, but also about the changes in my life philosophy and my view of the world. There are many people who have offered me enormous help and support at different points. Without their help, it would have been impossible for me to accomplish what I have done. My gratitude towards them can be hardly expressed.

I wish to express my deep appreciation to my major professor, Dr. Don W. Dareing, for his invaluable guidance, encouragement, patience and generous support throughout this study and also for funding me for my graduate studies. Through course and detailed discussions Dr. Dareing has provided the background on which this work was based and also the inspiration for carrying this work to completion. I also would like to express my special thanks to Dr. Thomas Thundat for his generous advice and help during the completion of this thesis. This thesis would not be completed without his support.

I am very grateful for Dr. J.A.M Boulet and Dr. Arnold Lumsdaine, who graciously agreed to take their precious time, serving on my thesis committee and offering many valuable suggestions.

I would like to express my special thanks to Dr. Patrick Christle who helped me in editing and read through this thesis and also giving me much helpful advice concerning writing skills.

Abstract

Atomic Force Microscopes (AFM) are typically used to image surfaces along with small particulates that may be deposited on the surface. Surface imaging can be made down to the atomic level but usually it is conducted at the nano and micro scales. It is highly desirable to identify the constituency of particulates on the surface and if possible determine the chemical and physical identity of particulates. The objective of the research presented in this thesis is to establish the feasibility of using dual micro cantilevers to determine the physical constituency of nano particles deposited to the micro surface. The goal at this point is not to determine the physical properties of a particulate but rather to determine whether the particulate is hard or soft and categorize it. The research addresses this goal by predicting the vibration response of dual micro cantilever when the cantilever tip engages a surface and a particulate. Five different particulate models are analyzed: elastic, viscous, visco-elastic in parallel, visco-elastic in series and visco-elastic in series/parallel. Each model represents different possible physical constituencies of particles. The analysis shows that each particle model produces unique signatures and vibration responses of the dual micro cantilever. Properties that are identified in the research are signatures. Signatures can be shifts in natural frequencies, change in response amplitudes and phase angles.

Table of Contents

List of Tables

List of Figures

Nomenclature

AFM	**Atomic force microscope**
STM	Scanning Tunneling Microscope
PSD	Position Sensitive Detector
TMAFM	Tapping Mode Atomic Force Microscope
Å	Armstrong (10^{-10} meter)
nm	Nano-Meter(10^{-9} meter)
μm	Micro-Meter(10^{-6} meter)
EBD	Electron-beam-deposited
kHz	Kilo Hertz
nN	Nano-Newton (10^{-9} N)
y_0	Base amplitude of the excitation force, nm
$k_{1,2}$	Spring constants of first and second mass , N/m
k_3	Spring constant for lower spring , N/m
$c_{1,2}$	Damper constants of first and second mass , N-s/m
c_3	Damper constant for lower dashpot , N-s/m
$f_{1,2}$	Frequency of first and second mass , kHz
$m_{1,2}$	Mass 1 and mass 2, kg
ω	Driving frequency, rad/sec
ω_n	Natural frequency, rad/sec
$\xi_{1,2}$	Damping Coefficients for the first and the second mass.
$\varsigma_{1,2}$	Modal damping coefficients for the first and the second mass

$r_{1,2}$	Frequency ratio for the first and the second mass
$w_{1,2}$	Deflection at point 1 and point 2 due to applied load , nm
$x_{1,2}$	Combined deflection at point 1 and point 2, nm
[k]	Stiffness matrix, N/m
[α]	Flexibility matrix, m/N
[m]	Mass matrix, kg
[c]	Damper constant matrix, N-s/m
E	Young's Modulus, N/m^2
I	Moment of Inertia of the beam, m^4
$F_{1,2}$	Applied force at point 1 and point 2, N
ω^2	Eigenvalue
{X}	**Eigenvector, nm**
$\left[\vec{X}\right]$	Modal Matrix
{x}	Local Coordinates
{η}	Modal Coordinates
{F}	Force Vector
{Q}	Modal Force
ϕ	Phase angle
Y_r	Base Amplitude
u	Displacement of damper, nm
r,R	Radius, nm
F_c	Capillary force, nN

h	Film Thickness, nm
σ	Surface tension, dyne/cm
α	Wetting angle, rad
θ	Contact angle, rad
F_m	Meniscus Force, nN
V	**Velocity, nm/ns**
P_c	Capillary pressure, nN/mm^2
P_{lv}	Liquid Vapor Pressure
P_{sl}	Solid liquid pressure
W	Constant load

CHAPTER 1

BACKGROUND

The Atomic Force Microscope (AFM) is one of about two-dozen types of scanned-proximity probe microscopes. It has been used primarily to image the surfaces of insulating materials with nanometer-scale resolution. The AFM was developed in 1986 by Binnig [1], who also developed the Scanning Tunneling Microscope (STM) along with Heinrich Rohrer in the early 1980's [2]. They both were awarded the Nobel Prize for the discovery of the STM. The STM is not only a tool for detailed investigation of surfaces, but also for the study of atoms and molecules on the surface. The introduction of the AFM has revolutionized the idea of the mechanical measurement of surfaces and the sensitivity of the surface forces on an unprecedented scale [3]. The AFM utilizes an atomically sharp tip to scan a surface [4]. The force of interaction between the tip and the surface is used to map the surface. The typical AFM used for topographic imaging of the surface is shown in Figure 1. This can operate in one of the several modes, such as contact mode, tapping mode and non-contact mode. The different types of modes are discussed later in this section.

The basis of all scanning probe techniques is that a sharp tip is brought close to a surface, and measurement is then made of some property that depends on the distance between the tip and the surface. In the STM the tip is made of tungsten or platinum/iridium wire, and when it is brought within a few nanometers of a conducting surface, a voltage difference is applied to it. The current is then measured as the tip scans across the surface, and these measurements lead to the image of the surface. Many

Figure 1: Digital Instruments Multimode™ AFM optimized for high-resolution force measurements and topographic imaging [9].

materials are not conductors; therefore the STM cannot be used to image the surface. Soft interfaces and biological molecules may be sensitive to electron bombardment, which motivated the scientists to seek an alternative for the STM, which is the AFM. Some of the disadvantages of the STM are that the electro-magnetic force between the tip and the surface affects the resolution of the images, and that it can only be used for conductive materials. The AFM was developed to control these forces and for imaging non-conductive surfaces too [5]. The basic principle of the STM depends on the tunneling current between a metallic tip, which is sharpened to a single atom point, and a conductive material. Since the STM uses current, it can image only conductive surfaces whereas the AFM can be used to image conductive as well as insulating surfaces. The AFM can be used to image insulating materials such as BN, NaCl and polymers with a very high atomic resolution, and it is even used to find magnetic forces with a spatial resolution of <10 nm using a magnetic tip [6].

In the original AFM, a tip at the end of a small cantilever beam was placed in contact with a surface. A typical AFM is shown in Figure 1. It is used to image and to find forces between the tip and the surface [7]. The sharp tip at the end of cantilever is used by the AFM to measure the forces between the tip and the surface with piconewton sensitivity and subnanometer lateral resolution. This has enabled the AFM to generate images of surfaces with an atomic resolution equal to that of STM. Because of the sensitivity of the AFM, an understanding of the tip and its interaction with the sample is important for the interpretation of images [8].

The AFM currently used has an optical lever that (shown later in Figure 4) reflects the laser beam from the cantilever. The reflected laser beam is sensed by a

photodiode, which magnifies the small cantilever deflections. The reflected laser beam is then passed on to the computer (shown in Figure 2) to get a plot for laser deflection versus tip position. In this way, the AFM makes a topographic map of the sample surface [9].

The heart of a scanning force microscope is the force interaction between the sharp tip and the sample surface. The tip is mounted on a flexible cantilever beam whose geometrical and material properties make it possible to probe the surface forces with high sensitivity. The role of the laser beam is to translate the force acting on the tip into a deflection that subsequently can be monitored by various means. Among these methods, electron tunneling, capacitance, optical interferometry, optical polarization, and optical deflection have recently been developed to a high degree of sophistication [3]. The most common AFM configuration has a laser beam that reflects from the backside of a very short (100- 200 μm) cantilever. Deflections in the cantilever are thereby precisely measured by an optical position-sensitive detector (PSD) [10]. In operation, a servo-circuit is employed to keep the detector signal constant by raising or lowering the sample. The slope of the cantilever where the laser beam is directed is, therefore, maintained at a constant value by the servo action [11].

The working of the AFM is shown in Figure 2. As shown in the figure, when the cantilever beam deflects the laser beam, it is sensed by the PSD. This detector senses where the ray is deflected and compares it with the basic position. Then this is passed on to a computer to map the surface of the sample.

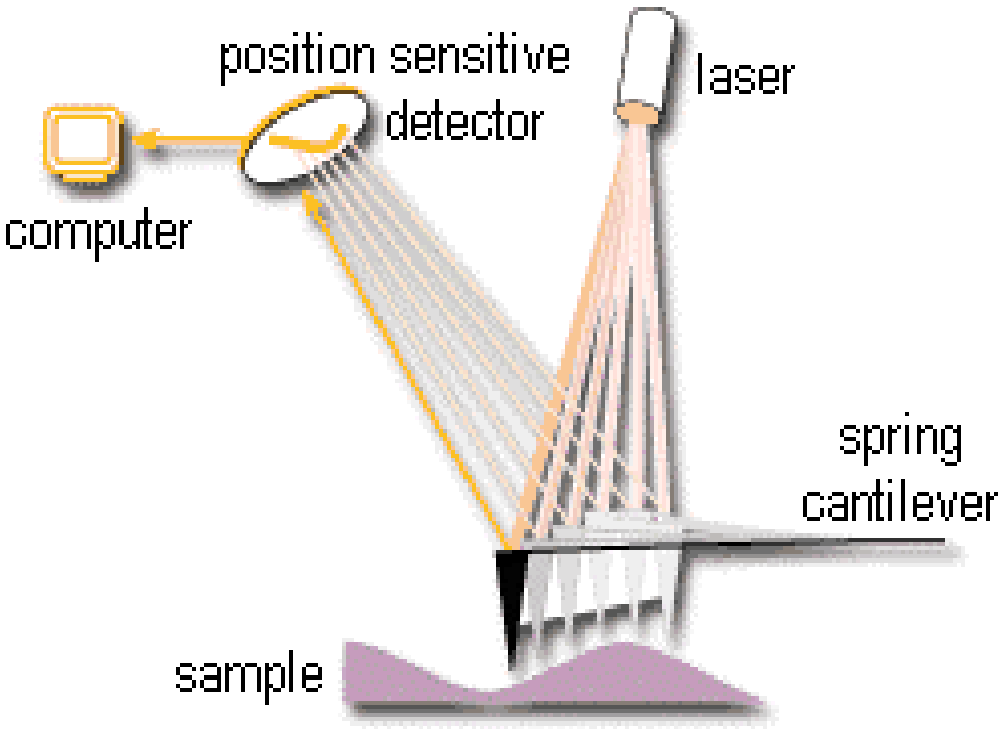

Figure 2: Working of AFM [9]

The AFM can be operated in two principal modes; one is with feedback control and other is without feedback control. With feedback control the tip-sample force is constant; hence, this can also be called constant force mode. Thus if there is any change in the forces between the tip and the sample, the tip-sample separation automatically changes to restore the constant force. In this mode a reasonably good image of the surface can be obtained (hence the alternative name, height mode). Without feedback mode only a small amount of feedback is present to control problems arising due to thermal drift or rough sample, which will damage the tip. Hence this mode is known as error signal mode and used primarily for very flat surfaces at high resolution [12].

The image contrast can be obtained in many ways. The three main classes of interaction are contact mode, tapping mode and non-contact mode. Contact mode is the most common method of operation of the AFM, and as the name suggests, the tip and sample remain in close contact as the scanning proceeds. It is commonly called deflection mode because, when the sample has any rough surface, the cantilever beam deflects. Even though this mode is generally believed to be the easiest to use, the images contain a mixture of friction [11,13,14], adhesion forces [13-16], capillary force [17] and elastic effects as well [11]. The drawback in contact mode is that as the sample moves it produces high lateral forces.

Tapping mode is the next most common mode used by the AFM. In this mode the AFM tip oscillates at its fundamental resonant frequency above the surface. The time the tip is in contact with the sample is less, so the lateral forces developed due to tip interaction are also less. An image obtained from tapping mode is far better than the image obtained from contact mode [12]. The tapping mode atomic force microscope is

an ideal tool for imaging surfaces. A rich variety of forces can be sensed by atomic force microscopy. In the non-contact mode (of distances greater than 10 Å between the tip and the sample surface), Van der Waals, electrostatic, magnetic or capillary forces produce images of topography, whereas in the contact mode, ionic repulsion forces take the leading role in producing the images.

Tapping mode is preferable to contact mode for soft samples. In contact mode the lateral forces, capillary forces and Van der Waals forces may damage the samples, but in tapping mode, a vibrating cantilever, is driven in resonant frequency taps over the sample [18]. In general, tapping mode operation in air requires a stiff cantilever to avoid the tip getting stuck on the sample surface due to capillary bridge formation. However, it is also possible with soft cantilevers, as long as the amplitude of oscillation is several microns as demonstrated by Putman et al [19]. In summary, the tapping mode AFM operating in air requires a very stiff cantilever, while operation in a liquid requires a very soft cantilever [20]. When the vibrating cantilever approaches the sample, it experiences an attractive force. This force will have an effect on the force gradient. As the force gradient increases, the free resonant frequency will decrease, so to restore this, a stiffer cantilever is used in air. Tapping mode AFM (TMAFM) operation in liquids rather than in air is preferred due to a number of factors, such as the reduction of Van der Waals forces by a factor of up to ten or more [21], the elimination of capillary forces, consequent minimization of friction forces, and reduced tip and sample contamination [22]. Liquids are also the ideal physiological media for biological samples. However, resonant motion of the cantilever for the TMAFM in liquids is impeded by the large damping and added

inertial mass of the liquid [23]. In spite of this, TMAFM under liquids has been demonstrated for DNA molecules and cells [19,22].

There are two ways to accomplish the resonant motion of the TMAFM. (i) The sample can be oscillated vertically up and down to excite the cantilever oscillation. The amplitude and phase of the cantilever beam changes when the tip begins to contact the sample position. (ii) By giving an acoustic excitation to the cantilever at frequencies well above the fundamental. While the tip scans the top of the surface, the oscillation amplitude of the cantilever senses the force derivative of the tip-sample interaction. The amplitude of the cantilever vibration changes when the tip begins to contact the sample surface and is held constant by a feedback circuit controlling the tip holder's position. In this way the surface topography under fluids can be recorded.

One of the most important factors influencing the resolution that may be achieved with an AFM is the sharpness of the scanning tip. The first tips used were made by glueing diamond onto pieces of aluminum foil. For the best tip the radius of curvature must be around 5 –10 nm. However, the AFM incorporates a number of refinements that enable it to achieve atomic-scale resolution [9]:

- Sensitive detection: Measures vertical deflection of the cantilever with high resolution.
- Flexible cantilevers: When using a flexible cantilever, the stylus exerts low forces on the sample, which reduces distortion and damaging of the tip while scanning. To have a flexible cantilever, the spring constant should be low and the resonant frequency should be high. To achieve this, the mass has to be low. Therefore, AFM cantilevers are of small size.

- Sharp tips: Generally tips are evaluated based on their end radius. Force microscopists use one of three tips; normal tip, super-tip and ultralever tip (shown in Figure 3).
- High-resolution tip-sample positioning
- Force feedback: In this the force between tip and sample is maintained as a constant value. The height between tip and sample is adjusted to restore the constant force value.

The main influences for a sharp tip are [12]:

- Broadening: Tip broadening arises when the radius of curvature of the tip is comparable with, or greater than, the size of the sample to be imaged.
- Compression: This occurs when the tip is over the sample.
- Interaction forces: Forces between the tip and sample are important for the contrast of the AFM. Selection of a tip depends on the material to be imaged.
- Aspect ratio (cone angle): This is crucial when imaging steep sloped samples.

The normal tip (Figure 3a; Albrecht et al., 1990) is a 3 μm tall pyramid with ~ 30 nm end radius. The electron-beam-deposited (EBD) tip or super-tip (Figure 3b; Keller and Chih-chung, 1992) is formed by an electron-beam-induced deposit of carbonaceous material made by pointing a normal tip straight into the electron beam of a scanning electron microscope. The super-tip offers a higher aspect ratio (it is long and thin, good for probing pits and crevices) and sometimes a better end radius than the normal tip.

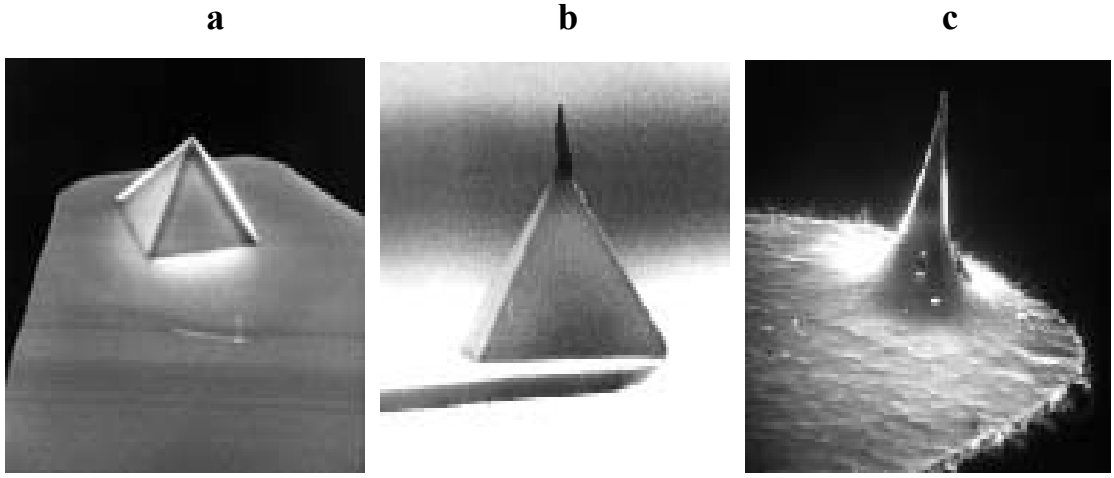

Figure 3: Three common types of AFM tip. (a) Normal tip (3 μm tall); (b) Super tip; (c) Ultralever tip (also 3μm tall) [9].

(Figure 3c). The ultralever tip offers a moderately high aspect ratio and on occasion a ~10 nm end radius [9].

The cantilever is the important component in the AFM. Cantilevers are made of flattened and polished tungsten wires whose ends are bent and then etched to obtain sharp tips. The cantilevers thus obtained will have stiffness in the range of 100 – 250 N/m. The length of the cantilever will range ~ 200 μm, width ~ 10 μm and thickness ~ 1 μm. The spring constant and cantilever length varies for various AFM modes, which are tabulated in Table 1. The stiffness of the cantilevers is calculated by measuring the thermal oscillation amplitude and also by laser interferometer. The cantilevers will have resonant frequencies in the range of 11 – 20 kHz [24].

The principal component of an AFM is the small cantilever, which measures the force between the tip attached to the cantilever and the surface of interest. The force is

Table 1: Length and spring constants for various AFM Modes

Cantilever	**Cantilever Length**	**Spring constant**
Standard Silicon Nitride	100 – 200 μm	0.01 – 0.6 N/m
Oxide-Sharpened Silicon Nitride	100 – 200 μm	0.01 – 0.06 N/m
Contact AFM Etched Silicon	450 μm	0.02 – 0.1 N/m
Force Modulation Etched Silicon	225 μm	1 – 5 N/m
Tapping Mode Etched silicon	225 μm	20 – 70 N/m
Tapping Mode Etched Silicon	125 μm	20 – 100 N/m

determined by multiplying the measured cantilever deflection by the calibrated spring constant of the cantilever as a function of the sample position. This measured force versus sample position generates a force map, or image of the surface. The measurement starts with the sample far away and the cantilever in its rest position. As the sample is moved towards the cantilever tip, the cantilever bends towards the sample due to attractive surface forces. The forward deflection is then multiplied by the spring constant to get the attractive force. When the sample is further moved forward, then the sample pushes back the cantilever to its original position. When plotting the deflection versus the distance moved a force plot can be drawn, and from this plot, the force between tip and sample at any desired point on the surface can be determined [25].

Surface forces are important in image interpretation. Surface forces alone create large contact areas, even before the cantilever applies any external load. The size of the contact area will also depend on the mechanical properties of the tip and sample. Assuming that the contact area between tip and sample determines the image resolution, an awareness of surface forces and mechanical properties is important in order to interpret contact-mode images. In non-contact mode imaging, if the surface forces vary from spot to spot on a sample through changes in the chemistry of the surface, the detected image will be a convolution of the topography and the surface forces [26].

The way to measure the forces with the AFM is to position the tip over a desired point of the sample and allow the piezoelectric scanner to scan the surface, and decreasing the distance between the tip and sample until the tip touches the sample. The curve obtained represents the cantilever deflection as a function of sample extension. The curve is called a force spectrum. When the tip is far from the sample, then the force is

repulsive, and when the tip is moved closer to the sample, then the force is attractive, so the cantilever deflects towards the sample [7].

When the base of the cantilever beam is given excitation, it produces vibration. Due to excitation, amplitude, frequency and phase angle will change. These changes are measured and used in a feedback loop to control the forces and the vertical distance between the tip and the sample. Tapping mode of the AFM is used commonly to image wide range of organic materials with nanometric-scale resolution. Other techniques such as, boundary excitations base motion excitation are also used to excite the base of cantilever to obtain the nanoscale information about elastic properties of materials [27].

The AFM shown in Figure 4 operates by measuring repulsive or attractive forces between tip and sample. When it is in repulsive mode (contact mode) the tip of the cantilever lightly touches the sample. A raster-scan drags over the sample and it measures the vertical deflection of the cantilever, which indicates the sample height [9]. In noncontact mode, the AFM derives topographic images from measurements of attractive forces; the tip does not touch the sample (Albrecht Et.al., 1991). On the nanometer scale, several investigators have measured the interaction forces between the tip and the sample during STM and AFM measurements. Martin and Williams and Wickramasinghe measured the attractive forces between AFM tip and sample as a function of tip-surface separation in the 3-18 nm range. The attractive forces are on the order of 10nN [8];

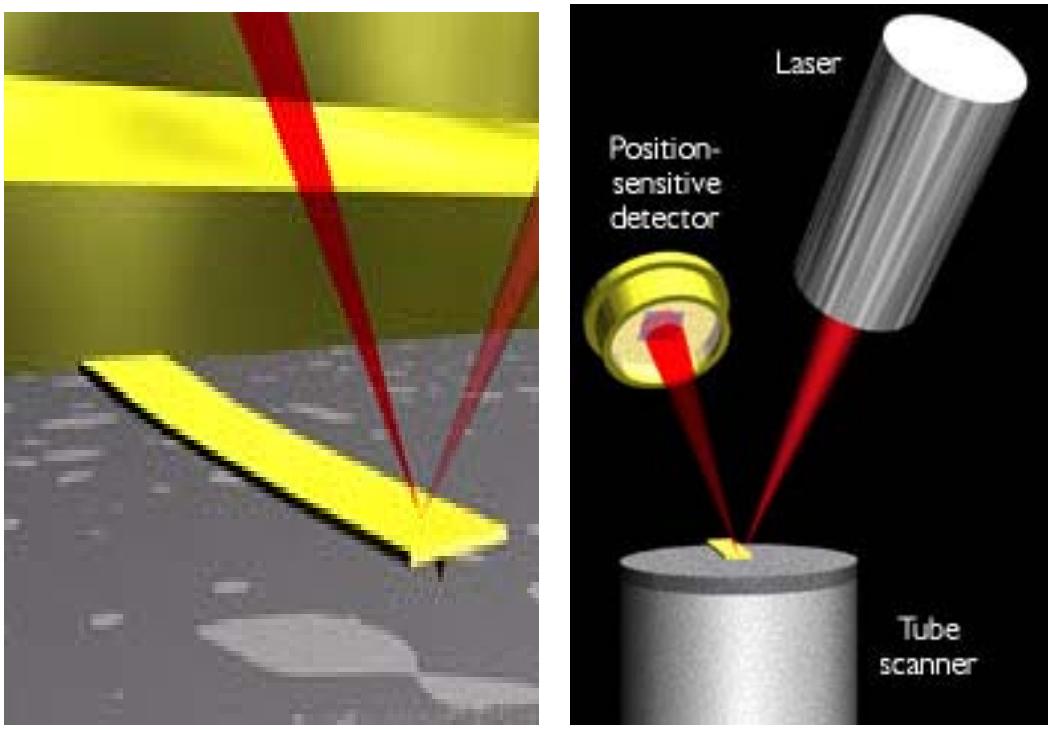

Figure 4: Concept of AFM and the optical lever; (left) a cantilever touching a sample; (right) the optical lever [9]

The AFM is being used to solve processing and materials problems in a wide range of technologies affecting electronics, telecommunications, biological, chemical, automotive, aerospace, and energy industries. The materials being investigated include thin and thick film coatings, ceramics, composites, glasses, synthetic and biological membranes, metals polymers, and semiconductors. The AFM is being applied to studies of phenomena such as abrasion, adhesion, cleaning, corrosion, etching, friction, lubrication, plating and polishing [28].

Recently, the AFM has also been used to investigate the mechanical properties of materials including atomic-scale friction, elastic modulus, and surface forces. The modulus can be determined from the loading part of the indentation curve for elastic materials. For elasto-plastic materials, elastic modulus and hardness can be found from the unloading curve. Force magnitudes range from millinewton and depend on the sample materials and the medium in which the experiment is conducted (air, vacuum, liquid) [8].

In most applications of AFM, only lower atomic resolution is achieved because of the extreme sensitivity and instability of soft levers against high force gradients of short interactions. But now atomic resolution can be achieved using high resonant cantilevers with large ~ 100 Å oscillation amplitudes in ultrahigh vacuum [24].

One of the most exciting results for atomic force microscopy has been the discovery of achieving atomic resolution when the tip is in contact with the sample while scanning. The AFM is able to achieve such a high resolution by using a very small loading force on the tip, typically ranging from 10^{-7} to 10^{-11} N, which makes the area of contact between the tip and sample exceedingly small [2].

The AFM can also image the softness of a sample by pressing the cantilever into it at each point in a scan. The scanner raises the sample or lowers the cantilever by a preset amount, called modulation amplitude (usually 1-10 nm) [9]. In response, the cantilever deflects an amount dependent on the softness of the sample: the harder the sample, the more the cantilever deflects. This type of analysis is also done using a single cantilever, as shown in Figure 5. Only information like frequency response and phase angle can be obtained by the use of a single cantilever beam. When a dual cantilever beam is used, one can expect to get more information about a particle.

In Figure 6, the dual cantilever proposed for imaging and identifying particles is shown. The second cantilever is attached to the end of the first cantilever. The tip is attached to the underneath end of the first cantilever. When the tip engages with any particle on the surface it produces some force. Due to this force and the cantilever's base motion, response is produced. The image of the surface can be interpreted by the response obtained from the dual cantilever. Two-degrees of freedom have an advantage over a single-degree of freedom. In the former, the response obtained for the second mass may provide some more information about the particle. In single degree of freedom we will have only one frequency response peak where as in dual cantilever we will have four-frequency response peak. This additional 3-frequency responses peak can provide some additional information about the particles.

The dual cantilever is given a base excitation with which it vibrates. As mentioned earlier the dual cantilever is assumed to be in tapping mode so that the cantilever vibrates over the surface at its resonant frequency. When it encounters any particle on the surface then the tip of the cantilever engages with the particulate. The

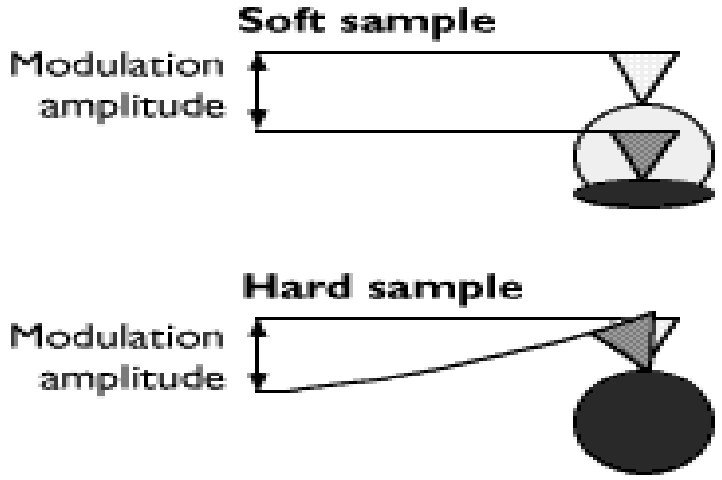

Figure 5: AFM's can image sample elasticity by pressing the tip into the sample and measuring the resulting cantilever deflection [9]

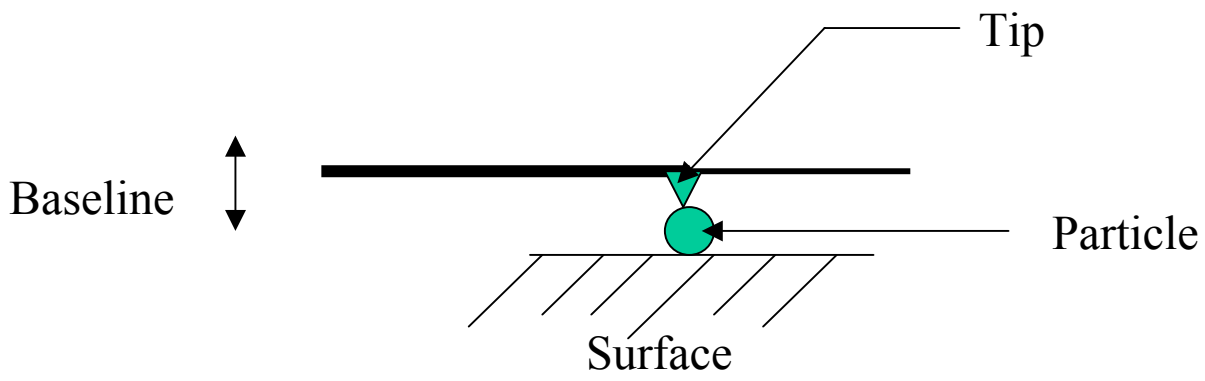

Figure 6: Dual cantilever proposed for imaging the particulate attached to a surface.

response obtained can be interpreted in some way to find the particle's properties. This forms the basis of the research work proposed. In this thesis we explore how the dual cantilever can be used to identify and image the surface and some of its advantages over a single cantilever beam.

Biological applications of atomic force microscopy, though technically challenging, are destined to be of great importance. The AFM is already used to image individual biological molecules such as amino acids and DNA [2]. It can also be used in finding the difference in shape of many biological molecules, such as single stranded, double-stranded and triple-stranded DNA, and protein channels in membranes [29].

CHAPTER 2

OBJECTIVE OF RESEARCH

Single microcantilevers are used in the AFM to image nano and micro surfaces. AFM imaging can also show the shapes of nano size particulates attached to surfaces. In some cases, particulates can be identified through the history of the surface. Known particles are sometimes simply placed on a test surface, either directly or indirectly. However, in some cases, the identity of imaged particles is unknown. Establishing the physical properties of nano size particulates at the same time a surface is being imaged would provide important supplemental information.

The objective of this research is to evaluate the possibility of using dual or compound microcantilevers in AFM to establish physical properties of particulates at the same time surfaces are being imaged. A dual microcantilever can be achieved has a direct modification of a single microcantilever. One needs only to extend a second cantilever away from the end of the first microcantilever. If the motions of the two cantilever tips are measured, the proposed cantilever configuration would convert a typical microcantilever from a single-degree of freedom vibration system to a two-degree of freedom vibration system. AFM would have to be modified with a second laser beam in order to measure the dynamic response of the tip of the second cantilever. Here the AFM is assumed to be in tapping mode because in contact mode the method used to solve the frequency response is complicated.

Assuming that the vibratory motion of both the tip and the end of the second cantilever can be measured simultaneously by AFM, how these measured responses can

be interpreted to extract both the image of a surface and identify particulates that might be attached to the surface is the objective of this research. The possible result of this research is to show how the frequency response obtained from the dual cantilever can be used to identify the particles.

In dual cantilever the modal stiffness and modal damping can be determined experimentally. Knowing the stiffness of the dual cantilever and stiffness matrix for the dual cantilever model, we can determine the type of particle on the surface. Moreover, in dual cantilever we will have four-frequency response peak whereas in single cantilever we will have only one frequency response peak. This also gives some additional information about the particle on the surface. The following sections explain vibration models used in the analysis and define various responses and signatures that can be used to identify particulates through their physical behavior.

CHAPTER 3

METHOD OF SOLUTION

The objective of this research is to image and identify a particle on a surface of a sample at the nano-scale level. In this research, the AFM is used to image the surface with atomic resolution. The single cantilever, shown in Figure 5, is commonly used to image a surface with atomic resolution. With the single cantilever model, frequency response can be obtained for only one point, whereas in dual cantilever model, frequency response can be obtained for two points. The frequency response for the second point in the dual cantilever model may provide some additional information about the particle that cannot be obtained from the single-degree cantilever model. In this chapter, the basic mathematical model used for the research is developed and analyzed with some numerical values for spring constants, damper constants and frequencies provided by the manufacturers of microcantilevers. This research is based on five basic models; they are the elastic model, the viscous model, the visco-elastic model in parallel (Kelvin-Voigt model), the visco-elastic model in series (Maxwell model) and the visco-elastic model in series/parallel (Standard solid model). This last model is also called the second viscous model. For each model, natural frequency, mode shape and frequency response are obtained. Frequency response is plotted as the function of the driving frequency with which the base vibrates. The signature for the models is noted and discussed briefly in the Chapter 4.

The dual cantilever used in this research is shown in Figure 7; it has two beams of

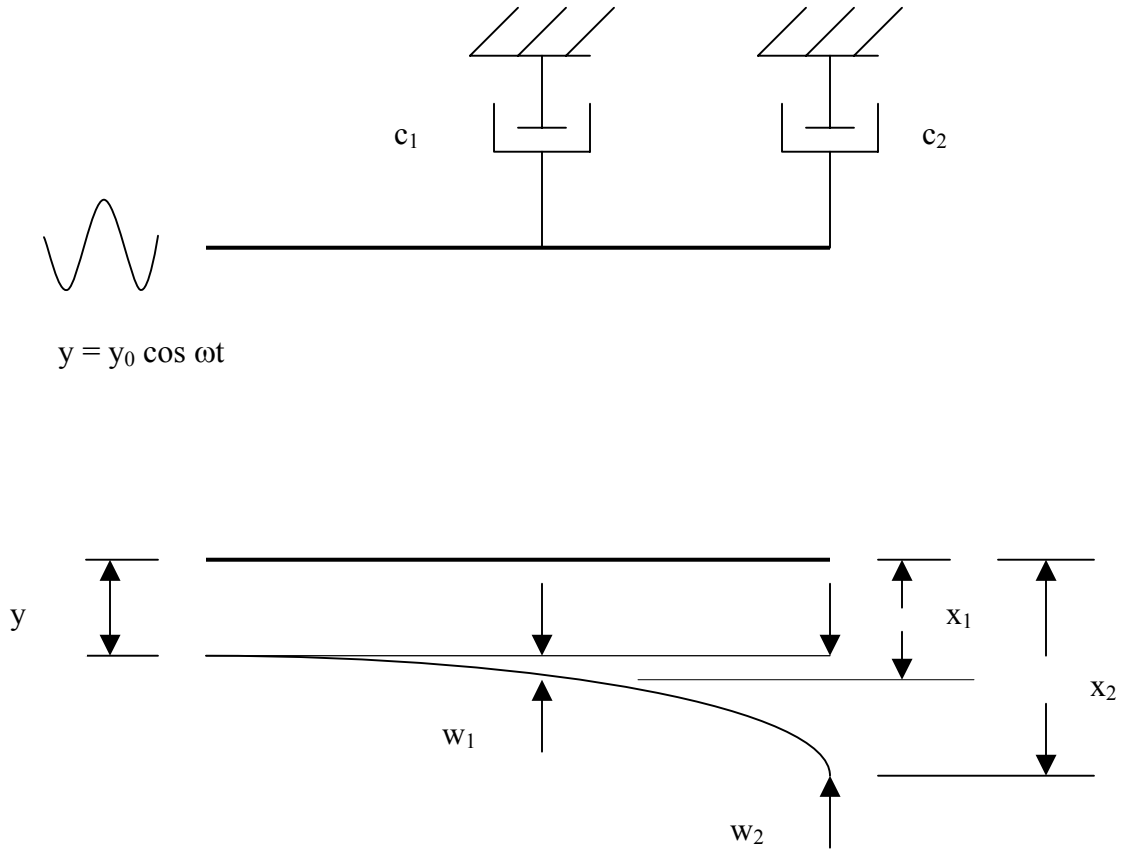

Figure 7: Dual cantilever with base motion of $y = y_0 \cos(\omega t)$ in tapping mode

different sizes that are attached together. Each beam has its own mass and stiffness. The AFM tip is attached to the underneath end of the first mass. In this research we are making two assumptions. First, the dual cantilever used in this research is assumed to be in tapping mode. In tapping mode the dual cantilever vibrates over the surface at its resonance frequency, and its response is altered when it encounters any particle. The use of tapping mode has some advantages over contact mode, which have been discussed in the background section. The basic purpose of using tapping mode is to reduce lateral forces. Lateral forces are produced while scanning the surface, and will result in damaging the tip. The second assumption is a steady state for calculating the frequency response (i.e. the tip is attached to the particle when response is obtained). In reality, though, is not the case; the tip does not stick to the particle. When the tip does not stick, then the calculations involve a lot of complication. But the complex calculations required to model this phenomenon are beyond the scope of this research. In this research, continuous systems are discretized, and so higher modes of the dual cantilever are neglected (beyond fundamental natural frequency).

The motion of a system subjected to any given excitation is commonly referred to as the system response. The response is generally described by displacement and, less frequently, by velocity or acceleration. The excitation can be in the form of initial displacement and velocities or in the form of externally applied force, or both.

The elements constituting a discrete mechanical system are of three types, namely, those relating forces to displacements, to velocities, and to accelerations, respectively. The most common example of a component relating forces to displacements is the spring. Springs are generally assumed to be massless, so that force acting at one end must be

balanced by force acting at the other end, where the latter force is equal in magnitude but opposite in direction to the former. The element relating forces to velocities is generally known as a damper. The damper is also assumed to be massless, so that a corresponding force at one end must balance a force at the other end. In this research, springs and damper are attached in various combinations and the corresponding response is analyzed.

In the basic dual cantilever model, it is assumed that the tip is not engaged with any particle. For this basic model, the equation of motion is derived. Using the equation of motion, we obtain the natural frequency, mode shapes and frequency response. This model is used as a baseline for all subsequent models. The frequency response obtained from this model is used to compare with the frequency response obtained from the other models. When the frequency responses are compared, one can see the difference, which may be useful in determining the physical nature of the particle on the surface. The frequency response for the basic dual cantilever model is obtained by substituting numerical values given by the micro-cantilever manufacturers. The same set of values for spring constants and frequencies are used through out the research.

The dual cantilever can be excited using an external force or by boundary force. In this research a boundary force modeled as $y_0 \sin\omega t$ excites the beam, where y_0 is the amplitude of the base motion and ω is the driving frequency. Physical properties of the particulate can be discovered in some way using the response obtained from the various models. The whole research is subdivided as follows. First, the model is attached to a spring alone, then with damper alone. Later spring and damper are connected in parallel, and lastly spring and damper are connected in series. Each model has its own signatures, and they are discussed briefly in the next chapter.

3.1 DUAL CANTILEVER MODEL

The unattached dual cantilever is the basic model used for this research. As stated before, in order to understand subsequent models, it is important to know how the dual cantilever model works. The few sections in this chapter deal with the basic dual cantilever model. Tapping mode is assumed for the dual cantilever. The basic dual cantilever used in this research is shown in Figure 7. In this model the assumptions made are, first, that the base of the dual cantilever is fixed to a vibrating support and, second, that the tip is not engaged with any particle on the surface. The system is allowed to vibrate under the influence of the base motion. The base motion has an amplitude of y_0 and a driving frequency of ω. In this section we are going to discuss how the basic equation of motion for the dual cantilever model is obtained. To derive the equation of motion, some of the concepts of strength of materials and dynamics are used.

In Figure 7, the displacement of the mass due to base motion can be related to the deflections as

$$x_1 = y + w_1 \tag{1}$$

$$x_2 = y + w_2 \tag{2}$$

where y is the base motion amplitude, w_1 is the deflection of mass m_1, w_2 is the deflection of mass m_2, x_1 is the combined amplitude of base motion and deflection of mass m_1 and x_2 is the combined amplitude of base motion and deflection of mass m_2.

In this particular case, the differential equation can best be developed in terms of the flexibility matrix [α] instead of the stiffness matrix [k], because it is easier to derive the flexibility influence coefficients than stiffness influence coefficients. The elements in the flexibility matrix are called influence coefficients. Moreover, the use of influence

coefficients facilitates the writing of differential equations of multi-degree of freedom systems directly in matrix form. The use of equations in matrix form facilitates the application of computer methods to get their solutions.

When load F_1 is applied at point 1 as shown in Figure 8, the deflection obtained at point 1 is α_{11} and the deflection due to load F_1 at point 2 is α_{21}. When a load F_2 is applied at point 2, the deflection at point 1 due to load F_2 is α_{12} and the deflection at 2 is α_{22}. Maxwell's reciprocal theorem states that the deflection at any point in the system due to unit load acting at any other point of the system is equal to the deflection at the second point due to unit load acting at the first point. Therefore, $\alpha_{12}=\alpha_{21}$.

Writing all the influence coefficients in matrix form gives the flexibility matrix $[\alpha]$

$$[\alpha]=\begin{bmatrix}\alpha_{11} & \alpha_{12}\\ \alpha_{21} & \alpha_{22}\end{bmatrix} \tag{3}$$

The stiffness matrix is the inverse of the flexibility matrix, i.e., $[k] = [\alpha]^{-1}$

$$[k]=\frac{1}{\alpha_{11}\alpha_{22}-\alpha_{12}\alpha_{21}}\begin{bmatrix}\alpha_{22} & -\alpha_{21}\\ -\alpha_{12} & \alpha_{11}\end{bmatrix}=\begin{bmatrix}k_{11} & k_{12}\\ k_{21} & k_{22}\end{bmatrix} \tag{4}$$

The deflection matrix is related to the force matrix by

$$[w]= [\alpha]\ \{F\} \tag{5}$$

Applying the above relation to the dual cantilever model shown in Figure 7 gives

$$\begin{Bmatrix}w_1\\ w_2\end{Bmatrix}=[\alpha]\begin{Bmatrix}-m_1\ddot{x}_1-c_1\dot{x}_1\\ -m_2\ddot{x}_2-c_2\dot{x}_2\end{Bmatrix} \tag{6}$$

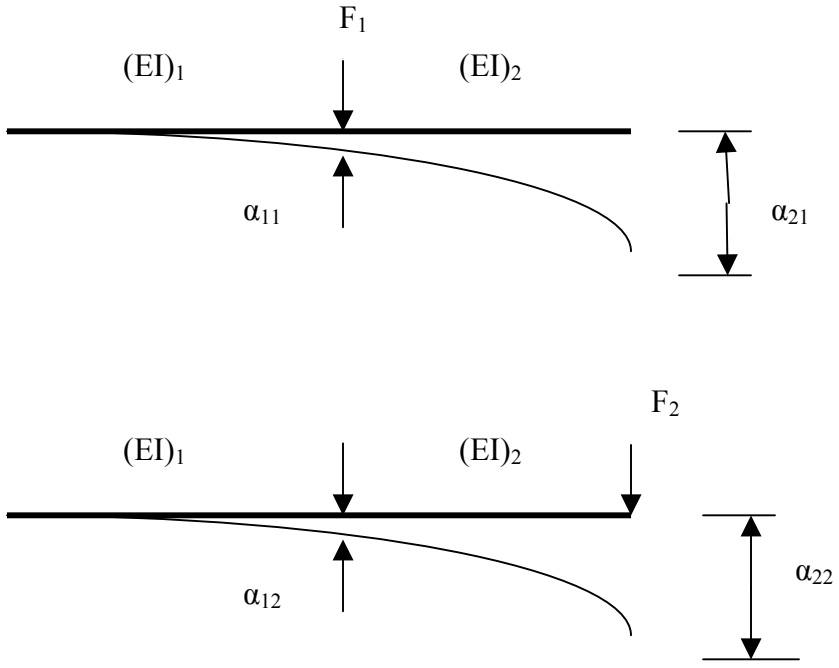

Figure 8: Elements in flexibility matrix; $\alpha_{12} = \alpha_{21}$

Since the flexibility matrix is the inverse of the stiffness matrix, equation (6) becomes

$$[k]\begin{Bmatrix} w_1 \\ w_2 \end{Bmatrix} = -\begin{bmatrix} m_1 & 0 \\ 0 & m_2 \end{bmatrix}\begin{Bmatrix} \ddot{x}_1 \\ \ddot{x}_2 \end{Bmatrix} - \begin{bmatrix} c_1 & 0 \\ 0 & c_2 \end{bmatrix}\begin{Bmatrix} \dot{x}_1 \\ \dot{x}_2 \end{Bmatrix} \tag{7}$$

Applying equations (1) and (2) to equation (7) gives

$$[k]\begin{Bmatrix} x_1 - y \\ x_2 - y \end{Bmatrix} = -\begin{bmatrix} m_1 & 0 \\ 0 & m_2 \end{bmatrix}\begin{Bmatrix} \ddot{x}_1 \\ \ddot{x}_2 \end{Bmatrix} - \begin{bmatrix} c_1 & 0 \\ 0 & c_2 \end{bmatrix}\begin{Bmatrix} \dot{x}_1 \\ \dot{x}_2 \end{Bmatrix} \tag{8}$$

(or)

$$\begin{bmatrix} m_1 & 0 \\ 0 & m_2 \end{bmatrix}\begin{Bmatrix} \ddot{x}_1 \\ \ddot{x}_2 \end{Bmatrix} + \begin{bmatrix} c_1 & 0 \\ 0 & c_2 \end{bmatrix}\begin{Bmatrix} \dot{x}_1 \\ \dot{x}_2 \end{Bmatrix} + [k]\begin{Bmatrix} x_1 \\ x_2 \end{Bmatrix} = [k]\begin{Bmatrix} y \\ y \end{Bmatrix} \tag{9}$$

where $y(t) = y_0 \cos(\omega t)$ represents the base motion of the dual cantilever.

In equation (9), m_1 is mass 1, m_2 is mass 2, c_1 is the damper constant for the first mass, c_2 is the damper constant for the second mass and [k] is the stiffness matrix, which is obtained by applying load at each point and getting the deflection at each point. Simplifying equation (9), the equation of motion for a two-degree of freedom system is

$$[m]\{\ddot{x}\} + [c]\{\dot{x}\} + [k]\{x\} = [k]\{y\} \tag{10}$$

where [m] is mass matrix, [c] is damper constant matrix , [k] is stiffness matrix and {y} is the base motion amplitude vector. How the natural frequencies and mode shapes are determined using the equation of motion derived for the dual cantilever is discussed in the next section.

3.1.1 EIGENVALUES AND EIGENVECTORS

It is helpful in the vibration analysis of any system to have a clear picture of the vibration mode shapes and their natural frequencies. This section establishes these vibration elements, which are commonly called eigenvectors and eigenvalues, respectively. An n-degree of freedom system requires n independent coordinates to define the system completely at any instant. In most cases, the coordinates are taken from the equilibrium position. The two-degree of freedom system requires 2 independent coordinates to specify the system. In this dual cantilever model, the two coordinates used to represent the system are x_1 and x_2, respectively as shown in Figure 9.

The differential equation for the two-degree freedom system given in equation (9) has both static and dynamic coupling between coordinates. The physical concept of static coupling is that if one coordinate is given a displacement, the other coordinate also undergoes some displacement. The differential equation (9) also has the second derivatives of x_1 and x_2, so it also has dynamic (inertial) coupling. The physical concept of dynamic coupling is that if acceleration is given to one coordinate, the other coordinate also has acceleration. The systems having two degrees of freedom are important because they introduce the phenomenon called coupling. The motion of any two independent coordinates, in general, depends also on the motion of the other coordinates through the coupling of springs and dampers.

One way to find a solution for a coupled system is to decouple the equations into two independent single-degree of freedom problems. Then, for a single-degree of freedom, the solution can be obtained easily. In order to decouple the differential

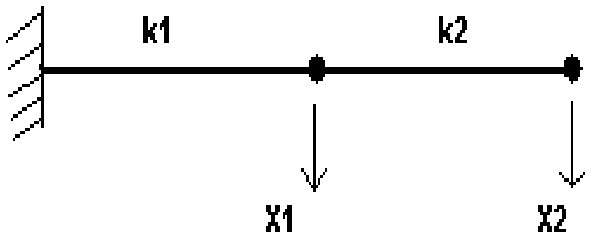

Figure 9: Dual cantilever with two-degree of freedom in free vibration.

equations, the modal matrix is used. In this section we are going to see how the modal matrix is obtained from the characteristic equation.

Making the mass matrix a diagonal matrix can eliminate dynamic coupling; similarly, making the stiffness matrix diagonal can eliminate static coupling. The method used to diagonalize both the mass and stiffness matrices is called decoupling. It decouples the two-degree of freedom equations into two single degree of freedom equations. Pre-multiplying the stiffness matrices by the transpose of the modal matrix and post-multiplying by the modal matrix gives the modal mass and stiffness matrices, which are diagonal.

The two-degree of freedom problem has two natural frequencies. Under certain conditions, any point in the system may execute harmonic vibrations in any of the two natural frequencies, and these are known as the principal modes of vibration. Amplitude ratio is the ratio between the displacement amplitude of mass and the amplitude of the base displacement. When the system is driven by harmonic excitation (base motion) with a frequency near one of the system's natural frequencies, the amplitude ratio will be high.

The differential equation for the two-degree system without any damping is

$$[m]\{\ddot{x}\} + [k]\{x\} = \{0\} \tag{11}$$

The classical approach to find the eigenvalues, natural frequencies, eigenvectors, mode shapes and the modal matrix is to assume solution of the form

$$x_1 = X_1 \sin \omega t \tag{12}$$

$$x_2 = X_2 \sin \omega t \tag{13}$$

substituting these two initial solution in the differential equation (11) gives

$$\left[[k] - \omega^2 [m] \right] \begin{Bmatrix} X_1 \\ X_2 \end{Bmatrix} = \{0\} \tag{14}$$

The above equation is said to be the amplitude equation or the eigenvector equation.

The stiffness matrix for the two-degree of freedom system is derived using relation $[k] = [\alpha]^{-1}$

$$[k] = \begin{bmatrix} (k_1 + k_2) & -k_2 \\ -k_2 & k_2 \end{bmatrix} = \begin{bmatrix} k_{11} & k_{12} \\ k_{21} & k_{22} \end{bmatrix} \tag{15}$$

where $k_{12} = k_{21} = -k_2$ and $(k_1 + k_2) = k_{11}$, here in this case k_1 and k_2 are obtained from the manufacture of the microcantilevers. The mass matrix is

$$[m] = \begin{bmatrix} m_1 & 0 \\ 0 & m_2 \end{bmatrix} \tag{16}$$

Natural frequency can be obtained from the characteristic equation

$$\left| [k] - \omega^2 [m] \right| = 0$$

(or)

$$\left| [m]^{-1} [k] - \omega^2 [I] \right| = 0 \tag{17}$$

where ω^2 is the eigenvalue, ω is the natural frequency and [I] is the identity matrix. There are two natural frequencies. The lower one is called the first, or the fundamental, frequency and the higher one is called the second frequency.

The eigenvector for each mode is calculated by substituting each natural frequency or the eigenvalue into the eigenvector equation (14). The eigenvectors obtained are the columns in the modal matrix. The modal matrix is given by

$$\left[\vec{X}\right] = \begin{bmatrix} X_{11} & X_{12} \\ X_{21} & X_{22} \end{bmatrix} \tag{18}$$

where $\begin{Bmatrix} X_{11} \\ X_{21} \end{Bmatrix}$ and $\begin{Bmatrix} X_{12} \\ X_{22} \end{Bmatrix}$ are the eigenvectors (mode shapes) of first and second vibration modes of the dual cantilever.

When the modal displacements are normalized with respect to the displacement of the first mass, then the modal matrix becomes

$$[\vec{X}] = \begin{bmatrix} 1 & 1 \\ X_{21} & X_{22} \end{bmatrix} \tag{19}$$

where X_{21} and X_{22} are given by

$$X_{21} = \frac{k_2}{\left(k_2 - m_{2eff}\ \omega_{n1}^2\right)} \tag{20}$$

$$X_{22} = \frac{k_2}{\left(k_2 - m_{2eff}\ \omega_{n2}^2\right)} \tag{21}$$

The ratio of the amplitude of the two masses being positive means that the motions are in phase, that is, the two masses move up or down together. This is the case for the system's first mode. The ratio of the amplitudes of the two masses being negative means that two motions are out of phase, that is, one mass moving down and the other moving up, and vice versa. This is the case for the second mode. In the first mode, every point in the system executes harmonic motion of the first natural frequency and in the second mode that of the second natural frequency. A system having two degrees of freedom can vibrate in two principal modes of vibration, corresponding to its two natural frequencies.

EXAMPLE CALCULATION:

The purpose of the following discussion is to describe numerically the typical mode shapes and the natural frequencies of the dual cantilever. Usually manufacturers of the microcantilevers gives the spring constants and natural frequencies of single microcantilevers, and their effective mass is calculated from the given numbers. We assume that the second cantilever in the dual cantilever is attached to the single microcantilever. The values of spring constants for different modes are tabulated in Table 1. If we choose the values for k_1, k_2, f_1 and f_2 as given below, for example $k_1 = 42$ N/m, $k_2 = 20$ N/m, $f_1 = 300$ kHz and $f_2 = 350$ kHz .

Extracting effective masses m_1 and m_2 from the single-degree cantilever information, effective masses are given as

$$m_{1eff} = \frac{k_1}{(2\pi f_1)^2} \tag{22}$$

$$m_{2eff} = \frac{k_2}{(2\pi f_2)^2} \tag{23}$$

where m_{1eff} and m_{2eff} are the effective mass for the dual cantilever; k_1 and k_2 are the spring constants for mass 1 and mass 2, respectively; and f_1 and f_2 are the frequencies with which the masses vibrate. It is assumed that the effective mass for each cantilever in isolation may be used for the dual cantilever system. It is recognized that this is an approximation, but is used for this initial study. Equation (22) and (23) are obtained from the standard equation, which is given by

$$f = \frac{1}{2\pi}\sqrt{\frac{k}{m}} \tag{24}$$

Knowing the frequency (f) and stiffness (k) of the cantilever, the effective mass of the cantilever can be determined. The effective masses for the system are calculated using equations (22-23), and they are found to be $m_{1eff} = 1.18\ e^{-11}$ kg and $m_{2eff} = 0.435e^{-11}$ kg.

Using the effective masses calculated and the stiffness matrix (Equation 15), we find the natural frequencies using the characteristic equation (17). The natural frequency for the first mode is found to be 193 kHz and for the second mode is 266 kHz. Substituting the first natural frequency in equation (20), and the second natural frequency in equation (21), the elements in the modal matrix are determined. The columns of the modal matrix are the first and second mode shapes. The modal matrix for the given set of numerical values is found to be

$$\left[\vec{X}\right] = \begin{bmatrix} 1 & 1 \\ 1.8158 & -1.5741 \end{bmatrix}$$

Mode shapes for the typical example values of spring constant and frequency are shown in Figures 10 and 11. In the first mode, mass m_1 and mass m_2 vibrates in phase, i.e., they move together. In the second mode, they are out of phase, i.e., as the first mass moves up the second mass moves down.

The mode shapes for the dual cantilever model have the same relative phase values of stiffness and mass. In the first mode, the two masses will always be in phase

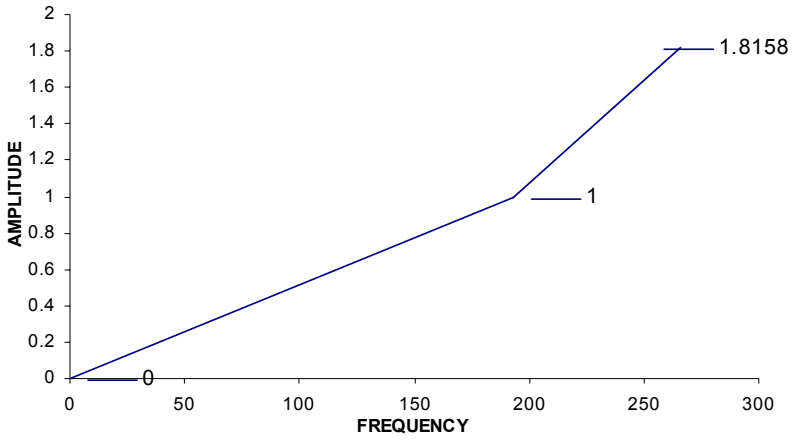

Figure 10: Mode shape 1; First natural frequency = 193 kHz

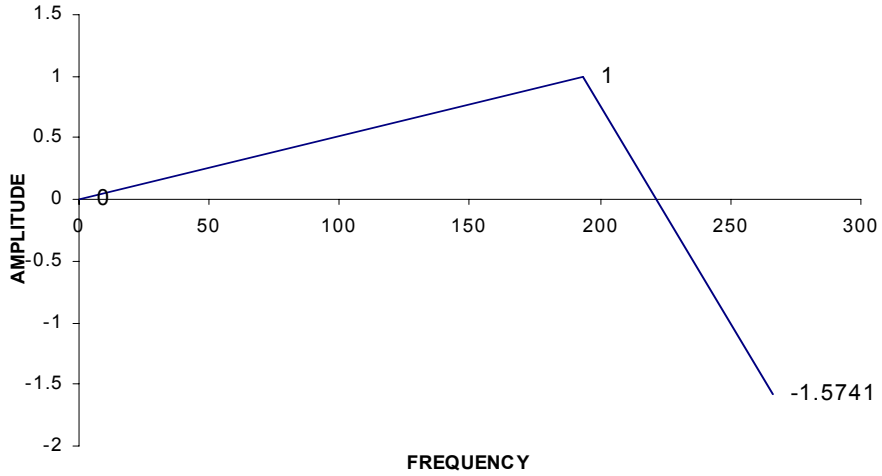

Figure 11: Mode shape 2; Second natural frequency = 266 kHz

and in the second mode, they will be out of phase. The mode shapes for the other models are discussed in Chapter 4.

3.1.2 FREQUENCY RESPONSE OF THE DUAL CANTILEVER

The response of the system is the movement of mass due to excitation by the base motion. The simple diagram for the dual cantilever used in this research is shown in Figure 7. In the previous section we discussed the mode shapes and the natural frequencies for the dual cantilever model. In this section we are going to discuss, using the mode shape and natural frequencies, how the frequency response for the dual cantilever model is determined. The frequency response obtained from this model forms the baseline for the other models in later sections. As mentioned previously this model is based on two assumptions. First, the cantilever is in tapping mode and the experiment is done in open space. Second, the tip is not engaged with any particle. In subsequent models, the tip will be engaged with a particle. So, when the solutions for those models are compared with the baseline solution, we may be able to say whether the particle is soft or hard. The response obtained for the system will be for a particular driving frequency. Therefore, the frequency response curve can be plotted by varying the driving frequency, i.e., frequency response is a function of driving frequency.

In this research the frequency response for the system is solved using the modal summation method. Here {x} contains the local coordinates, and {η} contains the modal coordinates. The local and modal coordinates are related by

$$\{x\} = \left[\vec{X}\right]\{\eta\} \tag{25}$$

where $\left[\vec{X}\right]$ is the modal matrix .

The differential equation in terms of local coordinates can be written as

$$[m]\left\{\ddot{x}\right\}+[c]\left\{\dot{x}\right\}+[k]\{x\}=\{F\} \tag{26}$$

where {F} is the local force matrix, given by

$$\{F\}=[k]\begin{Bmatrix} y \\ y \end{Bmatrix}=[k]\begin{Bmatrix} y_0 \\ y_0 \end{Bmatrix}\cos\omega t \tag{27}$$

The differential equation in terms of modal coordinates can be written as

$$[M]\left\{\ddot{\eta}\right\}+[C]\left\{\dot{\eta}\right\}+[K]\{\eta\}=\{Q\} \tag{28}$$

where [M] is the modal mass matrix

$$[M]=[\vec{X}^T][m][\vec{X}] \tag{29}$$

[K] is the modal stiffness matrix

$$[K]=[\vec{X}^T][k][\vec{X}] \tag{30}$$

[C] is the modal damping matrix

$$[C]=[\vec{X}^T][c][\vec{X}] \tag{31}$$

In this research , damping is assumed to be proportional, i.e.,

$$[c]=\alpha[m]+\beta[k] \tag{32}$$

where α and β are arbitrary constants. This assumptions makes the modal damping matrix to be diagonal, and so allows the two modal differential equations to be completely decoupled.

{Q} is the modal force , given by

$$\{Q\} = [\vec{X^T}]\{F\} \tag{33}$$

where [k] is the stiffness matrix, [m] is the mass matrix, [c] is the damper constant matrix. The modal matrices are all diagonal matrices, because the modal matrix decouples the differential equations to two single-degree of freedom equations.

The differential equation given in equation (28) can be expanded into two separate differential equations

$$M_1 \ddot{\eta}_1 + C_1 \dot{\eta}_1 + K_1 \eta_1 = Q_1 \tag{34}$$

and

$$M_2 \ddot{\eta}_2 + C_2 \dot{\eta}_2 + K_2 \eta_2 = Q_2 \tag{35}$$

where Q_1 and Q_2 are given by

$$Q_1 = X_1^T [k]\{y_0\}\cos\omega t \tag{36}$$

$$Q_1 = Q_{01}\cos\omega t \tag{37}$$

$$Q_2 = X_2^T [k]\{y_0\}\cos\omega t \tag{38}$$

$$Q_2 = Q_{02}\cos\omega t \tag{39}$$

Therefore, simplifying all the above equations, differential equations represented in equation (34) and (35) can be generally written as

$$\ddot{\eta}_r + 2\xi_r \omega_r \dot{\eta}_r + \omega_r{}^2 \eta_r = \frac{Q_{0r}}{M_r}\cos(\omega t) \tag{40}$$

We will proceed to solve the above differential equation using complex notation. Replacing cos ωt by e $^{i\omega t}$ gives

$$\ddot{\eta}_r + 2\xi_r \omega_r \dot{\eta}_r + \omega_r{}^2 \eta_r = \frac{Q_{0r}}{M_r} e^{i\omega t} \tag{41}$$

One can find a real solution as well as a complex solution for the same problem. In this particular research we are finding only the complex variable solution. The differential equation given in equation (41) can be solved by assuming an initial solution of the form

$$\eta_r = \bar{Y}_r \, e^{i\omega t} \tag{42}$$

where $\bar{Y}$ is the complex amplitude, ω is the driving frequency.

By substituting the complex function given in equation (42) into the differential equation (41) we get

$$\eta_r = \frac{\frac{Q_{0r}}{K_r}}{\left(\left(1 - r_r^2\right) + i\left(2\,\xi_r\, r_r\right)\right)} e^{i\,\omega\,t} = \bar{Y}_r \, e^{i\,\omega\,t} \tag{43}$$

where r_1 and r_2 are the frequency ratios for the first and the second masses. Frequency ratio is the ratio between the driving frequency and the natural frequency.

$$r_1 = \frac{\omega}{\omega_{n1}} \tag{44}$$

$$r_2 = \frac{\omega}{\omega_{n2}} \tag{45}$$

The modal solution η_r can also be written as

$$\eta_r = Y_r e^{-i\phi} e^{i\omega t} = Y_r e^{i(\omega t - \phi)} \tag{46}$$

where ϕ is the phase angle between the base motion and the modal response. Note that $\bar{Y}$ contains both amplitude and phase angle. The relationship between phase angle and the amplitude is shown graphically in the Nyquist phase diagram (Figure 12).

When both the numerator and the denominator of equation (43) are multiplied by the complex conjugate of the denominator, equation (43) becomes

$$\eta_r = \frac{\frac{Q_{0r}}{K_r}\left(\left(1 - r_r^2\right) - i\left(2\xi_r r_r\right)\right)}{\left(1 - r_r^2\right)^2 + \left(2\xi_r r_r\right)^2} = \bar{Y}_r e^{i\omega t} \tag{47}$$

Equation (47) has both the real part as well as the imaginary part. It can be written separately as

$$\bar{Y}_r = \frac{\frac{Q_{0r}}{K_r}\left(1 - r_r^2\right)}{\left(1 - r_r^2\right)^2 + \left(2\xi_r r_r\right)^2} - \frac{\frac{Q_{0r}}{K_r}\left(i2\xi_r r_r\right)}{\left(1 - r_r^2\right)^2 + \left(2\xi_r r_r\right)^2} \tag{48}$$

where the first term represents the real part and second term represents the imaginary part.

The response can be converted from modal coordinates back to local coordinates as

$$\begin{Bmatrix} \bar{x}_1 \\ \bar{x}_2 \end{Bmatrix} = \begin{bmatrix} X_{11} & X_{12} \\ X_{21} & X_{22} \end{bmatrix} \begin{Bmatrix} \bar{\eta}_1 \\ \bar{\eta}_2 \end{Bmatrix} \tag{49}$$

This can be written in another form as

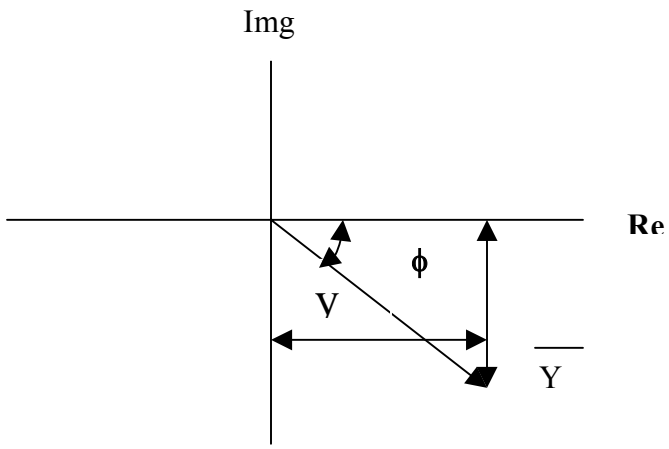

Figure 12: Nyquist phase diagram

$$\bar{x}_1 = X_{11}\bar{\eta}_1 + X_{12}\bar{\eta}_2 \tag{50}$$

$$\bar{x}_2 = X_{21}\bar{\eta}_1 + X_{22}\bar{\eta}_2 \tag{51}$$

As a classical approach, the initial solution is assumed to be of the form

$$\bar{x}_1 = \bar{X}_1 e^{i\omega t} \tag{52}$$

$$\bar{x}_2 = \bar{X}_2 e^{i\omega t} \tag{53}$$

substituting the complex variable solution given in equation (42) and using equation (52),(53) equation (50) and (51) becomes

$$\bar{X}_1 = X_{11}\bar{Y}_1 + X_{12}\bar{Y}_2 \tag{54}$$

$$\bar{X}_2 = X_{21}\bar{Y}_1 + X_{22}\bar{Y}_2 \tag{55}$$

The complex solution can be separated into real and imaginary parts as given below.

$$\mathrm{Re}\left[\bar{X}_1\right] = \sum X_{1r} \frac{\frac{Q_{0r}}{K_r}\left(1 - r_r^2\right)}{\left(1 - r_r^2\right)^2 + \left(2\xi_r r_r\right)^2} \tag{56}$$

$$\mathrm{Im}\left[\bar{X}_1\right] = -\sum X_{1r} \frac{\frac{Q_{0r}}{K_r}\left(2\xi_r r_r\right)}{\left(1 - r_r^2\right)^2 + \left(2\xi_r r_r\right)^2} \tag{57}$$

$$\mathrm{Re}\left[\bar{X}_2\right] = \sum X_{2r} \frac{\frac{Q_{0r}}{K_r}\left(1-r_r^2\right)}{\left(1-r_r^2\right)^2 + \left(2\xi_r r_r\right)^2} \tag{58}$$

$$\mathrm{Im}\left[\bar{X}_2\right] = -\sum X_{2r} \frac{\frac{Q_{0r}}{K_r}\left(2\xi_r r_r\right)}{\left(1-r_r^2\right)^2 + \left(2\xi_r r_r\right)^2} \tag{59}$$

The frequency response obtained is for the complex variable solution. The frequency response of the system, X_1 and X_2 are obtained by combining the real and the imaginary solution. It is given as

$$X_1 = \sqrt{\left(\mathrm{Re}\left[\bar{X}_1\right]\right)^2 + \left(\mathrm{Im}\left[\bar{X}_1\right]\right)^2} \tag{60}$$

$$X_2 = \sqrt{\left(\mathrm{Re}\left[\bar{X}_2\right]\right)^2 + \left(\mathrm{Im}\left[\bar{X}_2\right]\right)^2} \tag{61}$$

EXAMPLE CALCULATION:

This part of the section discusses numerically the values obtained for frequency response for the given example values. Values for the spring constants and frequencies are given by manufacturers of the microcantilevers. For example, considering a typical values for springs k_1= 42 N/m and k_2= 20 N/m, damping coefficient for first mass ξ_1=0.0012, frequencies f_1=300 kHz and f_2= 350 kHz . The damper coefficient for the first mass is assumed as given when the experiment is done in open space [41]. The damping coefficient for the second mass is taken proportional to the mass and is given by

$$\xi_2 = \xi_1 \left(\frac{m_{2eff}}{m_{1eff}} \right) \tag{62}$$

In this case, we assume that the damping for the second mass is proportional to the first mass, because the second cantilever is just an add-on cantilever to the single cantilever. The effective masses for the example values are already calculated and discussed in the previous section. Using the effective masses and damper coefficient for the first mass, we find from equation (62) that ξ_2 is 0.0034 . The modal matrix for the given example values is also calculated in the previous section. The modal mass matrix, modal stiffness matrix and modal damping matrix are calculated using modal matrix, mass matrix, stiffness matrix and damping constant matrix, respectively. The equations used to calculate these are given in the frequency response section of the dual cantilever model (Equations 29-31). The modal force is calculated from the modal matrix and the force vector. Knowing the natural frequency, we can calculate the frequency ratio for any given driving frequency. Knowing frequency ratio, damper coefficients, modal force and modal stiffness, we can determine the frequency response for the given driving frequency by using equation (48). Equation (48) has both real and imaginary parts; plots can be obtained separately for each of them. The total response or the combined response of the system is calculated using equations (60) and (61).

Figure 13 represents the real part of the frequency response for the first mass. From the plot it is clear that once the driving frequency is larger than the first natural frequency then the amplitude is negative because the system vibrates in second principal mode. Figure 14 represents the imaginary part of the frequency response for the first mass. Figure 15 gives the frequency response of the combined real and imaginary parts of the dual cantilever. From the plot it is clear that when the driving frequency is equal to the natural frequency the amplitude ratio is high. As the driving frequency increases initially the amplitude ratio increases until it reaches the first natural frequency, and then it decreases and again increases until it reaches the second natural frequency, and then it is steady after that. When the driving frequency increases beyond 350 kHz, the response is negligible.

Figure 16 is the real part of the frequency response for the second mass. When we compare Figure 13 and Figure 16 the difference can be easily seen. In Figure 13 as the driving frequency increases beyond the first natural frequency, the amplitude ratio is negative and it gradually increases as driving frequency increases. But in Figure 16, when the driving frequency increases beyond the first natural frequency the amplitude ratio is negative and until it reaches the second natural frequency it is negative. Figure 17 gives the imaginary part of the frequency response for the second mass. In the same way, if you compare Figure 14 and Figure 17, the difference can be easily seen. In Figure14, when the driving frequency is near the second natural frequency still the amplitude ratio is negative but in Figure 17, the amplitude ratio is positive. Figure 18 gives the frequency response for the combined real and imaginary parts for the second mass.

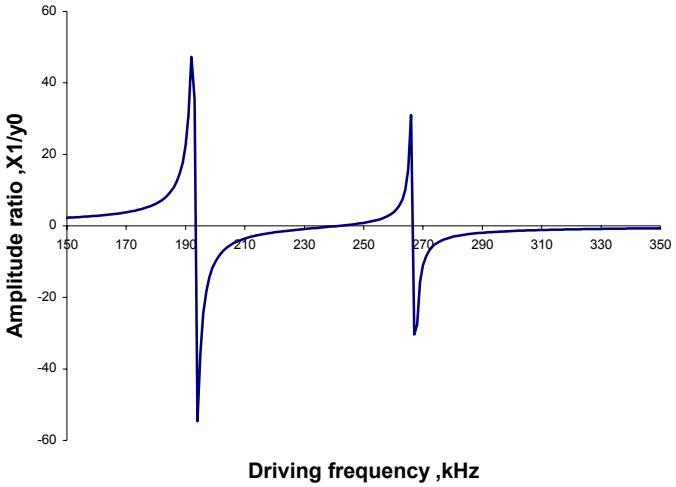

Figure 13: Real part of the complex solution for the first mass

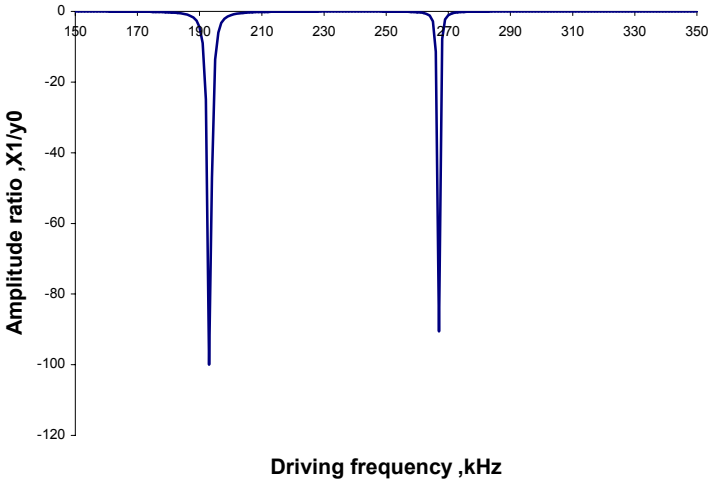

Figure 14: Imaginary part of the complex solution for the first mass

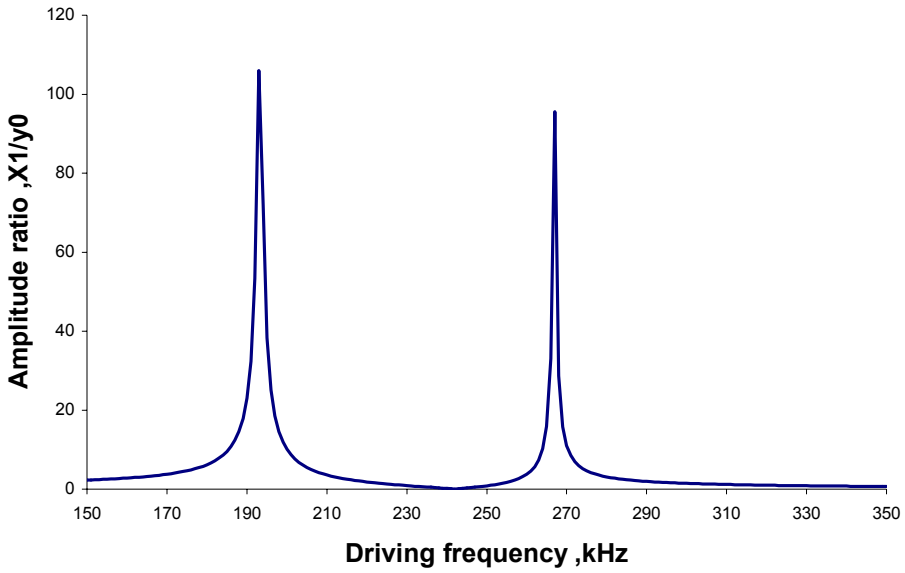

Figure 15: Combined frequency response of two-degree damped system for the first mass

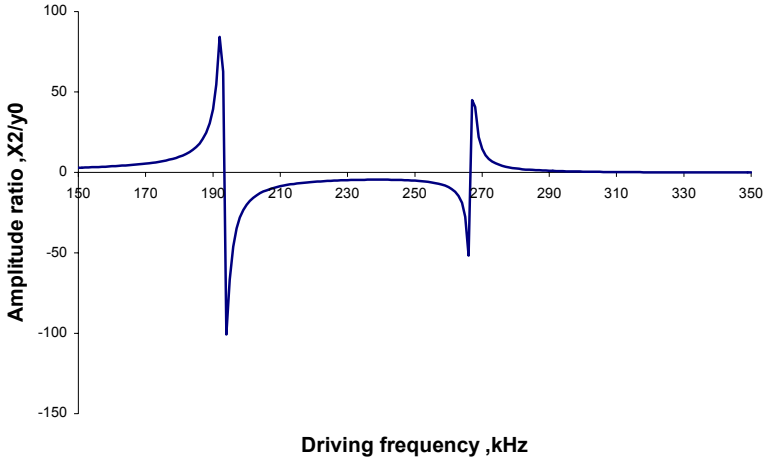

Figure 16: Real part of the complex solution for the second mass

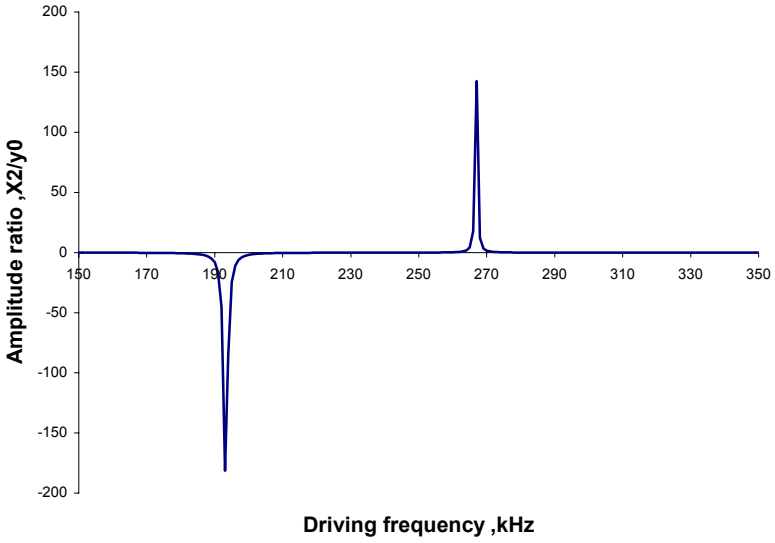

Figure 17: Imaginary part of the complex solution for the second mass

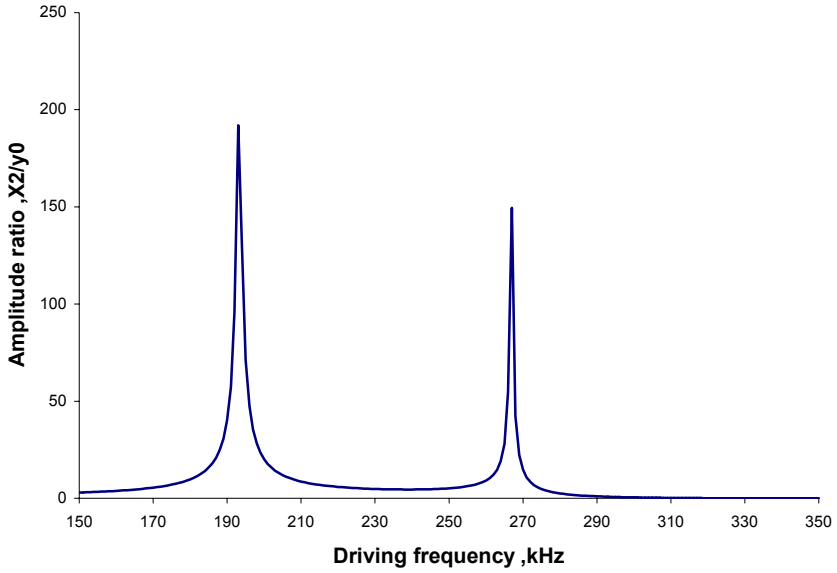

Figure 18: Combined frequency response of the two-degree damped system for the second mass

3.2 ELASTIC MODEL

The objective of this research is to identify and image particulates on the surface. Until now we have discussed how the basic dual cantilever model is built, and how the frequency response for the dual cantilever model is obtained. Moving on to the research, first we are going to discuss the elastic model in this section. The elastic model, as the name suggests, is used to find whether the particulates on the surface are hard or not. The block diagram for the classic elastic model is shown in Figure 19(a). In this model, the dual cantilever tip is connected to a lower spring. The spring attached to the tip is considered to be the particle on the surface, which we have to identify. The assumptions made in the dual cantilever model are applied here also i.e., tapping mode and steady state response. The response obtained from this model is then compared with the frequency response of the dual cantilever model or the baseline model. By comparing the two frequency response curves, one can identify the signature of this model.

In Figure 19 (b), k_3 represents the lower spring attached to the tip of the dual cantilever. Here x_1 and x_2 are the displacements of the first and second masses, respectively. The dual cantilever is given a base motion with an amplitude of y_0 and a driving frequency ω. As mentioned earlier, the dual cantilever beam has different stiffness; k_1 and k_2 are the stiffness for the first and second beam, respectively. The lower spring attached to the tip of the dual cantilever is considered to be parallel to the springs k_1 and k_2. Thus, the spring force acting on the tip is now the sum of the spring forces of springs k_1 and k_3. This will in turn increase the total stiffness of the first beam. When the stiffness of the beam increases, the natural frequency automatically increases

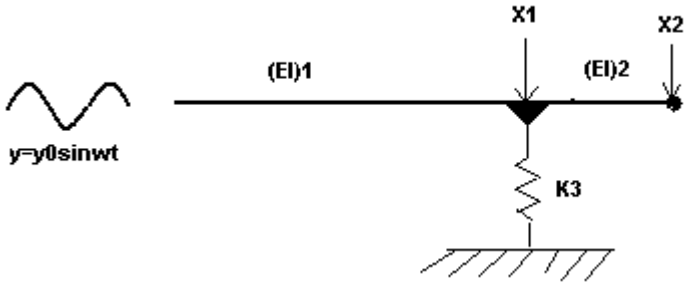

(a)

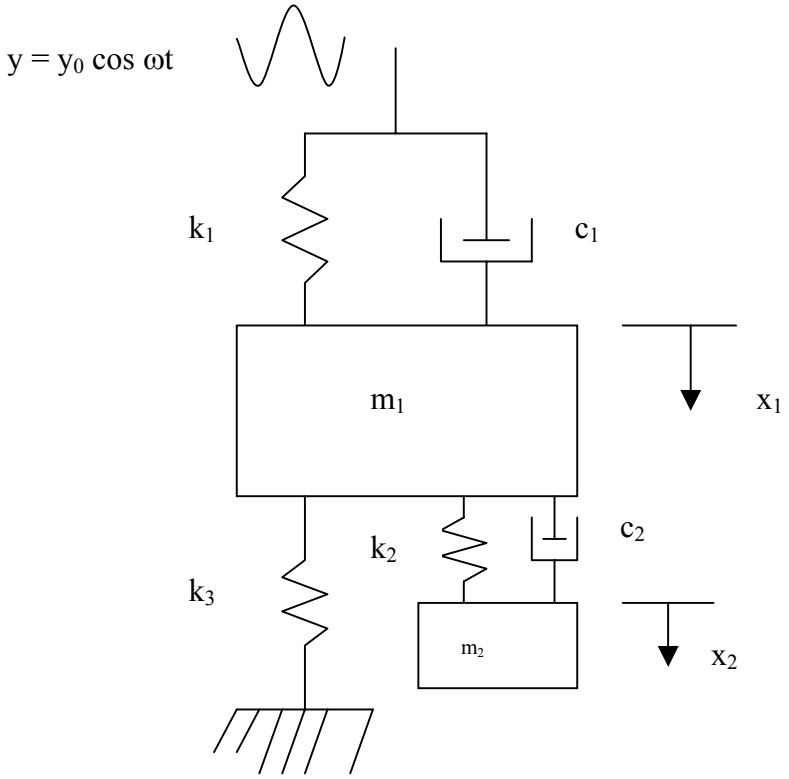

(b)

Figure 19: Elastic model. (a) Dual cantilever tip attached to a lower spring (b) Graphical representation for elastic model

The characteristic equation used to find the natural frequency of the elastic model is the same as the characteristic equation given in the dual cantilever model. The stiffness matrix used to find the natural frequency is

$$[k] = \begin{bmatrix} (k_1 + k_2 + k_3) & -k_2 \\ -k_2 & k_2 \end{bmatrix} \tag{63}$$

Comparing the stiffness matrix used in the dual cantilever model (equation 15) and the one given in equation (63), we can see all the terms are the same except the first term. The first term has an extra term, which is the spring constant of the lower spring. Therefore, when the lower spring constant has some non-zero value, the natural frequencies will increase. When comparing the natural frequencies of the dual cantilever model with that of the elastic model, the elastic model has the higher natural frequencies. Shift in natural frequency is one of the signatures of this model. Shift in natural frequency occurs only due to that extra term in the stiffness matrix, so the lower spring has direct impact on the natural frequency.

The dual cantilever will be vibrating in its resonance frequency over the surface, which has to be imaged. While the tip is scanning the surface, it is just moving over the surface and does not have any contact with the surface. When the tip encounters any particle on the surface, then this model is applied, i.e., the particle is considered to be a spring and is attached to the tip. The equations used to find the frequency response are already discussed in the previous section. The same set of equations is used here too. The frequency response obtained for the elastic model is then compared with the frequency response obtained in the dual cantilever model. If there is any frequency shift, then one can say that the particle on the surface is hard. This is so because, when the

particle is hard, it will increase the stiffness of the beam, which results in a higher natural frequency. When the lower spring constant value is zero, then the frequency response obtained from this model will be the same as the frequency response obtained in the dual cantilever model. Some of the particles that can be found using this model are sand, lead, and steel.

The frequency response obtained will be for a particular value of driving frequency. Therefore, varying the driving frequency, the frequency response curve is drawn. Frequency responses are obtained for different values of the lower spring constants, and they are compared. A plot between the lower spring constant and the shift in natural frequencies is also drawn to see how natural frequencies vary with the change of lower spring constant values.

EXAMPLE CALCULATION:

This part of the section deals with some numerical values for the elastic model. Let us take the same example values given in the previous section and k_3 =10 N/m for the lower spring constant. The effective masses calculated (Equations 22-23) from the spring constant and the frequencies given by the manufacturers are

$m_1 = 1.18\times10^{-11}$ kg $\quad m_2 = 0.0435\times10^{-11}$ kg

Using the stiffness matrix and the effective masses, the natural frequencies are calculated from the characteristic equation (17). The natural frequencies are found to be

First natural frequency = 200.82 kHz

Second natural frequency = 270.886 kHz

Mode shape is given by $X = \begin{pmatrix} 1 & 1 \\ 2.1017 & -1.36 \end{pmatrix}$

The frequency responses for this example model are shown in the Figure 20 and Figure 21. Figure 20 represents the frequency response of the first mass and Figure 21 represents the frequency response of the second mass.

In both figures, the frequency response obtained from the elastic model is compared with the frequency response obtained from the dual cantilever model or the baseline model. The solid line represents the frequency response of the elastic model, and the dotted line represents the frequency response of the baseline. It can be seen that the natural frequency of the elastic model is higher than the natural frequency of the baseline model. Therefore, by inferring this, one can say the particle on the surface is harder. In order to see what happens to the natural frequency when the lower spring constant value changes, a different value for the lower spring constant is taken and the same procedure is followed to get the frequency response. For example take k_3 = 20 N/m, the frequency response for this value is given in Figure 22 and Figure 23.

Comparing the frequency responses obtained for the lower spring constant values of 10 N/m and 20 N/m, it can be seen that there is a shift in natural frequencies. The natural frequency increases with the increase in k_3. When the lower spring constant is 10 N/m, then the first natural frequency is 200 kHz, and when the lower spring constant is 20 N/m, the first natural frequency is 207 kHz. From the Figures 20 and 22, it is clear that as the lower spring constant increases the natural frequency tends to shift outwards. Plots can be drawn between shifts in natural frequency versus lower spring constant. The shift in the first natural frequency is given in Figure 24 and for the second natural frequency in Figure 25. In both figures, the natural frequency obtained for this model is compared with the baseline natural frequency. The change in natural frequency is linear.

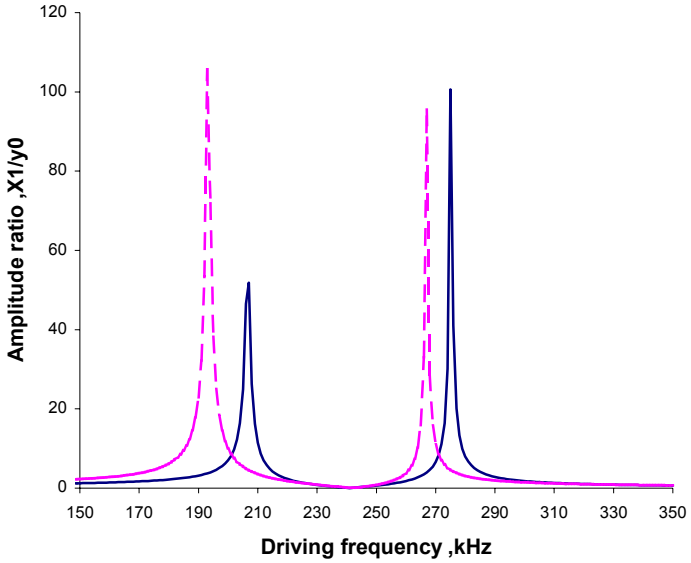

Figure 20: Frequency response of first mass for two-degree damped system adding a lower spring with spring constant k_3= 10 N/m
_____ k_3=10 N/m ; ------- Baseline with k_3 = 0 N/m

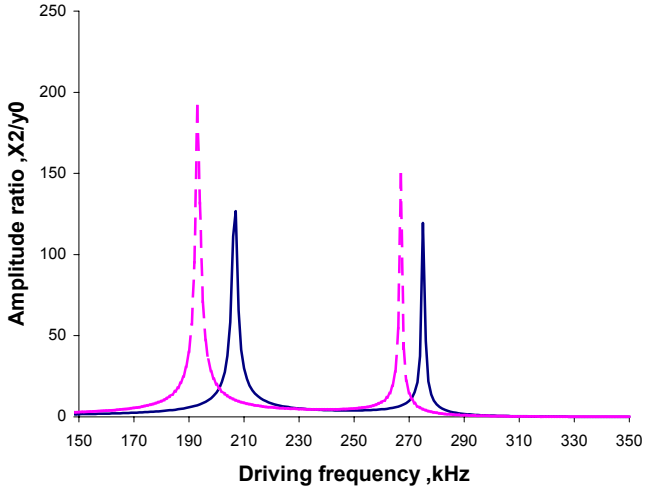

Figure 21: Frequency response of second mass for two-degree damped system adding a lower spring with spring constant k_3= 10 N/m
_____ k_3=10 N/m ; ------ Baseline with k_3=0 N/m

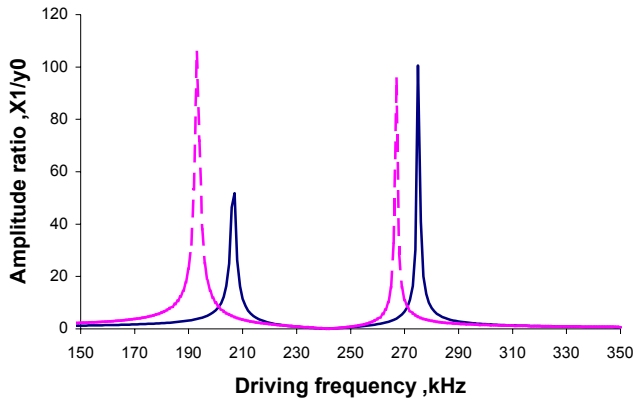

Figure 22: Frequency response of first mass for two-degree damped system adding a lower spring with spring constant k_3= 20 N/m

_____ k_3=20 N/m ; ------- Baseline with k_3 = 0 N/m

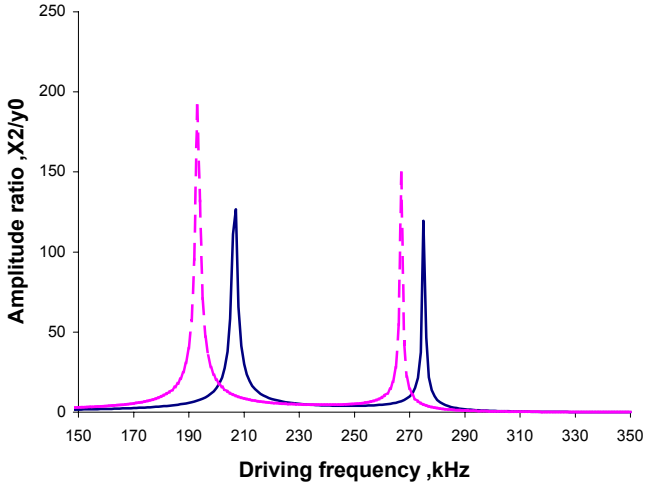

Figure 23: Frequency response of second mass for two-degree damped system adding a lower spring with spring constant k_3= 20 N/m

_____ k_3=20 N/m ; ------- Baseline with k_3 = 0 N/m

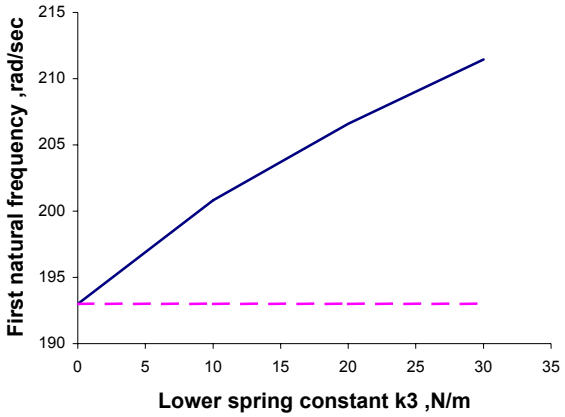

Figure 24: Spring constant k_3 versus first natural frequency
_____ With k_3; -------- Baseline with k_3 = 0 N/m

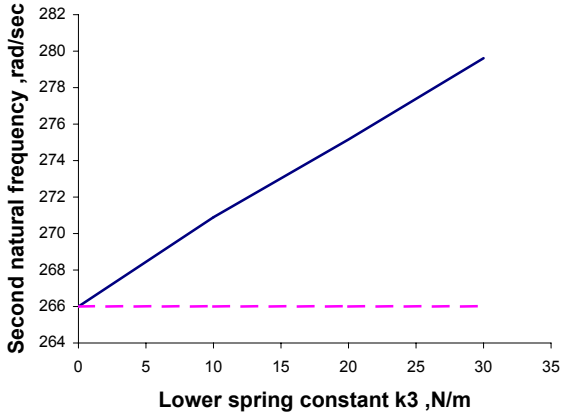

Figure 25: Spring constant k_3 versus second natural frequency
_____ With k_3 ; -------- Baseline with k_3 = 0 N/m

The signature of this model and some more examples for this model are discussed briefly in Chapter 4. In Chapter 4, it is explained how the response obtained from this model can be linked to the particle properties.

3.3 VISCOUS MODEL

Viscous model is the second model used in this research to identify and image particle on the surface. In the previous section we have seen how the elastic model is used to identify hard particles. In this section we are going to discuss how soft particles are being identified. As the name suggests, the viscous model is used to image whether the particle on the surface is soft or not. In the elastic model only the spring is connected to the tip of the dual cantilever, but in the viscous model only the damper is connected to the tip. A block diagram for the viscous model is shown in Figure 26(a). In Figure 26(b), c_3 represents the lower damper, and x_1 and x_2 are the displacements of the first mass and the second mass, respectively. The dual cantilever is given a base motion with an amplitude of y_0 and a driving frequency of ω. The dual cantilever has a stiffness of k_1, k_2 and damper constants c_1, c_2 for the first and second masses, respectively.

In this model, when the lower damper is connected to the tip of the dual cantilever, the energy exerted by the damper will be high and hence can be used to identify soft particulates. In this model the lower damper added is parallel to the main system (i.e., to the dual cantilever). Therefore, the damper constant for the first beam will be the sum of the lower damper constant and the damper constant for first mass. In this model the stiffness matrix, which is used to find the natural frequency, is the same as the stiffness

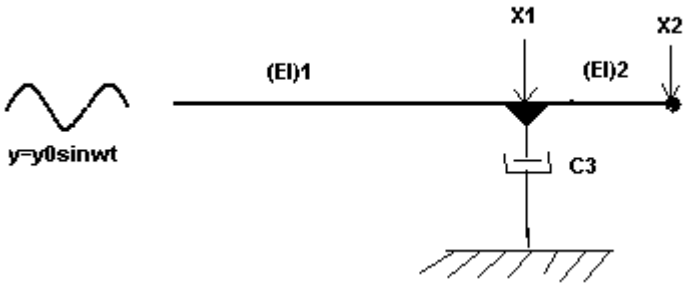

(a)

(b)

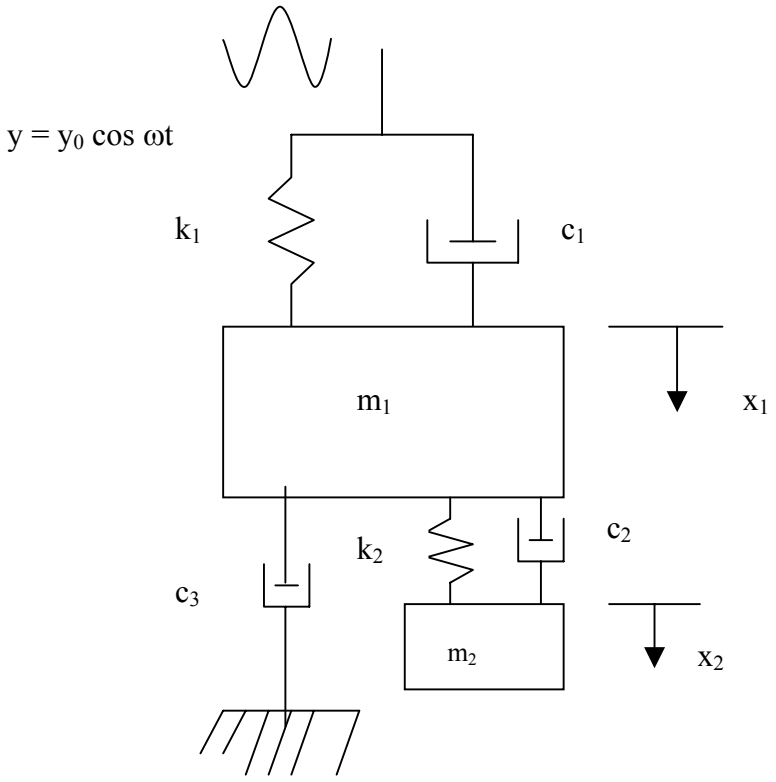

Figure 26: Viscous model. (a) Dual cantilever tip attached to a lower damper (b) Graphical representation of viscous model

matrix used to find the natural frequency of the dual cantilever model. Hence, the natural frequency for this model is going to be the same as the natural frequency of the baseline model. The natural frequency increases only when there is any extra spring force acting. In this model, there is no extra spring force, but there is an extra damper force because of the damper. Therefore, the only changes in this model will be the damper coefficient and the damper constant matrix. The damper constant in this model is taken proportionally to the effective mass ratio. Knowing the damper coefficient for the first mass from the manufacturer and calculating the effective mass and the natural frequencies from given values of spring constants and frequencies, the damper constant for the first mass can be determined by using the relationship given in

$$damper\ \ coefficient\ (\ \xi\ ) = \frac{Damper\ \ const}{Critical\ \ damping} = \frac{c}{c_c} \tag{64}$$

where the critical damping is determined from the effective mass and the natural frequency. The damper constant for the first mass is

$$c_1 = \xi_1\, 2\, m_{1eff}\ \omega_{n1}^2 \tag{65}$$

where ξ_1 is the damper coefficient of the first mass, ω_{n1} is the first natural frequency, and m_{1eff} and m_{2eff} are the effective masses for mass 1 and mass 2, respectively.

Equation (65) is obtained from the standard equation, which is given by

$$\xi = \frac{c}{c_c} = \frac{c}{2m\omega_n} \tag{66}$$

The damper constant for the second mass, which is proportional to the effective mass, is

$$c_2 = c_1 \left(\frac{m_{2eff}}{m_{1eff}} \right) \tag{67}$$

We assume that the effective masses are same for all the modes. Equation (67) is derived from

$$\frac{c_1}{m_1} = const \quad \text{and} \quad \frac{c_2}{m_2} = const$$

The lower damper attached to the dual cantilever is considered as the particulate on the surface. While scanning, the tip of the dual cantilever moves over the surface. When it encounters any particle then this model applies. When the tip of the cantilever touches the lower damper, a response is produced, and this response is recorded. Some of the particulates which can be determined from this model are DNA, blood etc.,

The damper force acting now on the tip is the addition of the first mass damper constant force plus the lower damper constant force because the lower damper is parallel to the dual cantilever. The damper constant at the tip is then given by

$$c_4 = c_1 + c_3 \tag{68}$$

The local damping matrix for the viscous model is

$$c = \begin{pmatrix} c_4 & -c_2 \\ -c_2 & c_2 \end{pmatrix} \tag{69}$$

The modal damping matrix is determined using the equation (31) given in the frequency response section of the dual cantilever model. Since we have assumed that there is proportional damping, the off diagonals are zero when the modal damping is calculated.

$$[C] = \begin{bmatrix} C_1 & 0 \\ 0 & C_2 \end{bmatrix} \tag{70}$$

where

$$C_1 = [X_1^T][c][X_1] \tag{71}$$

$$C_2 = [X_2^T][c][X_2] \tag{72}$$

Here X_1 and X_2 represents the first and second mode respectively.

The mathematical formulation of this model requires modal damping factor ς_1 and ς_2 to determine the frequency response, which can be now determined from

$$\varsigma_1 = \frac{C_1}{2M_1\omega_{n1}^2} \tag{73}$$

$$\varsigma_2 = \frac{C_2}{2M_2\omega_{n2}^2} \tag{74}$$

Equation (73) and (74) are formulated from the relation between the damper constant and the critical damping given in equation (64). Where ω_{n2} is the second natural frequency, C_2 is the second diagonal element in the modal damping matrix or the damper constant for the second mass in the modal coordinates, and M_2 is the second diagonal element in the modal mass matrix or the mass 2 in the modal coordinates.

After determining the modal damper coefficients (Equation 73 and 74) and the frequency ratios (Equations 44 and 45) for mass 1 and mass 2, the frequency response can be determined by using the same equations used to determine the frequency response in the dual cantilever model. The frequency response curve can be plotted as a function of driving frequency. The same procedure can be used to determine the frequency response for various values of the damper constants for the lower damper. By comparing the plots obtained with the baseline frequency response, one can determine what type of particle is on the surface. When the amplitude ratio of the viscous model is lesser than

the amplitude ratio of the baseline model then the particle on the surface can be identified as a soft particle. Therefore, change of amplitude ratio is considered to be one of the signatures of this model.

EXAMPLE CALCULATION:

In this part of the section we are going to discuss this model with some numerical values for the lower damper. Using some numerical examples will help us to understand better how the model is working and what happens when the damper constants change. A typical numerical example is used to see graphically what happens to the amplitude ratio when there is a change in lower damper constant value. Let us take some example values as given by the manufacturer of the microcantilevers $k_1 = 42$ N/m, $k_2 = 20$ N/m, $f_1 = 300$ kHz, $f_2 = 350$ kHz: The damper constant value for the lower damper is assumed initially to be c_3=0.00000005 N-s/m. The effective masses are calculated as

$$m_1 = 1.18\times10^{-11} \text{ kg and } m_2 = 0.0435\times10^{-11} \text{ kg.}$$

Using the effective mass and the stiffness matrix, natural frequencies of the two-degree of freedom are

First natural frequency = 193 kHz

Second natural frequency = 266 kHz

Corresponding mode shapes are displayed as columns in the modal matrix as

$$X = \begin{pmatrix} 1 & 1 \\ 1.8158 & -1.5741 \end{pmatrix}$$

These are the same as the dual cantilever model which has already been discussed.

The damper coefficient for the first mass is assumed to be 0.0012 [41]. The damper constant for the first mass is calculated using the relation given in (64). Knowing the

natural frequencies and the effective masses, damper constants for both mass can be determined from equations (65,67). Modal mass matrix, modal stiffness matrix, and modal damper matrix are calculated using modal matrix, mass matrix, stiffness matrix and damper matrix, respectively, using the equations (29-31). The modal damper coefficients for the first and the second mass are then calculated using equation (73) and (74).

After determining the values for modal damper coefficients, frequency ratio, modal force and modal stiffness, substituting them in the frequency response equation, we find the frequency response for the first mass as shown in Figure 27. Figure 27 is compared with the baseline frequency response (Figure 28) to see the difference in the model when a damper is added. The difference cannot be seen when both are shown in the same plot, so they are shown in two different plots. The amplitude change is very small for this value of damper constant value. When the damper constant value is higher, then one can see the difference clearly. Figure 28 represents the frequency response for the first mass of the dual cantilever when the tip is not attached to any particle. Figure 29 represents the frequency response of the second mass for the viscous model, and it is compared with Figure 30, which is the frequency response of the second mass for the dual cantilever model or the baseline frequency response. When the lower damper constant value increases, it offers more resistance for the masses to vibrate and hence the amplitude ratio is less. When the lower damper constant value is high, then it behaves more like rigid body. Hence the force exerted on the damper will be high, that's why the movement of damper will be high.

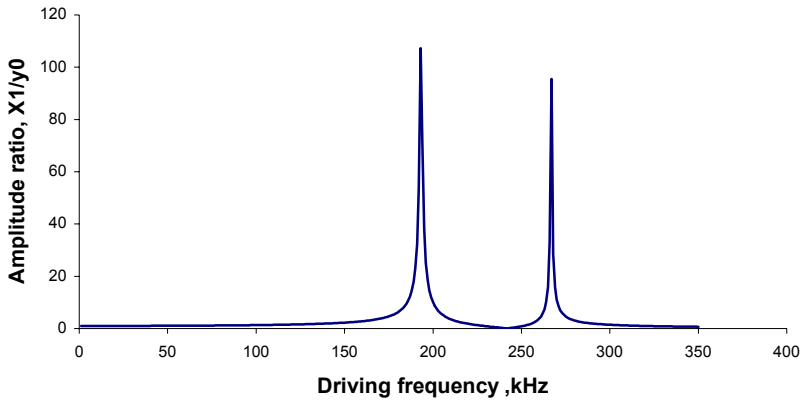

Figure 27: Frequency response for the first mass with a lower damper constant c_3 = 0.00000005 N –s/m

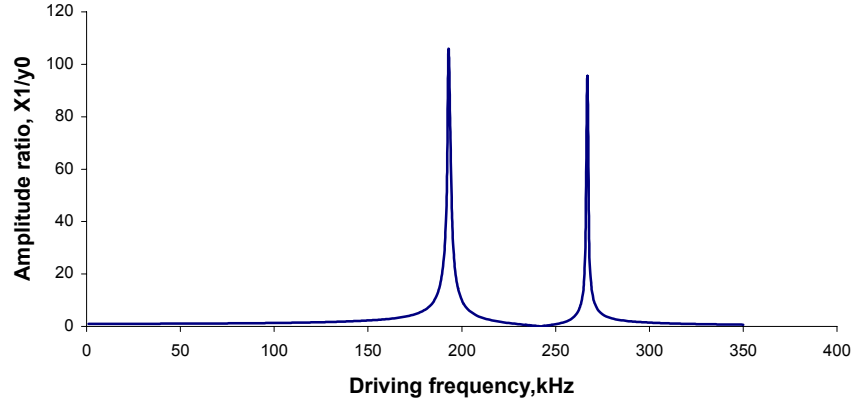

Figure 28: Frequency response for the first mass; baseline with c_3=0 N-s/m

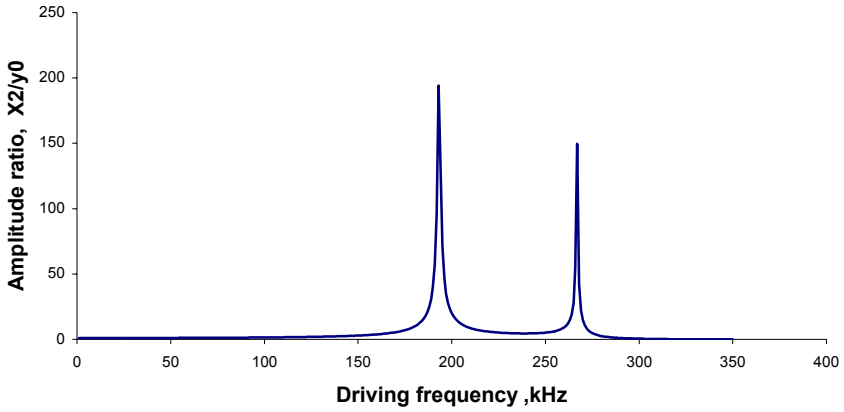

Figure 29: Frequency response for the second mass with a lower damper constant c_3= 0.00000005 N-s/m

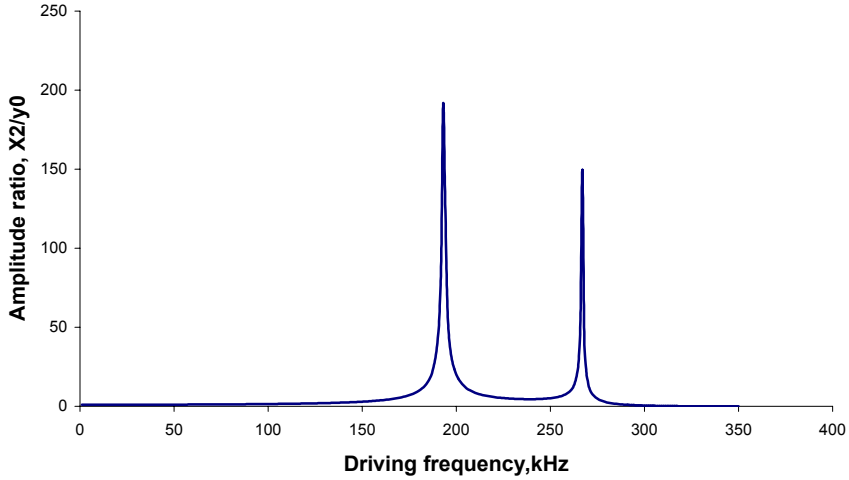

Figure 30: Frequency response for the second mass; baseline with c_3 = 0 N-s/m

Figure 31 represents the frequency response of the viscous model for the first mass when the damper constant value is 0.0000005 N s/m. Figure 31 has both the viscous model frequency response and the baseline frequency response. The solid line represents the viscous model frequency response, and the dotted line represents the baseline frequency response. When comparing both plots, we can infer that the amplitude ratio of the viscous model is less than the amplitude ratio of the baseline frequency response. From this we can infer that the particle on the surface is a soft particle. Figure 32 represents the frequency response of the viscous model for the second mass. It has both the frequency responses of the viscous model and the baseline. So, when the damper constant is higher, then the first mass will be fully restrained from vibrating. In that case we will have only amplitude for the second mass. A plot can be drawn for the change in amplitude ratio versus the lower damper constant value. From the plot we can see how the damper constant value changes the amplitude ratio of the system. Figure 33 represents the change of amplitude ratio versus the damper constant value for the first mass and Figure 34 represents the change of amplitude ratio versus lower damper constant value of the second mass. The change is linear, and as the damper constant value increases the change of amplitude ratio is almost constant. So, change in amplitude ratio is considered to be the signature of this model.

Comparing Figure 27 and Figure 31, it can be shown that when the damper constant value increases then the amplitude of vibration decreases at resonance. From this model one can say, when there is a change in damper constant then the amplitude ratio will also change. Change in amplitude ratio refers to whether the particulate is soft or not. When

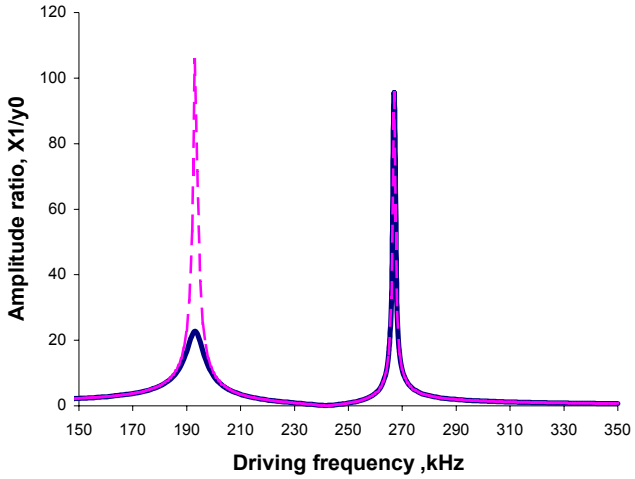

Figure 31: Frequency response for the first mass of the two-degree damped system adding a damper with c_3=0.0000005 N-s/m
_____ c_3=0.0000005 N-s/m ;-------- Baseline with c_3 = 0 N-s/m

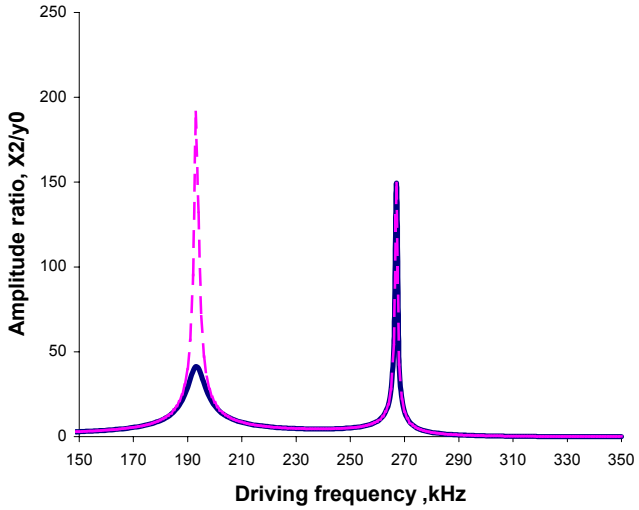

Figure 32: Frequency response for the second mass for the two-degree damped system adding a damper with c_3=0.0000005 N-s/m
_____ c_3=0.0000005 N-s/m ; -------- Baseline with c_3 = 0 N-s/

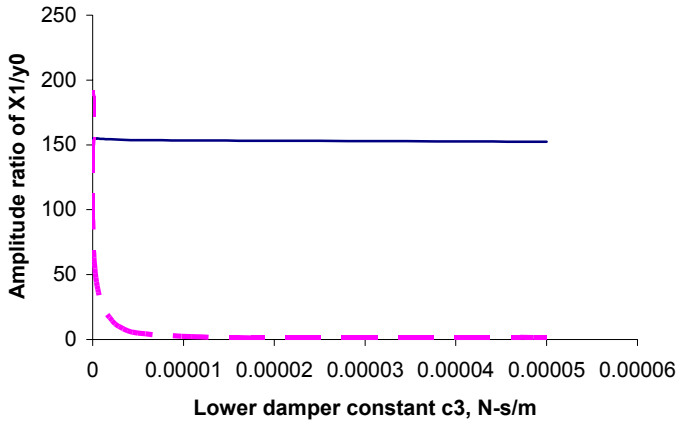

Figure 33: Damper constant versus shift in amplitude ratio for X_1
_____ with c_3; -------- Baseline with c_3 = 0 N-s/m

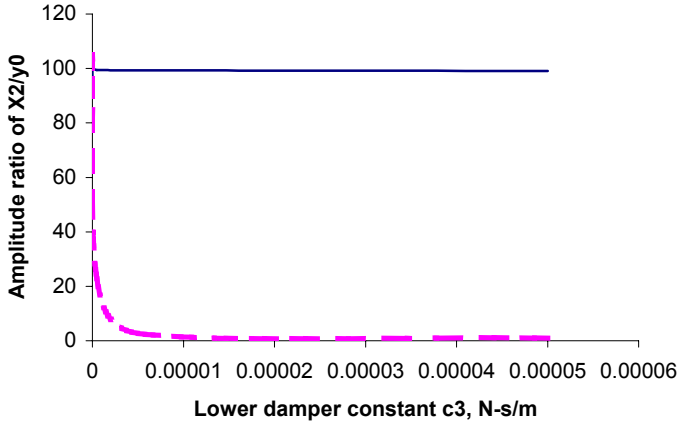

Figure 34: Damper constant versus shift in amplitude ratio for X_2
_____ with c_3; ------- Baseline with c_3 = 0 N-s/m

the amplitude ratio is higher then the particle is not soft. In the other case, when the amplitude ratio is less, then the particle is soft.

Figure 33 and Figure 34 show that as the damper constant increases the amplitude ratio decreases. It can be seen that as the damper constant is higher then the amplitude ratio is almost negligible. The mass does not vibrate because it is fully restrained from vibration. So we will have vibration for second mass alone.

In the viscous model, the tip can be assumed to experience a force consistent with either a capillary force model or a squeeze film model. Each model is discussed separately.

3.3.1 CAPILLARY FORCE MODEL

Condensation of water vapor takes place in the gap between contiguous bodies. The liquid bridge or meniscus thus formed will, on the one hand, draw up on the particle by means of surface tension forces ($F_{c,\,1}$) and on the other hand, will reduce the liquid pressure ($F_{c,\,2}$) by virtue of its concave shape, i.e.,

$$F_c = F_{c,\,1} - F_{c,\,2} \tag{75}$$

$$F_{c,\,1} = 2\pi a_1 \sigma \tag{76}$$

$$F_{c,\,2} = S\, p_c \tag{77}$$

where F_c is the capillary force, S is the contact area ($S = \pi a_1^2$); p_c is the capillary pressure and σ is the surface tension of the liquid. The capillary pressure indicates the difference in pressure between two bulk phases (in present case, liquid and gas) that are in a state of equilibrium and are separated by a curve surface. If a_1 and a_2 are the radii of the curvature of the water interlayer, the capillary force is determined as

$$F_c = \frac{2\pi\sigma r}{\left[1 + tg\left(\frac{\alpha}{2}\right)\right]} \tag{78}$$

As α (wetting angle) tends to zero, capillary force becomes

$$F_c = 2\pi\sigma r \tag{79}$$

The various angles and areas for calculating the capillary force are shown in Figure 35. If one of the contiguous surfaces is planar, the height of the interlayer will be twice as small. Then

$$F_c = 4\pi\sigma r \tag{80}$$

The capillary force depends on the wetting angle. It can be seen from Table 2, that as the wetting angle is increased i.e., as the surface becomes more hydrophobic, the forces of adhesion drop off; the particle diameter under these conditions determines how much the adhesive force drops. These forces are calculated not only for a single particle, but also for dust-covered surface.

When a drop of liquid is placed on the surface of a solid, the attraction of the solid causes a reduction in pressure within the liquid. This is designated as P_{sl}, while P_{lv} gives

Table 2: Force variation due to change in wetting angle

Wetting angle α, deg **Capillary force F_c, for particles of indicated diameter**	0	15	60	90
12 μm	416	407	252	135
4 μm	1240	1220	777	405

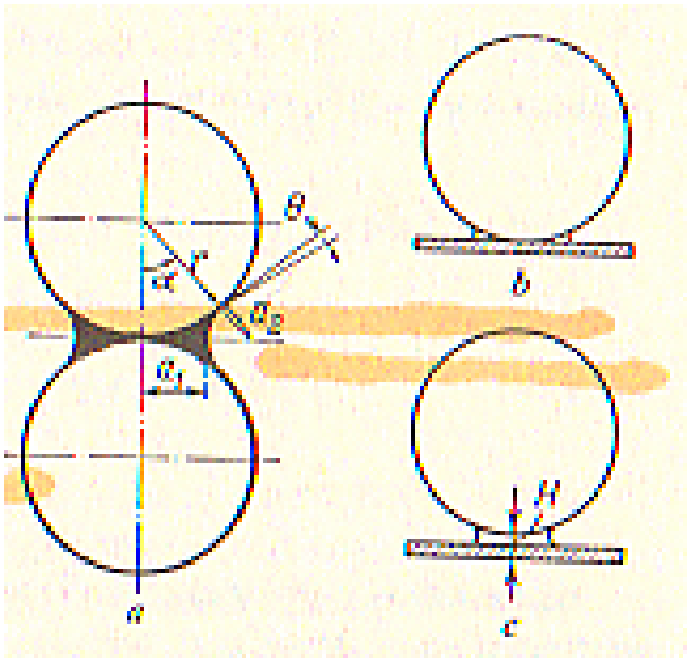

Figure 35: Capillary condensation upon contact of two particles (a) or contact of particle with surface (b, c): (a, b) without any interlayer in contact zone; (c) with liquid interlayer in contact zone.

inward pressure from the liquid vapor interface. The pressure P_{sl} is balanced by spreading of the drop until

$$P_{sl} = P_{lv} \cos \theta \qquad (81)$$

where θ is the contact angle. When there is no positive molecular attraction at the liquid-solid interface, P_{sl} is zero indicating a contact angle of 90°.

Surface Tension:

Surface molecules are subject to an attractive force from nearby surface molecules so that the surface is in the state of tension. This tensile force per unit of length along the surface is called surface tension. Surface tension is a property of the fluid and its adjacent fluid or solid. It is more properly called the interfacial tension because it appears at the interface between two fluids in contact with each other.

Surface tension is the tendency of the surface of a liquid to behave like a stretched elastic membrane. There is a natural tendency for liquids to minimize their surface area. For this reason, drops of liquid tend to take a spherical shape. For such a small droplet, surface tension will cause an increase of internal pressure p in order to balance the surface force. Surface tension generally appears only in situations involving either free surfaces (liquid/gas or liquid solid boundaries) or interfaces (liquid/liquid boundaries); in the latter case, it is usually called the interfacial tension.

When an interface between two fluids meets a solid surface, the interface forms an angle with respect to the solid surface called contact angle. This angle depends upon the nature of the two fluids and the solid. The values of the angle and the interfacial

tension then determine the effects of capillarity, such as the vertical rise height of a fluid in capillary tube.

Liquid mediated adhesive forces can be divided into two components; meniscus force due to surface tension force and a rate-dependent viscous force. These forces increase for smaller gaps and smoother surfaces so that the adhesion of ultra flat surfaces can be extremely strong. For an applied normal force less that the meniscus force there is no tendency for the surfaces to separate. When the force exceeds the meniscus force (F_M) at time t_m, then the viscous component in the normal direction ($F_{V\perp}$) is the excess over F_M. F_{AD} is the total force required to separate the two surfaces in time t_s,

$$F_{AD}=F_M + F_{V\perp} \tag{82}$$

If a drop of liquid is introduced between two surfaces under close proximity, surface tension effects will arise. The surface tension effects will attempt to pull the surfaces closer together; furthermore, surface tension will resist separation of the surfaces in a direction normal to the interface (Fan and O'Brien, 1975). This is because, whenever surface tension acts, the pressure inside the liquid is lower than it is outside the liquid. Force calculated using surface tension is

$$F_c = \frac{2\pi\sigma r}{\left[1+\tan(\theta)\right]} \tag{83}$$

where θ is the contact angle, σ is the surface tension of the liquid, r is the radius of the droplet.

By comparing, the force obtained from the frequency response curve and Table 3, we can conclude what type of particle is on the surface. This force is a constant force and it does not change with height. It is independent of height of the liquid film.

Table 3: Capillary force for various liquids and contact angle

Liquid	**Surface tension** In Dyne/cm	**Force in nN/m F_c**		
		$\theta = 30°$	$\theta = 45°$	$\theta = 60°$
Water	72.3	3.612	3.23	2.903
Blood	55.5- 61.2	3.0327	2.71906	2.4379
Crude oil	0.0320 N/m	1.58572	1.42172	1.2747
Olive oil	41	2.0317	1.82159	1.63323
Soap	25	1.2388	1.11066	0.9958
Mercury	470	23.2903	20.8816	18.7224

1 Dyne/cm = 0.001 N/m

3.3.2 SQUEEZE FILM MODEL

Consider two circular flat plates of radius approaching each other, or a single circular plate of radius R approaching a large surface (as in Figure 36). The space between is filled with a viscous liquid, which is being displaced radially outward by the relative motion of the plates. An elementary circular slot can be imagined through which liquid is being forced.

Load carrying capacity W is the product of the area and the average pressure

$$W = \pi R^2 p_{avg} \quad \text{(or)} \quad W = \frac{3\pi \mu V R^4}{2h^3} \tag{84}$$

This equation can be utilized in number of different ways, depending upon information known and what has to be determined. For a constant load W, the instantaneous velocity

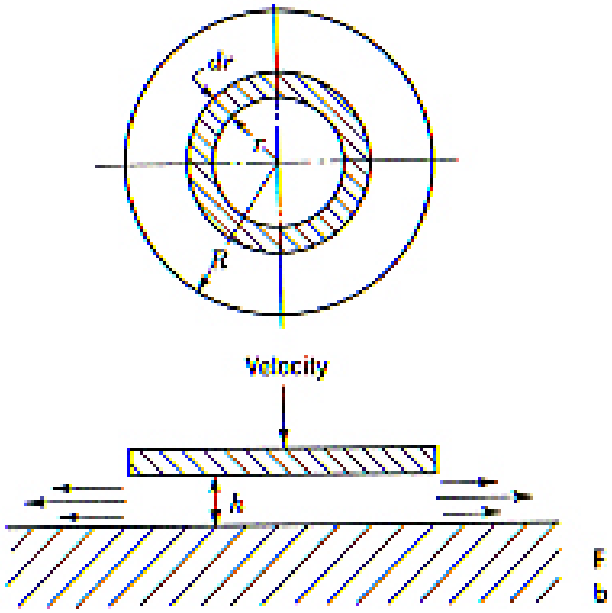

Figure 36: Squeeze film model

Table 4: Damper constant for various liquid

Liquid	Viscosity (μ)	Damper constant(c) in nN-s/nm
Water	1.002 cP	$0.00047942 \times 10^{-2}$
Honey	10000cP	47.1×10^{-2}
Soya bean oil	69.3cP	0.3264×10^{-2}
Mercury	1.554cP	0.007319×10^{-2}

of approach can be computed for a given thickness. The opposite condition can also be analyzed where there is a uniform velocity of approach. In this case, as the film thickness decreases, the build-up pressure of a load carrying capacity can be revealed.

$$c = \frac{W}{V} = \frac{3\pi\mu R^4}{2h^3} \tag{85}$$

Let us assume h= 100 nm, R= 10 nm and μ= bulk viscosity and it will differ for different liquid. The damper constant for various liquids can be determined by using the equation (85) and are tabulated in Table 4.

3.4 VISCO – ELASTIC MODEL #1 - SPRING/DAMPER IN PARALLEL (KELVIN-VOIGT MODEL)

In previous sections we discussed the elastic model, in which a spring alone is connected to the tip of the dual cantilever, and the viscous model in which a damper alone is connected to the tip of the dual cantilever. When both the spring and the damper are connected, either in series or in parallel, then the model is called a visco-elastic model. In this section we are going to discuss the first visco-elastic model, in which, the spring and the damper are connected in parallel to the tip of the dual cantilever. This

visco-elastic model is used to identify particulates, which are a little soft or a little hard. The lower spring and the lower damper, which are connected to the dual cantilever tip, are considered to be parallel to the springs and dampers in the dual cantilever. In this model, the particle that can be identified has to be a combination of spring and damper in parallel. This model has the advantages of both the elastic and the viscous model discussed in previous sections and has its own signature. The signature of this model is discussed briefly in Chapter 4. The concept used to identify the particles is the same as used in the viscous and the elastic models. The typical block diagram used for the visco-elastic model with spring/damper in parallel is shown in Figure 37(a).

In Figure 37(b), the dual cantilever tip is connected to the lower spring and the damper. The dual cantilever has springs k_1 and k_2 and dampers c_1 and c_2, respectively. Here c_3 and k_3 are the lower damper and the lower spring connected parallel to the main system. In this model, x_1 and x_2 are displacement of first mass and second mass respectively. A base motion with amplitude of y_0 and a driving frequency of ω excites the dual cantilever beam. Due to this base motion, the system vibrates. When the tip touches the lower system, which consists of a spring and a damper, response is produced. The response produced by the system can be linked to the properties of the particles in some way as explained in Chapter 4.

Some of the particles, which can be determined from this model, are DNA, tissues and cells. In this model, the stiffness matrix used to calculate the natural frequency is the same as the stiffness matrix discussed in the elastic model (Equation 63). The damper matrix for this model is the same as the damper matrix used for the viscous model (Equation 69). After knowing spring constants and frequencies of the beam from the

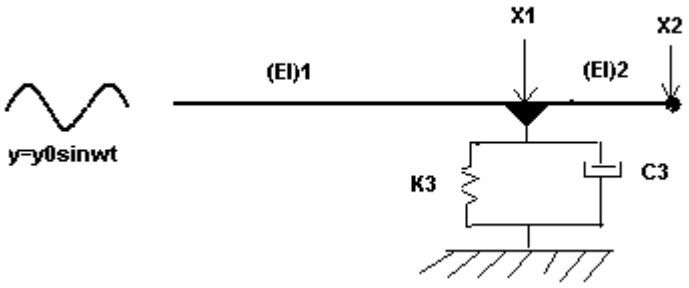

(a)

(b)

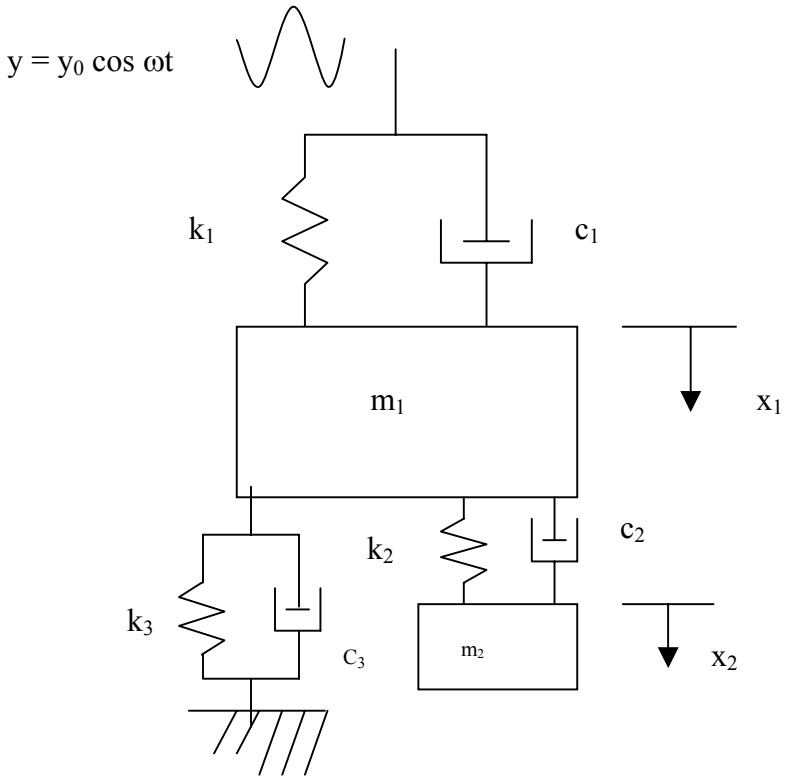

Figure 37: Voigt/Kelvin model. (a) Dual cantilever tip attached to the spring and the damper in parallel (b) Graphical representation of visco-elastic model

manufacturers, the effective masses for the dual cantilever are calculated. Using the stiffness matrix and the effective masses, the natural frequencies and the mode shape are determined. Modal mass matrix, modal stiffness matrix and modal damping matrix are calculated from mass matrix, stiffness matrix, damper constant matrix and modal matrix, respectively. After determining all of the above, the damper coefficient for the second mass is determined as discussed in earlier section (that is viscous model). The frequency response equations are given under the frequency response section in the dual cantilever model.

The response obtained from this model can be used to determine what type of particle on the surface and its corresponding physical properties. When the response obtained has a low amplitude ratio, then one can decide that the particle is soft and when there is a frequency shift, then it can be inferred that the particle is hard. These are the signatures expected from this model. The signature of this model is discussed briefly in Chapter 4 along with a parameter study.

In the parameter study the damper coefficient of the first mass is varied and the results are compared with the results obtained from this model. The frequency response for this model is obtained from the equations derived in section 3.1.2 for various values of k_3 and c_3. This is done to see how the frequency response varies corresponding to lower spring constant and lower damper constant values. By comparing this frequency response curve with the baseline, it will be easy to identify the particle.

EXAMPLE CALCULATION:

This model can be understood more clearly with some numerical examples than simply the mathematical model itself. The typical values for the dual cantilever taken are

already discussed in previous sections under example calculations. Therefore, taking some values for the lower spring constant and lower damper constant, the frequency responses are plotted and compared with the baseline frequency response for determining the signatures.

From Figure 38, when the lower spring has a spring constant of 10 N/m and lower damper has a damper constant of 0.00000005 N-s/m, the natural frequency is calculated as 207 kHz. When there is no spring connected to the tip of the dual cantilever, then the natural frequency is calculated as 193 kHz, so comparing this two we can say that as the spring constant increases the natural frequency shifts. Comparing with Figure 15 and Figure 38, we can see that the amplitude ratio when adding damper is less than the amplitude ratio in Figure 15. These things are seen in both the elastic model and the viscous model, where the natural frequency tends to move outwards and the amplitude of vibration is reduced respectively.

Comparing the plots obtained from adding a spring alone, i.e. Figure 20, and adding a spring and a damper, i.e. Figure 39, it is clear that as the lower damper constant value increases, the amplitude with which the masses vibrate is reduced and as lower spring constant increases the natural frequency tends to shift outwards. This will not be universally true, but in this model it is true.

3.5 VISCO – ELASTIC MODEL #2 - SPRING/DAMPER IN SERIES (MAXWELL MODEL)

This is the second visco-elastic model in this research. In the previous section we discussed the visco-elastic model in which the spring/damper are connected in parallel,

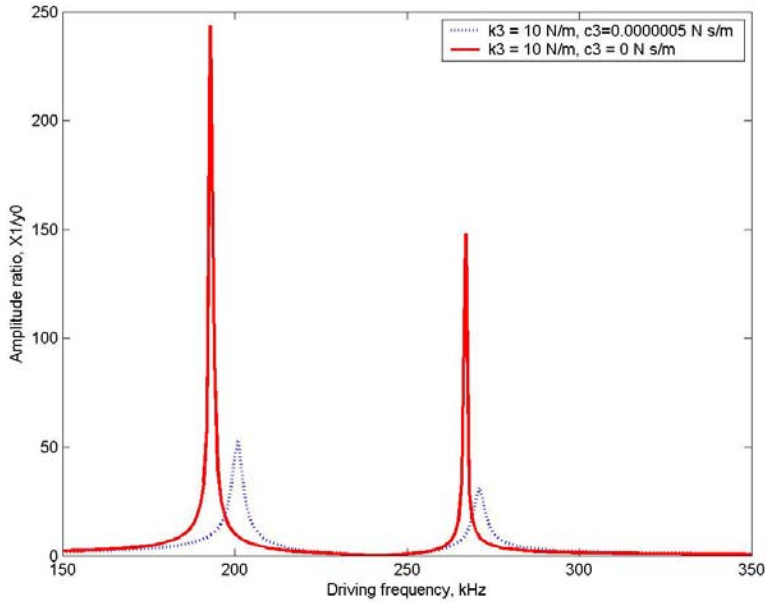

Figure 38: Frequency response for the first mass adding a lower spring k_3=10 N/m and damper constant c_3= 0.0000005 N-s/m

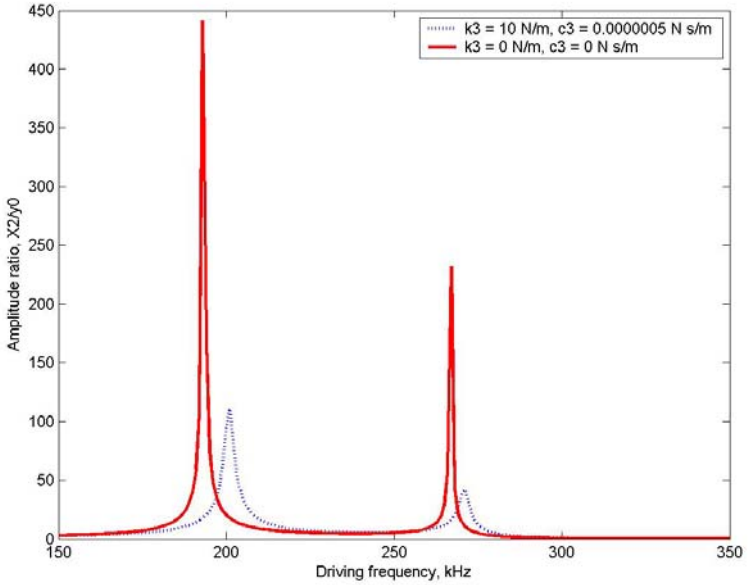

Figure 39: Frequency response for the second mass adding a lower spring k_3=10 N/m and damper constant c_3= 0.0000005 N-s/m

and in this section we are going to discuss the visco-elastic model in which the spring/damper are connected in series. In order to understand the physical nature of spring and damper connected in series, the visco-elastic model for the two-degree-of-freedom problem is done by building the classic single-degree-of-freedom model and then transferring it to the two-degree of freedom model.

A simple single-degree-of-freedom model is used to understand the concept of spring and dashpot in series. The simplest model is the one that has a mass connected to the spring and the damper in series. In this model, the mass is free to vibrate and no base motion is given. The next case will be a mass connected to the spring and the damper in series with the free end given a base motion. By studying the above two cases, we can understand how the spring and the damper behave when they are connected in series and when they are given any base motion. Using these models, a two-degree visco- elastic model with spring and damper connected in series is developed.

Concepts used in deriving the equation of motion for the two-degree model, when the spring and damper are connected in series, are derived from the two simple cases discussed above. This concept is different than the concept used for the dual cantilever model. All the equations derived here are based on the kinematics and dynamics of the model. The equation of motion derived is based on the free body diagram of the model and the forces acting on the body. The basic principle in deriving the equation of motion is to equate the external force and the applied force on the body.

In this model, the movement of the damper is also considered, and it is determined from the equation of motion of the system. The movement of the damper depends on the type of particle on the surface and on the exciting force between the tip and the particle.

When the particle is soft, then the movement of the damper is less, and when the particle is hard, then the movement will be greater.

3.5.1 SINGLE DEGREE OF FREEDOM WITH FREE END

This model is a classic example of single-degree of freedom with mass connected to the spring and the damper in series. The end where the mass is connected is free to vibrate. The simple single-degree model used to show how spring and damper work when they are connected in series is shown in Figure 40. In Figure 40, m is the mass of the system, k is the spring attached to the system and c is the damper. We can see from Figure 40, that the mass is connected to the spring and damper in series, and the mass is free to vibrate. Displacement of the spring is taken as x and the damper as u.

The equation of motion for this model is determined by considering the dynamics and kinematics of the system. The basic concept used in deriving the equation of motion, as mentioned earlier, is to equate applied force to the external force, which is best summarized by Newton's Law. In this model, the natural frequency is determined in a different way than in the other three models (elastic model, viscous model and visco-elastic model #1). In the other three models, the modal summation method is used to find the frequency response, but in this model, the response of the system is determined from the amplitude equation itself.

Imagine, at any instant, when the system is displaced through a distance x from the equilibrium position as shown in the Figure 40. The body has, at that instant, a velocity $\dot{x}$ in the downward direction and acceleration $\ddot{x}$ also in the downward direction. The

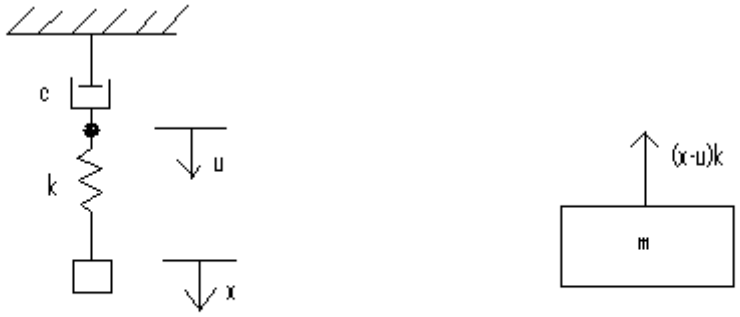

Figure 40: Single degree of freedom with free end and its free body diagram

damping resistance at any instant is equal to c $\dot{x}$, where $\dot{x}$ is the relative velocity between the piston and the cylinder of the damper.

The external forces acting on the body at this instant are

(i) The spring force kx acting in the upward direction, and

(ii) The damping force c $\dot{x}$ acting in the upward direction.

From the free body diagram shown in Figure 40, equating external force and applied force,

$$m\ddot{x} = -(x-u)k \tag{86}$$

or

$$m\ddot{x} + kx = uk \tag{87}$$

From kinematics, the force due to the displacement of the spring is equal to the force acting on the damper, so equating those two forces we get

$$(x-u)k = c\dot{u} \quad \text{(or)} \quad \frac{c}{k}\dot{u} + u = x \tag{88}$$

Combining equations (87) and (88)

$$m\ddot{x} = -c\dot{u} \tag{89}$$

Where $\ddot{x}$ is the second derivative of the displacement of the spring with respect to time or the acceleration of the mass, $\dot{x}$ is the first derivative of the displacement of the mass with respect to time or the velocity of the spring, and $\dot{u}$ is the first derivative of the displacement of the damper with respect to time. The mass of the system is m; k is the spring constant of the system, c is the damper constant of the system. Equations (88) and

(89) are the linear differential equations of the second order, and the initial solution is of the form

$$x = Xe^{st} \tag{90}$$

$$u = Ue^{st} \tag{91}$$

where s are the roots of the system.

Substituting for x and u in equations (88) and (89)

$$\begin{bmatrix} ms^2 & cs \\ -1 & \left(1+\frac{cs}{k}\right) \end{bmatrix} \begin{Bmatrix} X \\ U \end{Bmatrix} = \begin{Bmatrix} 0 \\ 0 \end{Bmatrix} \tag{92}$$

Equation (92) is called the amplitude equation of the single-degree of freedom model; it can be solved to get the roots.

$$\begin{vmatrix} ms^2 & cs \\ -1 & \left(1+\frac{cs}{k}\right) \end{vmatrix} = 0 \tag{93}$$

Equation (93) is called the characteristic equation and equating it to zero gives the roots of the equation, which is the natural frequency of the system. Substituting the roots in equation (92) the response for the system can be determined.

The relation between response of damper and response of the spring is

$$U = \frac{1}{\left(1+\frac{cs}{k}\right)} X \tag{94}$$

$$\alpha = \frac{1}{\left(1+\frac{cs}{k}\right)} \tag{95}$$

$$x(t) = X_1 e^{s_1 t} + X_2 e^{s_2 t} + X_3 e^{s_3 t} \tag{96}$$

$$u(t) = \alpha_1 X_1 e^{s_1 t} + \alpha_2 X_2 e^{s_2 t} + \alpha_3 X_3 e^{s_3 t} \tag{97}$$

The initial conditions are assumed to be

$$x(0) = X_0 \tag{98}$$

$$\dot{x}(0) = 0 \tag{99}$$

$$u(0) = 0 \tag{100}$$

where s_1, s_2, s_3 are roots of the characteristic equation, x (t) is the response of the system, u (t) is the displacement of the damper and α is the ratio between X and U. Then, applying the initial condition to equation (96) and (97), constants are determined and substituting this in the response equation, the total response is obtained.

The nature of the solution, and hence the equilibrium, depends on the roots s_1, s_2 and s_3 of the characteristic equation. If s_1, s_2 and s_3 are real and negative, then $e^{s_1 t}$, $e^{s_2 t}$ and $e^{s_3 t}$ reduce to zero as t tends to ∞, so the solution dies out as the time unfolds. If anyone of s_1 or s_2 or s_3 is real and positive, then the solution increases without bounds as t tends to ∞. If the roots s_1, s_2 and s_3 are complex, then they are complex conjugates. The nature of the solution depends upon the real part of the roots. Indeed, the solution can be expressed as the product of two factors, one corresponding to the real part of the exponents and the other corresponding to the imaginary parts. The factor corresponding to the real part plays the role of time-dependent amplitude, and the factors corresponding to the imaginary parts vary harmonically with time. If the real part is negative, then the time-dependent amplitude approaches zero as t tends to ∞, so that the solution represents a

decaying oscillation. If the real part is positive, then the time-dependent amplitude increases without bounds as t tends to ∞, so that the solution represents a divergent oscillation. If the real part is zero, in which case the roots are purely imaginary, the amplitude does not depend on time but is constant and the solution represents simple harmonic oscillation, which is bounded.

3.5.2 SINGLE DEGREE OF FREEDOM WITH BASE MOTION

In the previous section we saw how the single-degree of freedom model works when the spring and the damper are connected in series without any base motion. In this section, we are going to see how it works when a base motion is given. The principle, which is applied to derive the equations in single-degree of freedom with free end, is used in this model also. In this model, mass is attached to the spring and the damper in series as given in Figure 41. The free end is given a base motion with an amplitude of y_0 and a driving frequency of ω. Considering a classical spring-mass-dashpot system, where k is the stiffness of the spring, m is the mass of the body and c is the damper constant of the dashpot.

When the system is given a base motion and, at any instant, when the mass is displaced from the mean position through a distance x in the downward direction (positive direction of x), the external forces acting on the system are

(i) kx, in the upward direction.

(ii) $c\dot{x}$, in the upward direction.

(iii) $y_0 \sin\omega t$ in the downward direction.

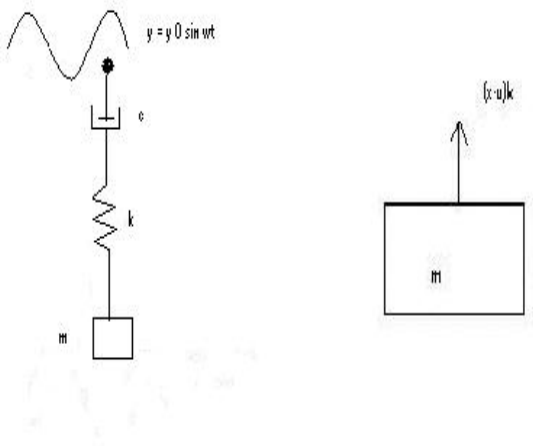

Figure 41: Single degree of freedom with base motion

Taking all these forces and using Newton's law of motion (that is equating applied force and external force), the differential equation for the system is derived. From the free body diagram shown in Figure 41, equating the applied force and external forces

$$m\ddot{x} = -(x-u)k \tag{101}$$

$$y = y_0 \sin \omega t \tag{102}$$

The force acting on the spring is equal to the force acting on the damper, so equating those two we get

$$(\dot{y}-\dot{u})c = (u-x)k \tag{103}$$

Let us assume the solution of the second order differential equation can be of the classical form

$$x = Xe^{i\omega t} \tag{104}$$

$$u = Ue^{i\omega t} \tag{105}$$

Substituting the initial solution for x and u equations (101) and (103), a matrix is obtained for the equation of motion, which can be solved directly to get the unknown displacement of the spring and the damper. Equation (101) and (103) are the two differential equations for the single degree model with base motion.

The matrix form of equation of motion is given by

$$\begin{bmatrix} -\omega^2 m + k & -k \\ k & -(\frac{ic}{k}\omega + 1) \end{bmatrix} \begin{Bmatrix} X \\ U \end{Bmatrix} = \begin{Bmatrix} 0 \\ -i\omega c y_0 \end{Bmatrix} \tag{106}$$

where y_0 is the amplitude with which the system vibrates, ω is the driving frequency, X is the complex response of the system and U is the complex response of the damper. Then substituting these back into the initial solution the real response for the system is determined.

3.5.3 TWO-DEGREE OF FREEDOM WITH BASE MOTION

In this section, the two-degree model of a dual cantilever with the spring and the damper connected in series to the tip of the dual cantilever is discussed. As we already discussed in previous sections, when there are two masses, spring and damper are connected in series, then the equation of motion for the system is obtained using free body diagram. Displacement of one mass is influenced by the other mass.

The mathematical formulation for an n-degree-of-freedom system consists of n simultaneous ordinary differential equations. Hence, the motion of one mass affects the motion of another. For a proper choice of coordinates, known as principal or natural coordinates, the system differential equations become independent of one another. The natural coordinates represent linear combinations of the actual displacements of the discrete mass and, conversely, the motion of the system can be regarded as a superposition of the natural coordinates. The differential equations for the natural coordinates posses the same structure those of single-degree-of-freedom systems.

The model for the proposed two-degree dual cantilever with spring and damper connected in series to the tip of the dual cantilever is shown in the Figure 42(a). The dual cantilever has stiffness k_1 and k_2, damper constants c_1 and c_2 respectively, k_3 is the stiffness of the lower spring, c_3 is the damper constant of lower spring. A base motion with amplitude of y_0 and a driving frequency of ω excites the dual cantilever. Due to

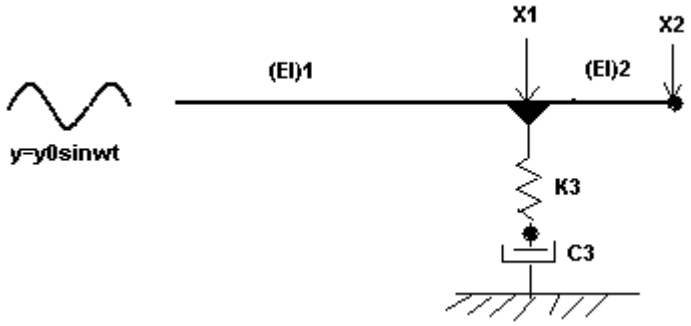

(a)

(b)

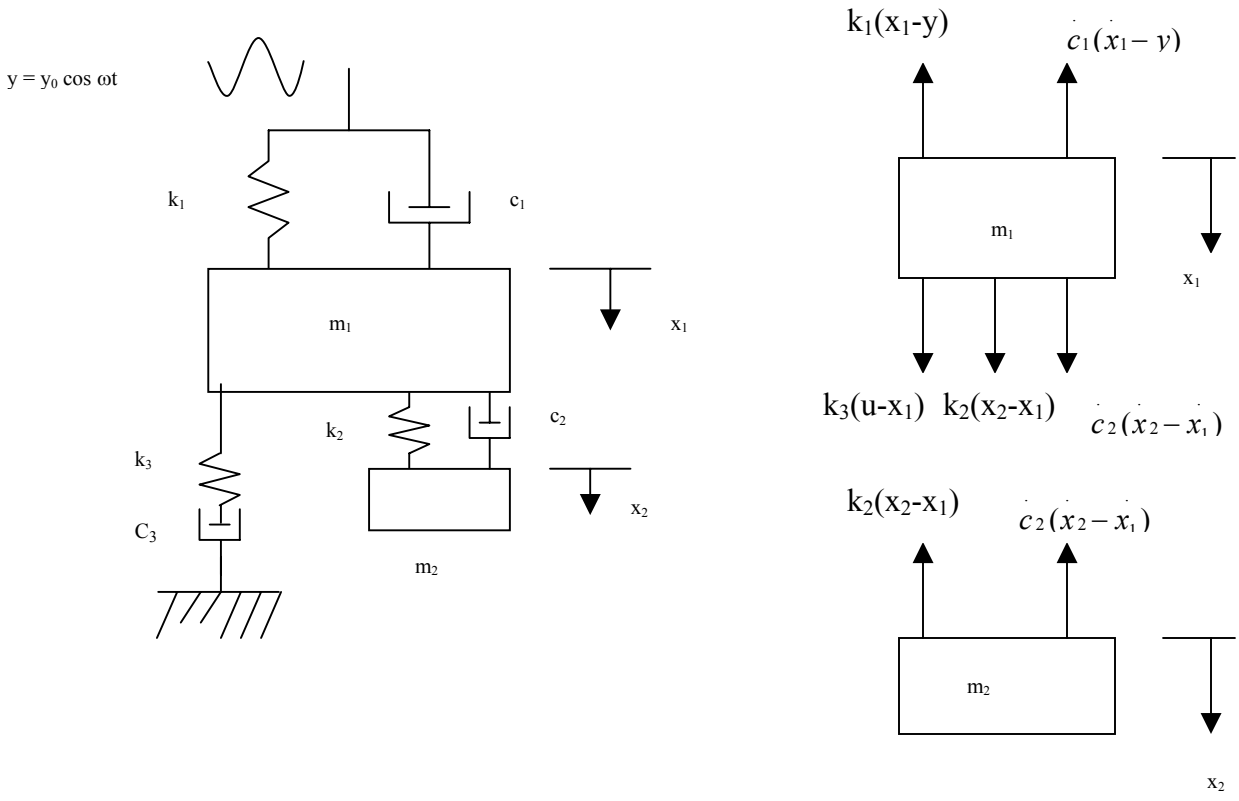

Figure 42: Maxwell model. (a) Dual cantilever tip attached with the spring and the damper in series (b) Graphical representation for the two-degree model with spring and dashpot in series.

excitation, the dual cantilever vibrates; the displacements of the masses are determined using the response equation. Here x_1 is the movement of mass 1, x_2 is displacement of mass 2 and u is displacement of lower damper. The free body diagram for this model is also shown in Figure 42(b) to get all the forces acting on the system. Equating the force acting on the body, equation of motion for the system to determine the natural frequency and frequency response is derived. Figure 42(b) represents the free body diagram for the two-degree dual cantilever with base motion. It shows the forces acting on mass m_1 and mass m_2 separately. The basic principle in deriving the equation of motion using free body diagram is to equate the applied force to external force. When the forces are equated, the equation obtained for first mass is given in equation (108) and for second mass in equation (110). In these two equations the external force is the acceleration force and the applied force are due to force spring and damper.

Natural vibration for a multi-degree-of –freedom system differ from that of a single-degree-of -freedom system in that for multi-degree-of-freedom systems natural vibration implies a certain displacement configuration, or shape, assumed by the whole system during motion. Moreover, a multi-degree-of-freedom system does not possess only one natural configuration but have a finite number of natural configurations known as natural modes of vibration. Depending on the initial excitation, the system can vibrate in any linear combination of these modes. To each mode corresponds a unique frequency, referred to as a natural frequency, so that there are as many natural frequencies as there are natural modes.

By equating the external and applied force for the system the three equation obtained are given below. Equation (109) is obtained by equating force acting on the spring to the force acting on the damper.

$$y = y_0 \sin\omega t \tag{107}$$

$$m_1 \ddot{x}_1 = c_3 \dot{u} + k_2(x_2 - x_1) + c_2(\dot{x}_2 - \dot{x}_1) - k_1(x_1 - y_0) - c_1(\dot{x}_1 - \dot{y}_0) \tag{108}$$

$$\frac{c_3 \dot{u}}{k_3} + u = x_1 \tag{109}$$

$$m_2 \ddot{x}_2 = k_2(x_2 - x_1) + c_2(\dot{x}_2 - \dot{x}_1) \tag{110}$$

Let us assume the initial solution to be of classical form

$$x_1 = X_1 e^{i\omega t} \tag{111}$$

$$x_2 = X_2 e^{i\omega t} \tag{112}$$

$$u = U e^{i\omega t} \tag{113}$$

Substituting the initial solution for x_1, x_2 and u in (108),(109),(110) and solving the equation (114) gives the unknowns of the matrix, in this case they are the displacement of first, second mass and damper.

$$\begin{bmatrix} -m_1\omega^2 + k_2 + k_1 + i\omega(c_1 + c_2) & -i\omega c_2 - k_2 & -ic_3\omega \\ -k_2 - ic_2\omega & -m_2\omega^2 + k_2 + ic_2\omega & 0 \\ -1 & 0 & \frac{ic_3\omega}{k_3} + 1 \end{bmatrix} \begin{Bmatrix} X_1 \\ X_2 \\ U \end{Bmatrix} = \begin{Bmatrix} k_1 y_0 + ic_1 y_0 \omega \\ 0 \\ 0 \end{Bmatrix} \tag{114}$$

The solution obtained from the above equation is the complex solution, to get the real response for the model we have to substitute the complex solution back to the initial solutions.

The Maxwell model shown in (Figure 43(a)) is similar to the visco-elastic model #2 shown in Figure 42. In this maxwell model, the spring with modulus g and damper with viscosity η are connected in series. The creep response and stress relaxation for this maxwell model are shown in Figure 43 (b). Where e is the strain, s is the stress acting, s_0 is the initial stress and e_0 is the initial strain. As seen from the plot, shown in Figure 43 (b), the creep is steep. When the stress is removed, the spring instantly relaxes but the damper remains extended. This model exhibits permanent deformation. A purely viscous material such as pitch, for example, may be thought of as a maxwell material. Maxwell model is fluid-like if the viscosity small and solid-like if it is large.

3.6 VISCO- ELASTIC MODEL # 3 - SPRING/DAMPER IN SERIES/PARALLEL (STANDARD SOLID MODEL)

This is the third visco-elastic model discussed in this research. This model is a slight modification of the second visco-elastic model. In this model we are not going to develop mathematical model for single degree of freedom, instead we are directly building the two degree freedom model using the concepts from previous section. The way of analyzing this model is to form a concept from which, the properties of the particulates can be identified.

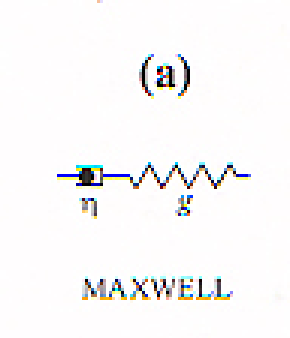

(b)

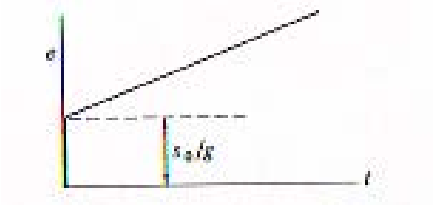

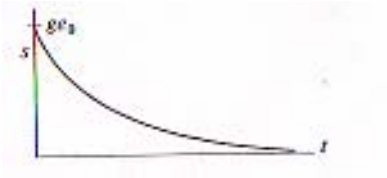

Figure 43: Maxwell model. (a) Maxwell model (b) Creep response and stress relaxation

3.6.1 TWO DEGREE OF FREEDOM MODEL

The block diagram for the third viso-elastic model is shown in Figure 44 (a). In the Figure 44 (b), k_3 and k_4 are the two springs attached to the tip of the dual cantilever, and c_3 is the damper. We can see from the figure, the spring k_3 is connected in series with the spring k_4 and damper c_3, which are connected in parallel. The displacement of mass 1 is x_1 and mass 2 is x_2 and displacement of spring k_4 and c_3 is taken as u. In this model we assume that k_4 is some proportional of k_3

Say $k_4 = \alpha\, k_3$

In this way, when α is zero then this model becomes similar to the visco-elastic model #2. From the free body diagram given in Figure 44(b), the forces acting on the body can be easily determined. Equating the external force to the forces due to spring and damper, we get the equation (116) and (119). Those two equations are for the first mass and the second mass respectively.

$$y = y_0 \sin \omega t \tag{115}$$

$$m_1 \ddot{x_1} = -k_1(x_1 - y_0) - c_1(\dot{x_1} - y_0) + k_2(x_2 - x_1) + c_2(\dot{x_2} - \dot{x_1}) + k_3(u - x_1) \tag{116}$$

Forces due to spring is equal to the force acting on the damper, so equating those two

$$k_3(x - u) = k_4 u + c_3 \dot{u} \tag{117}$$

or

$$\frac{c_3}{k_3}\dot{u} + \left(\frac{k_4 + k_3}{k_3}\right)u = x_1 \tag{118}$$

$$m_2 \ddot{x_2} = -k_2(x_1 - x_2) - c_2(\dot{x_1} - \dot{x_2}) \tag{119}$$

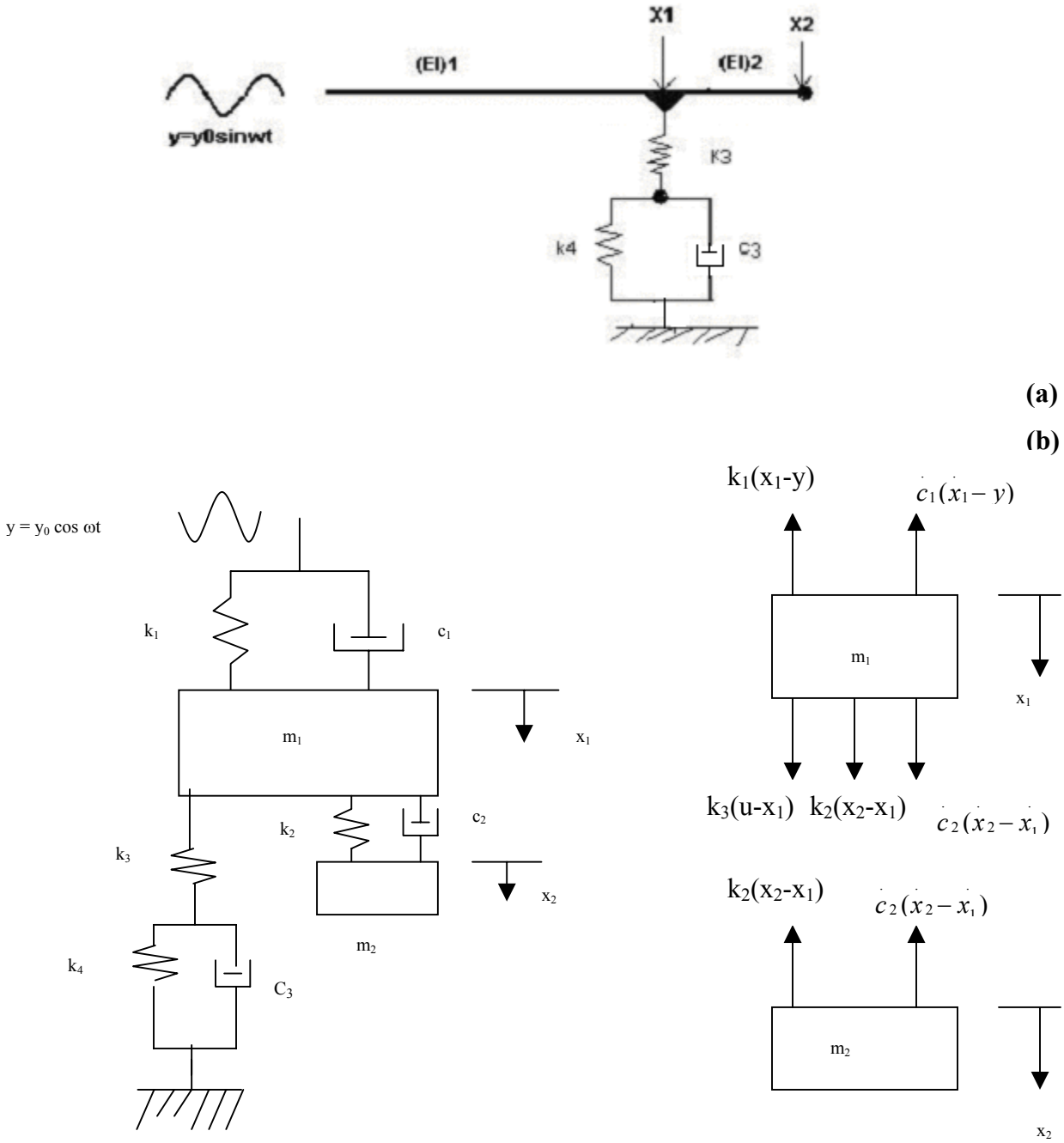

Figure 44: Standard solid model. (a) Second viscous model for two degree of freedom (b) Free body diagram for the two-degree freedom model

Equation (116), (118) and (119) are the three differential equations to determine the unknowns. Now, assuming an initial solution of the form

$$x_1 = X_1 e^{ist} \tag{120}$$

$$x_2 = X_2 e^{ist} \tag{121}$$

$$u = U e^{ist} \tag{122}$$

Substituting the initial solution in the equations (116)(118) and (119), and writing them in a matrix form

$$\begin{bmatrix} -m_1 s^2 + i(c_2 + c_1)s + (k_2 + k_1 + k_3) & -ic_2 s - k_2 & -k_3 \\ -ic_2 s - k_2 & -m_2 s^2 + ic_2 s + k_2 & 0 \\ -1 & 0 & i\frac{c_3}{k_3}s + \left(\frac{k_4}{k_3} + 1\right) \end{bmatrix} \begin{Bmatrix} X_1 \\ X_2 \\ U \end{Bmatrix} = \begin{Bmatrix} k_1 y_0 + c_1 \omega y_0 \\ 0 \\ 0 \end{Bmatrix} \tag{123}$$

Equation (123) is called the amplitude equation. Substituting the values for mass, spring constant and damper constants the response of the system can be determined and plotted. This model is similar to standard solid model or delayed elasticity model where a spring g_1 is connected in series with a spring g_2 and damper η in parallel as shown in Figure 45 (a) and (c). Figure 45 (b) gives the creep and stress response of standard solid model.

This model gives an overall better approximation to the response of polymers. If the loading varies cyclically at frequency ω as in dynamical mechanical testing, the response is characterized by a complex modulus and phase lag. This model has properties similar to a styrene-butadiene random co-polymer with glass transition temperature near room temperature [24,32]. At high frequency, the damper cannot respond and the system responds like an elastic spring with modulus. At low frequency, the damper can fully relax and the system again responds elastically but with modulus. These values are

(a)

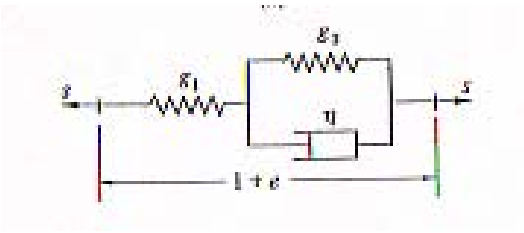

(b)

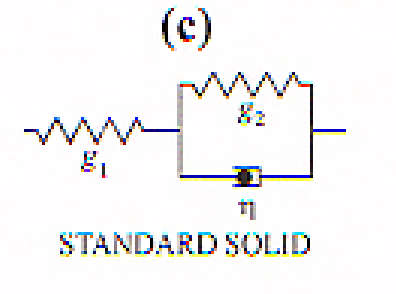

Figure 45: Standard solid model. (a) Standard solid model (b) Creep and stress relaxation response (c) Another way of representing standard solid model

similar to those measured experimentally for 1,2-polybutadiene freshly cast from toluene solution [20,21]. The standard solid model is more representative of contacts to polymeric solids and exhibits behavior intermediate between the maxwell and Voigt/kelvin models. The Voigt/Kelvin model has spring g_2 connected to damper η in parallel.

CHAPTER 4

DISCUSSION OF RESULTS

In this chapter we will discuss the dynamic response of each of the basic mathematical models explained in Chapter 3. Each model will be discussed in terms of specific response and signatures that may be useful in describing the physical properties of the particulates later. Results obtained for each model in Chapter 3 are discussed in this chapter along with their signatures and how they are used to identify the particulates on the surface.

4.1 ELASTIC MODEL

This is the first model discussed in the research. The block diagram for this model is shown in Figure 19. As shown in Figure 19, the tip of the dual cantilever is connected to a spring. If the particle on the surface that has to be identified is a combination of spring, then this model is applied. The signature expected from this model will be a shift in natural frequencies. The spring connected to the tip of the dual cantilever is parallel to the other springs (k_1 and k_2). Therefore, the lower spring k_3 increases the total spring force acting on the tip of the dual cantilever, hence the natural frequencies increases. When there is a shift in natural frequencies then one can conclude that the particle on the surface is hard. Depends on how much the shift in natural frequencies we can say how hard the particles are. In the mathematical model for the elastic model, we have discussed how this model works with some numerical examples. Also, a plot is drawn between different values of lower spring constant and change in

natural frequencies. These plots are shown in Figure 46 and Figure 47; from these figures we can see clearly that, as the lower spring constant increases the natural frequency also increases.

When the lower spring constant is zero, then the natural frequencies are same as the natural frequencies in the case of dual cantilever model discussed in 3.1 sections. But when the lower spring has any value, then the natural frequencies increases. It is seen from Figures 46 and 47 that, the change in natural frequencies is linear to the change of amplitude ratio. In the Figures 46 and 47, the solid line shows the natural frequency when the lower spring is connected to the tip where as the dotted line represents the natural frequency of dual cantilever when the tip is not connected to the lower spring.

In this model, the shift in natural frequencies can be linked in some way to the hardness of the particle from which we can determine what type of particle is on the surface. The particles, which can be identified by this model, are biological (DNA), engineering (Steel, Alloy, Aluminum etc.,). Each particle will be having its own stiffness, so when the response obtained from the elastic model is compared with the baseline frequency response we can determine the frequency shift. Based on the frequency shift, the spring constant can be determined from Figures 46 and 47. A table can be drawn for various particles and their corresponding stiffness, so we can determine the type of particle and their physical properties from that table, using the stiffness determined from the frequency response obtained form this model.

Here is an example application for the elastic model with some values for young's modulus and size of particle. Stiffness can be determined from the equation (124) given

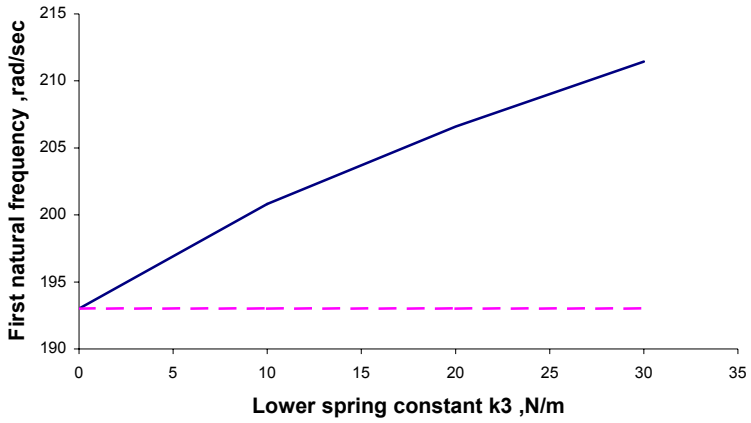

Figure 46: Change in first natural frequency versus lower spring constant

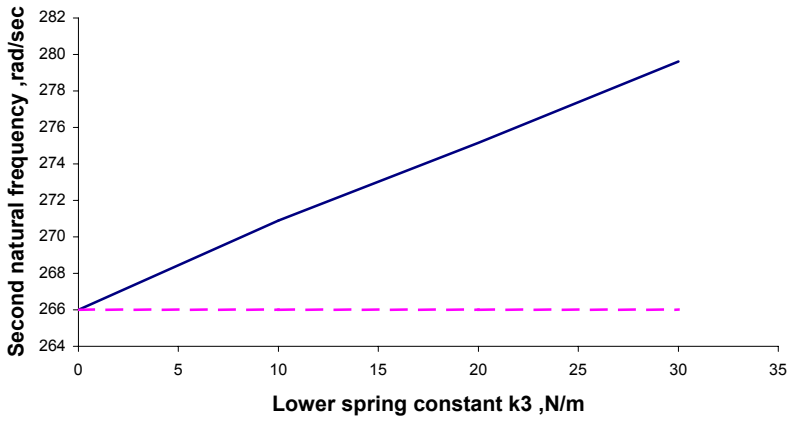

Figure 47: Change in second natural frequency versus lower spring constant

Table 5: Variation in stiffness due to size of the particle

Size	L in nm	K in nN/nm
10	10	2000
20	10	8000
30	10	12000

as.

$$k = \frac{EA}{L} \tag{124}$$

where E is young's modulus – it depends on type of material; for steel= 200 nN/(nm)^2, A is the area of the particle and L is the length of the particle. For example, consider a cubical steel particle of size say 10nm x 10nm x10nm on the surface, then the stiffness of the particle is determined as 2000 nN/nm. As the size varies stiffness also varies, it can be seen in Table 5.

From Table 5, one can say how the size of the particle can change the stiffness of the particle. The frequency response determined from the elastic model is compared with the baseline frequency response; the shift in natural frequencies can be determined. Using the shift in natural frequencies, we can determine the lower spring constant from Figures 46 and 47. After knowing the lower spring constant, then the type of the particle can be easily determined. In this model the particle on the surface does not have any damping (that is the particle is being considered as hard).

The mode shapes for the various values of lower spring constants are given in

Figures 48- 52. Mode shapes for various values of lower spring constants are drawn to see how it varies with lower spring constant. It can be seen from Figures 48-52 that, as the lower spring constant increases then the second mode decreases and the first mode increases steeply.

In this section, a parameter study is done by varying the damping coefficient for the first mass. First it is changed from 0.0012 to 0.002 and then to 0.005. Frequency response for various damper coefficient and various lower spring constant values are plotted against the driving frequency. Figures 53-58 gives the frequency responses for various damper coefficient values of the first mass

Figures 57 and 58 represents the frequency response of the first mass and the second mass of the elastic model, connected to a lower spring with a spring constant of 30 N/m and damper coefficient for the first mass of 0.0012. From Figure 57, when the damping factor is 0.0012, the amplitude ratio for the first mass is around 80 at the first natural frequency, where as the amplitude ratio for the first mass from Figure 53 when the damping coefficient for the first mass of 0.002 at the first natural frequency is around 50. In Figure 58 for the second mass, the amplitude ratio at first natural frequency when the damping factor for the first mass is 0.0012 is approximately 160, and when damping factor is 0.002, it is around 125. Similarly, when the damping factor for the first mass is still increased from 0.002 to 0.005 the amplitude ratios at first natural frequency points are 20 and 45 for the first and the second mass respectively. From this comparison we can infer that, as the damper coefficient for the first mass increases the amplitude ratio for both masses decreases.

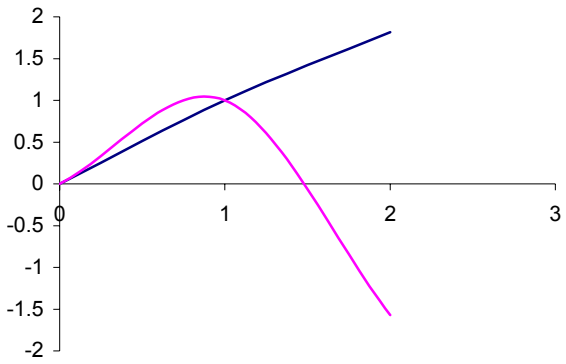

Figure 48: Mode shape when lower spring constant k_3 =0 N/m

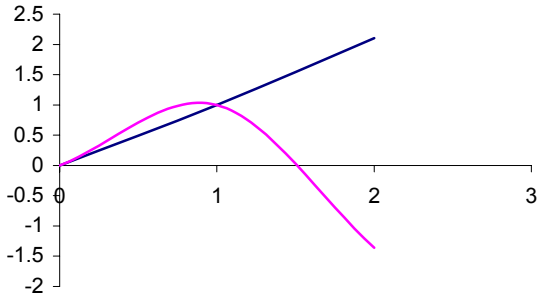

Figure 49: Mode shape when lower spring constant k_3 =10 N/m

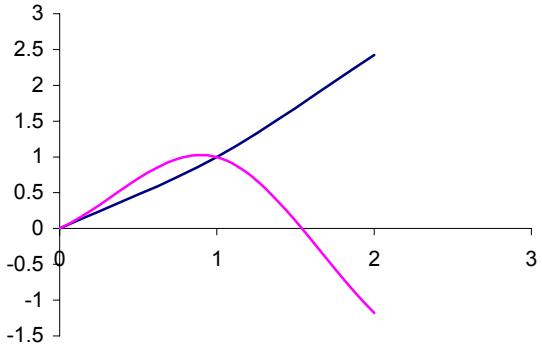

Figure 50: Mode shape when lower spring constant k_3= 20 N/m

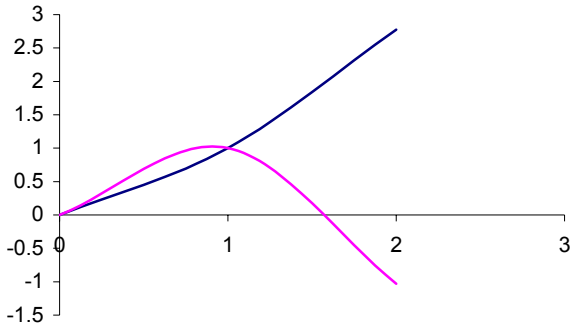

Figure 51: Mode shape when lower spring constant k_3=30 N/m

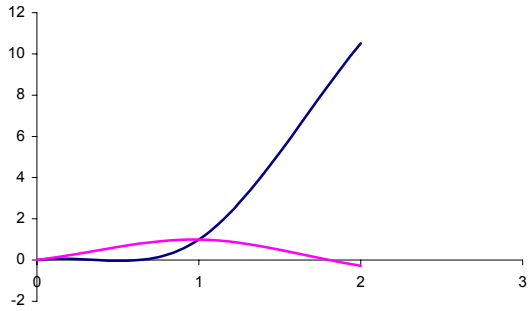

Figure 52: Mode shape when lower spring constant k_3= 200 N/m

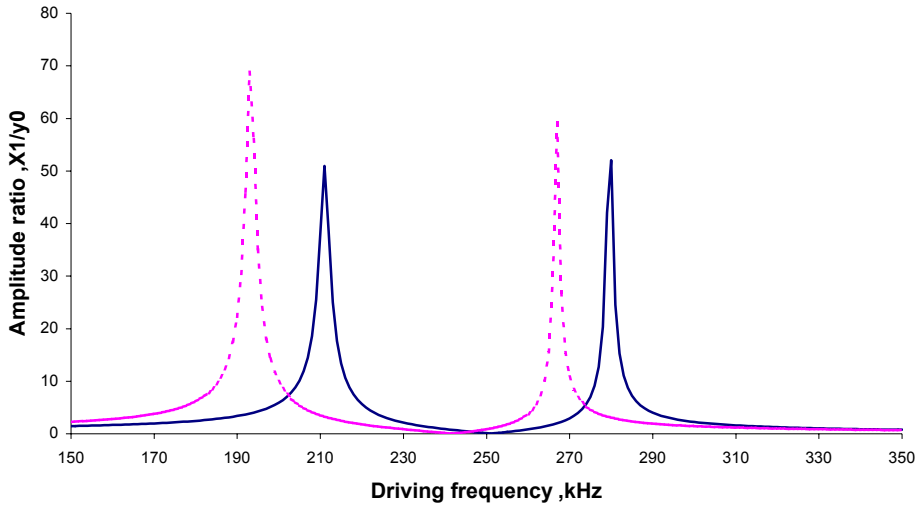

Figure 53: Frequency response for the first mass when lower spring constant k_3 = 30 N/m and damper coefficient for first mass = 0.002

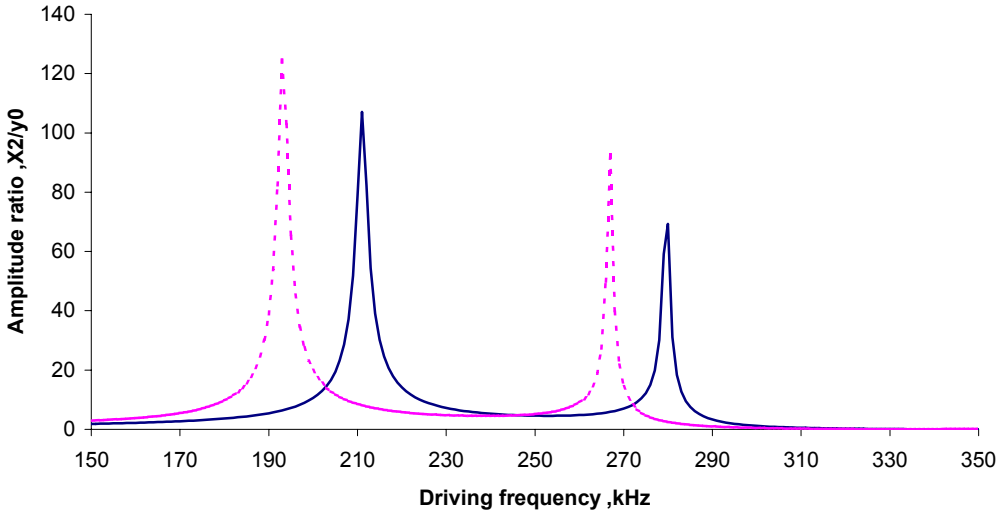

Figure 54: Frequency response for the second mass when lower spring constant k_3 = 30 N/m and damper coefficient for first mass = 0.002
_____with k_3 =30 N/m and ξ_1=0.002;-------- base line with k_3 = 0 N/m and ξ_1 =0.0012

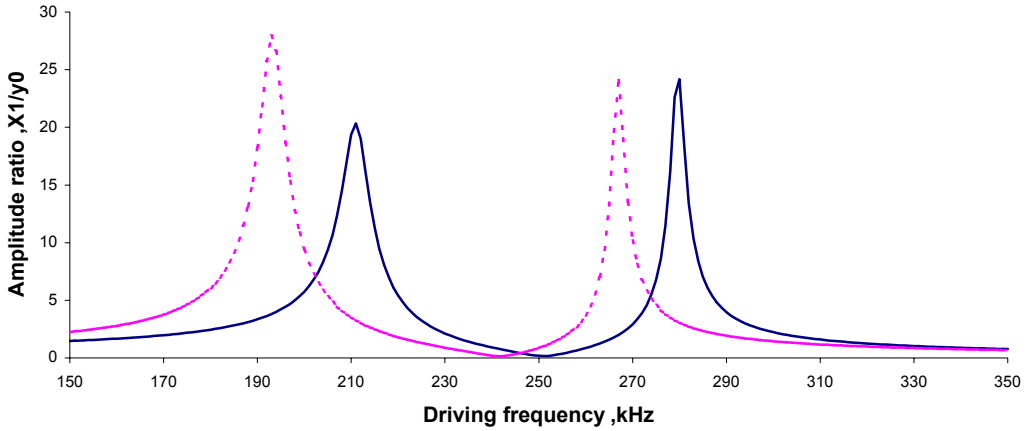

Figure 55: Frequency response for the first mass when lower spring constant k_3 = 30 N/m and damper coefficient for first mass = 0.005

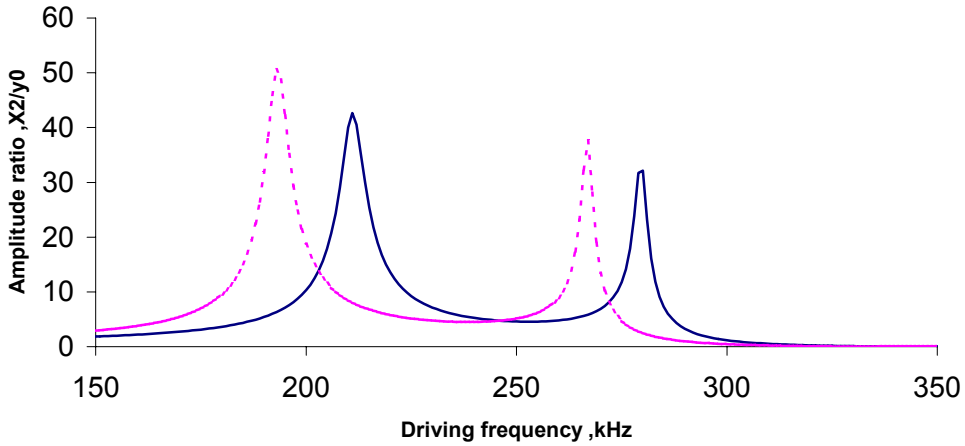

Figure 56: Frequency response for the second mass when lower spring constant k_3 = 30 N/m and damper coefficient for first mass = 0.005
_____ with k_3 =30 N/m and ξ_1=0.005; ------ base line with k_3 = 0 N/m and ξ_1 =0.0012

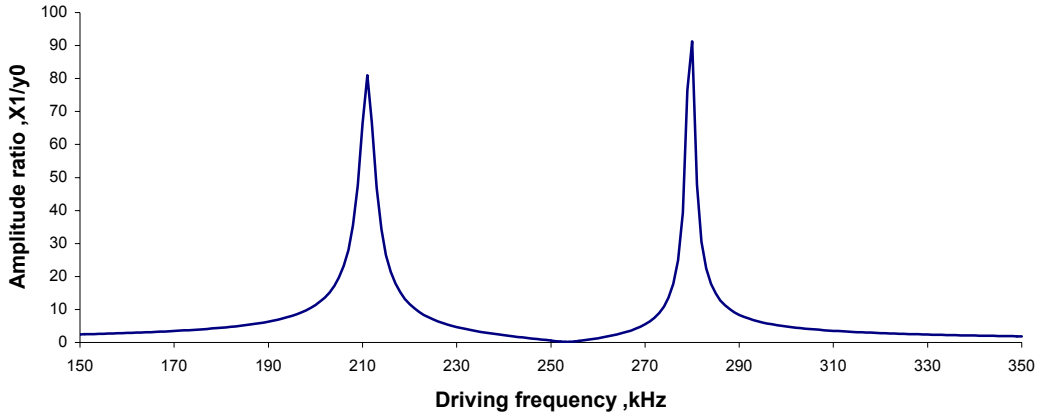

Figure 57: Frequency response for the first mass when lower spring constant k_3 = 30 N/m and damper coefficient for first mass = 0.0012

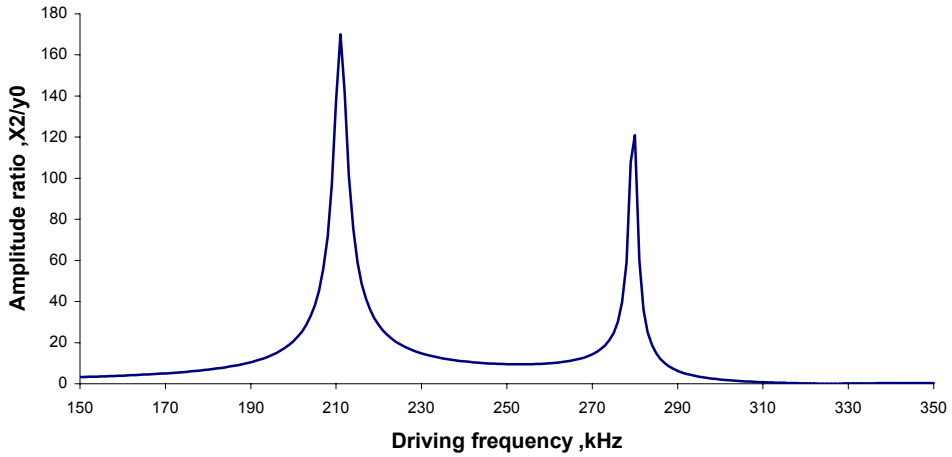

Figure 58: Frequency response for the second mass when lower spring constant k_3 = 30 N/m and damper coefficient for first mass = 0.0012

4.2 VISCOUS MODEL

This is the second model discussed in this research. The block diagram for the viscous model is shown in Figure 26. As seen in Figure 26, the tip of the dual cantilever is connected to a damper. In this case, the particle is considered to be a combination of damper. The lower damper connected to the tip of the dual cantilever is parallel to the other dampers (c_1 and c_2) of the dual cantilever. Therefore, the damping force acting on the tip of the dual cantilever will be now the addition of the damper force due to lower damper and damper force due to the first mass.

The expected signature from this model is, change in the amplitude ratio. The frequency response obtained from this model is compared with the frequency response obtained from the dual cantilever when the tip is not connected to any spring or damper. Comparing these two frequency responses, if the amplitude ratio of the viscous model is lesser then the amplitude ratio of the dual cantilever model, then the particle is said to be soft. Depends on the change in amplitude ratio, the damper constant of the particle can be interpreted. Plots can be drawn between various values of lower damper constants and the change in amplitude ratio for the first mass and the second mass. These plots are shown in Figures 59 and 60. In both the Figures, as the lower damper constant value increases, the amplitude ratio decreases. When a damper is connected to the tip of the dual cantilever, and if it has some damping constant value, then the amplitude ratio will differ from the baseline model. So this change in amplitude ratio can be linked in some way to the mechanical properties of the particulates.

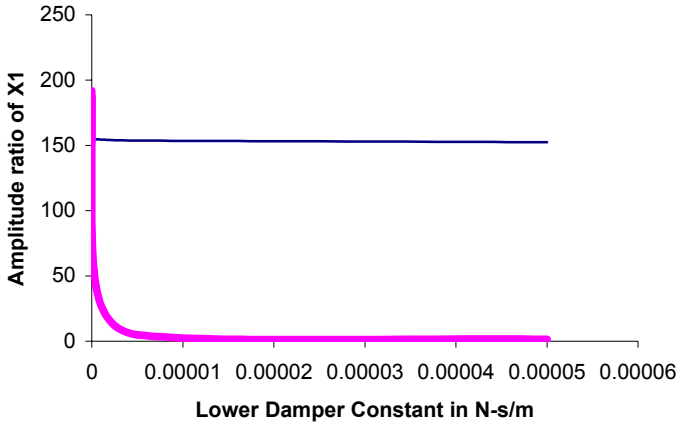

Figure 59: Change in amplitude ratio for first mass versus lower damper constant

_____ Baseline with c_3 = 0 N-s/m; _____ with c_3

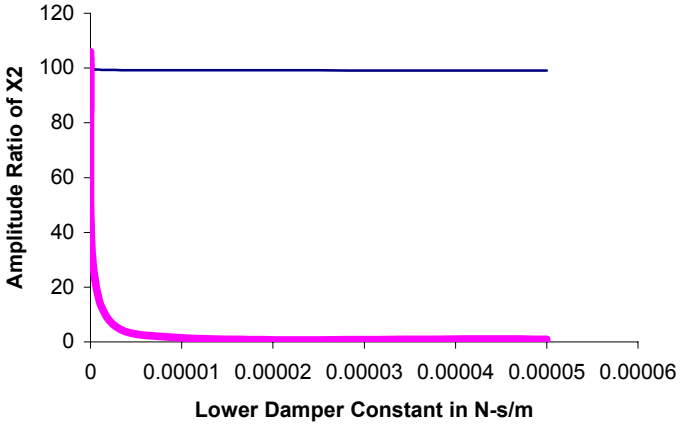

Figure 60: Change in amplitude ratio for second mass versus lower damper constant

_____ Baseline with c_3 = 0 N-s/m; _____ with c_3

When there is no damper attached to the tip of the dual cantilever, the frequency response for this case is shown in Figure 61 and when the tip is attached to a damper with damper constant of 0.000000005 N-s/m, then the frequency response is shown in Figure 62. By comparing these two plots, it is clearly seen that when there is no damper, then the amplitude ratio is little higher than 100. But when we add a damper, then the amplitude ratio is less than 100. These plots can be later used to compare with the baseline model to determine the damper constant of the particles on the surface.

Parameter Study:

In this case, we are varying the damping coefficient for the first mass and recording the frequency response. Therefore, the damping coefficient for the second mass will also be changing for each value of the damper coefficient for the first mass. Plots are obtained for different damping coefficient and are shown in Figures 63-70. From these Figures, it is clear that, as the damping factor increases the amplitude ratio tends to decrease and become low when it is high. Figures 69 and 70 are the frequency response for the first and the second mass when the damping factor is 0.0012. It is seen from the figures, that the amplitude ratio at the first natural frequency is around 110 when the damping factor is 0.0012, it is very low when the damping factor is 0.1, it is around 20 when the damping factor is 0.01 and it is around 105 when it is 0.001. Same way the amplitude ratio for X_2 also changes as the damping factor increases.

4.3 VISCO-ELASTIC MODEL #1- SPRING/DAMPER IN PARALLEL (VOIGT/KELVIN MODEL)

We have already discussed the signatures of the elastic model and the viscous model in the previous sections. The signature of this model is going to be similar to both the

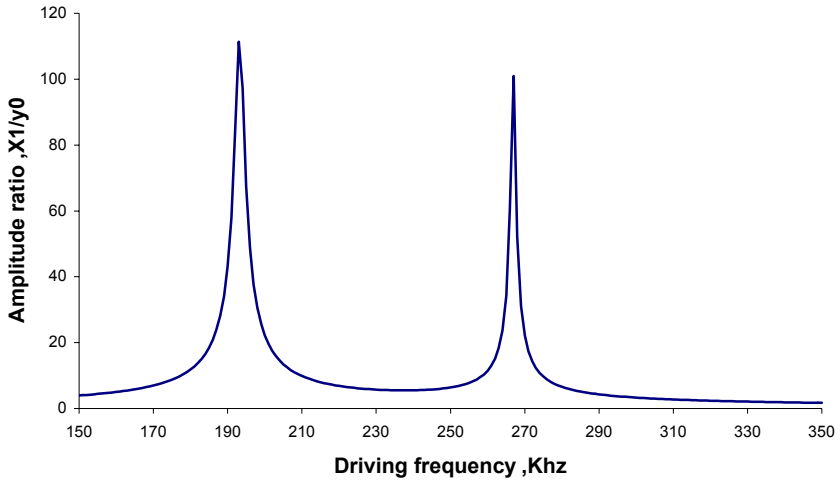

Figure 61: Frequency response for first mass when the tip is not connected to damper.

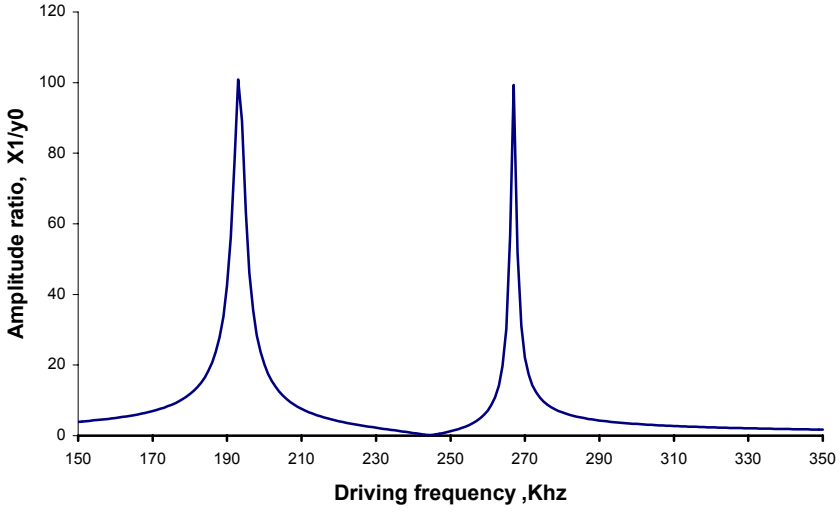

Figure 62: Frequency response for the first mass when the tip is connected to a lower damper c_3 =0.00000005 N-s/m

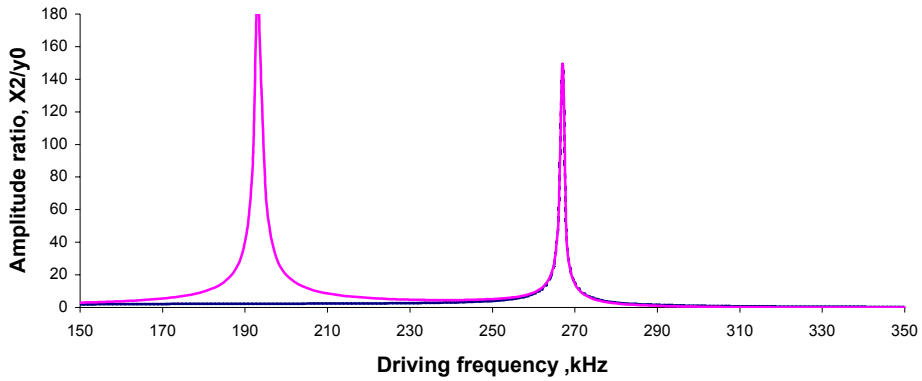

Figure 63: Frequency response for the first mass with damper constant c_3 = 0.00000005 N-s/m and damper coefficient for first mass = 0.1

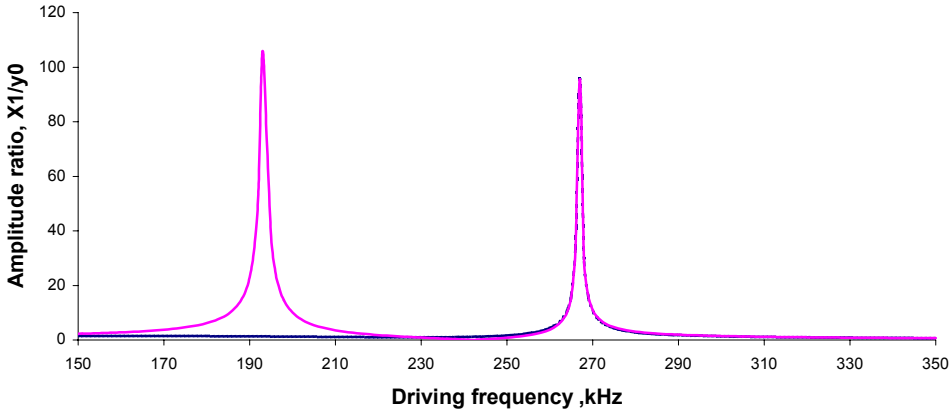

Figure 64: Frequency response for the second mass with damper constant c_3 = 0.00000005 N-s/m and damper coefficient for first mass = 0.1

------ with c_3 =0.00000005 N-s/m and ξ_1 =0.1;

_____ with c_3 = 0 N-s/m and ξ_1=0.0012

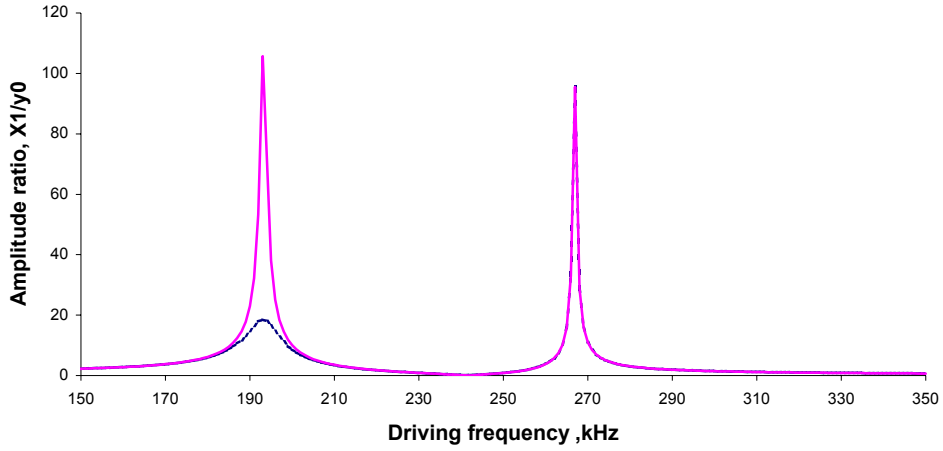

Figure 65: Frequency response for the first mass with damper constant c_3 =0.00000005 N-s/m and damper coefficient for first mass = 0.01

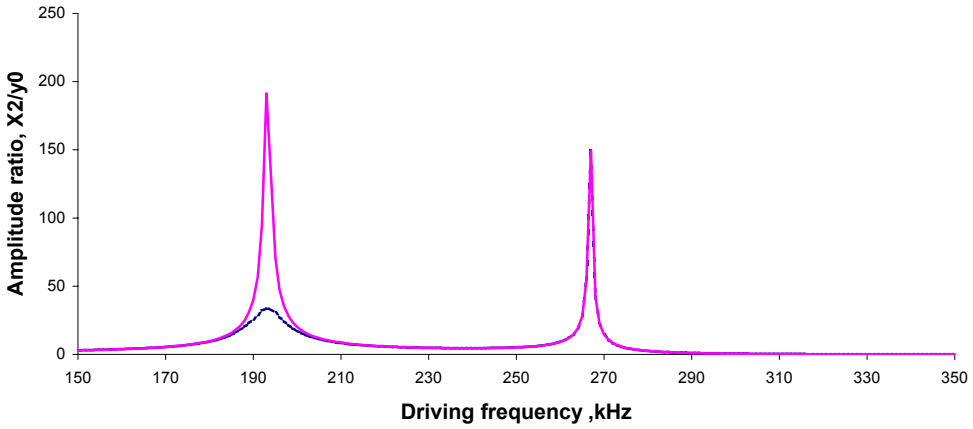

Figure 66: Frequency response for the second mass with damper constant c_3=0.00000005 N-s/m and damper coefficient for first mass = 0.01

------ with c_3 =0.00000005 N-s/m and ξ_1 =0.01;

_____ with c_3 = 0 N-s/m and ξ_1=0.0012

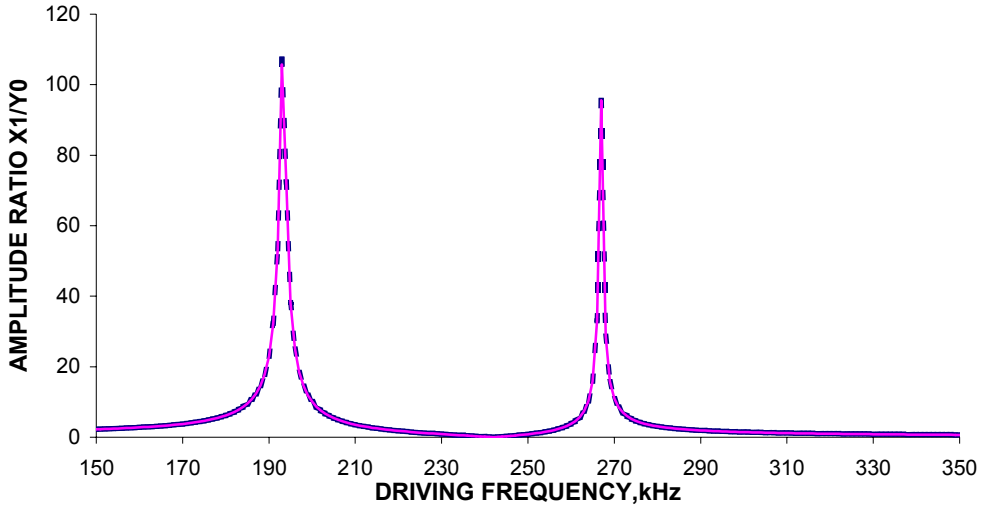

Figure 67: Frequency response for the first mass with damper constant c_3 = 0.00000005 N-s/m and damper coefficient for first mass = 0.001

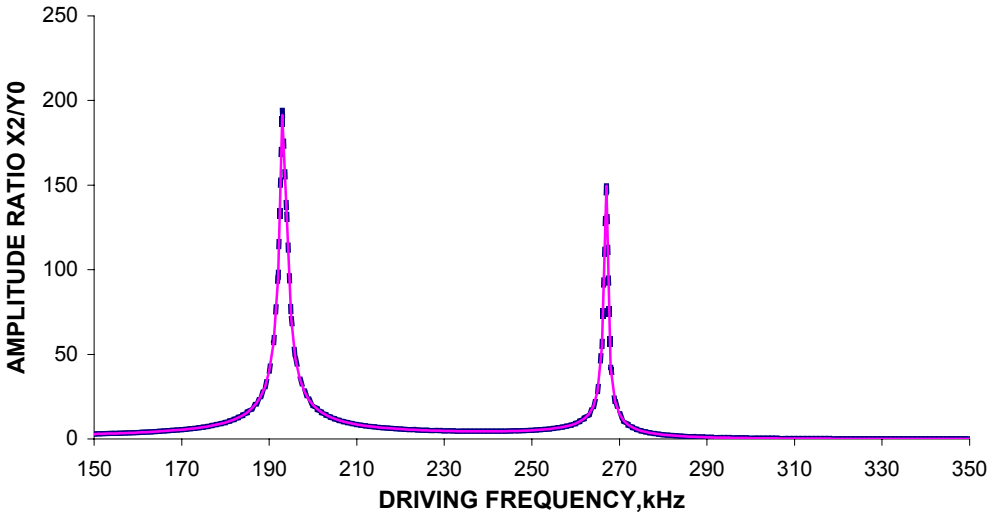

Figure 68: Frequency response for the second mass with damper constant c_3 = 0.00000005 N-s/m and damper coefficient for first mass = 0.001

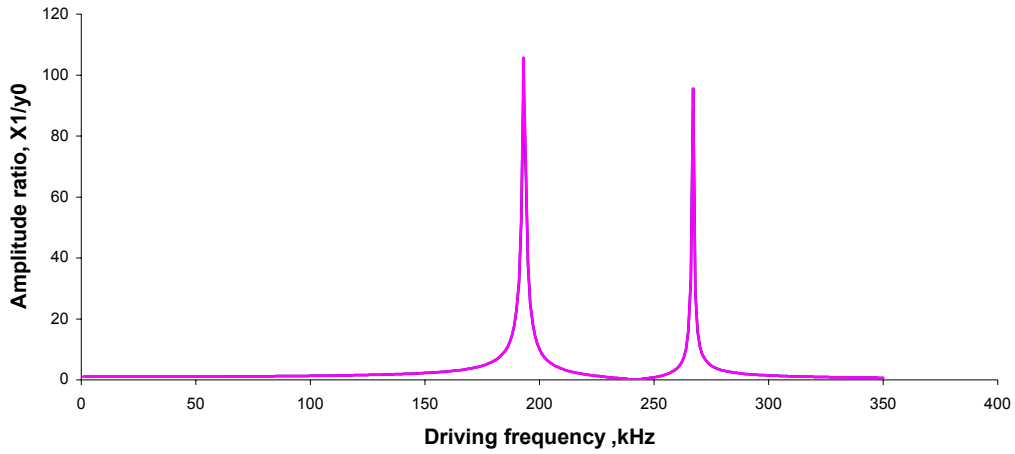

Figure 69: Frequency response for the first mass with damper constant c_3 =0.00000005 N-s/m and damper coefficient for first mass =0.0012

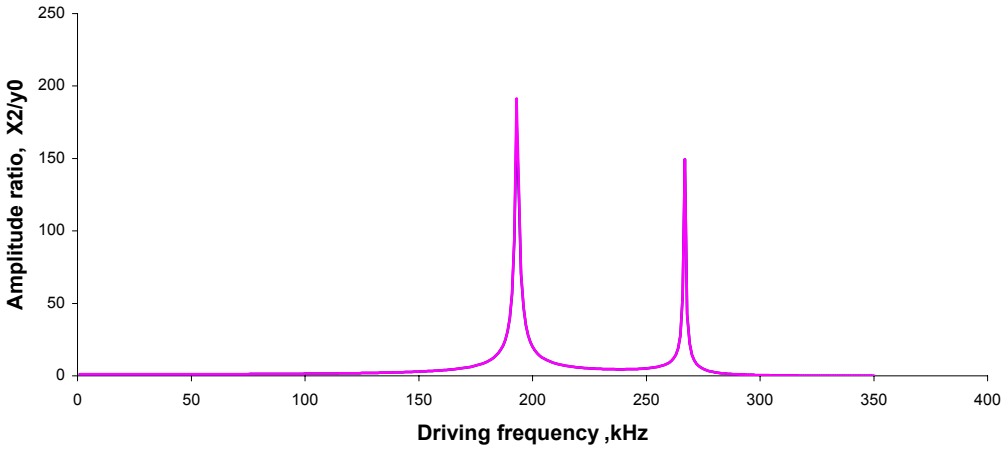

Figure 70: Frequency response for the second mass with damper constant c_3 = 0.00000005 N-s/m and damper coefficient for first mass = 0.0012

elastic and the viscous models. In the mathematical model, the frequency responses are determined for some numerical examples. Some of the particles that can be identified from this model are DNA, tissues and cell. The particle, which has to be identified on the surface, is considered to be a combination of spring and damper as shown in the Figure 37. If the particle has spring and damper in parallel, then this model can be applied to identify the particle on the surface. This model has the advantage of both the elastic and the viscous model. We can identify both the soft and the hard particles on the surface. As mentioned earlier, depends on the shift in the natural frequencies and the change in amplitude ratio we can determine the physical properties and identify the particles on the surface.

A parameter study is be done by varying the values of lower spring constant, damper constant values and damper coefficient for first mass. This study can reveal how some of the physical properties of the particles can be determined from the frequency response. For this initial study finding the physical properties of the particle is beyond scope.

4.4 VISCO-ELASTIC MODEL #2 - SPRING/DAMPER IN SERIES (MAXWELL MODEL) (SEE FIGURE 42)

This is the second visco-elastic model discussed in this research. As shown in Figure 42, the tip of the dual cantilever is connected to a spring and a damper in series. In the previous models (elastic, viscous and visco-elastic #1) we used modal summation method to find the frequency response, and in this model we are finding the complex amplitude from the amplitude equation directly. The equation of motion for this model is derived by equating the forces in the free body diagram shown in Figure 42 (b). In this

case we are plotting the movement of the damper as well. To see how the frequency response varies numerically, we can use some example values for k_1, k_2, k_3, c_1, c_2, c_3, f_1 and f_2. Usually stiffness and frequency can be obtained from the manufacturers of the microcantilevers. Frequency response for various values of the lower spring constant k_3 and the lower damper c_3 are obtained and discussed in this section. Some of the particles that can be identified by this model are pitch, polymers etc.,

Taking the values for $k_1 = 42$ N/m, $k_2 = 20$ N/m, $c_1 = 0.000000003$ N s/m, $c_2 = 0.000000008$ N s/m, $f_1 = 300$ kHz, $f_2 = 350$ kHz and varying the lower damper constant and the lower spring constant, plots are obtained for the frequency response. First, we are going to vary the lower spring constant and see how the frequency response is affected by this change. Figures 71,73,75 show the frequency response for the Maxwell model for the first mass, second and the damper respectively. In these figures, plots are compared with different lower spring constant values to see the shift in natural frequencies. We can infer that as the spring constant k_3 increases the natural frequencies also increases. Phase angle of the system can provide some additional information about the particle, but as if now, it is beyond the scope of this study. Phase angle for a system can be determined by

$$Phase\ angle = -\arctan\frac{\mathrm{Im}(\bar{X})}{\mathrm{Re}(\bar{X})}$$

Phase angle is the inverse tangent of the imaginary part to the real part of the response. Figure 72 and Figure 74 represents the phase angle for the first and the second mass respectively, as we see there is definite a phase shift between different values of the lower

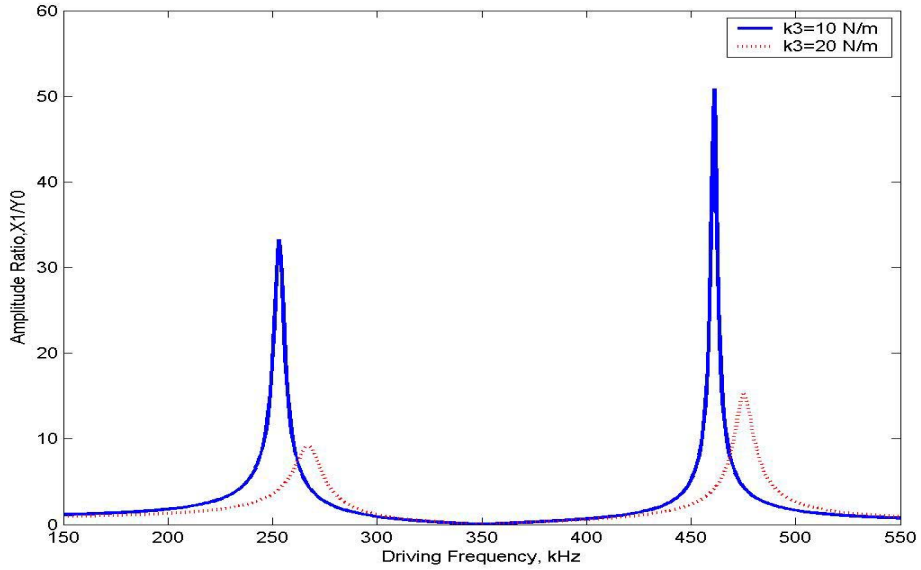

Figure 71: Frequency response of first mass in maxwell visco-elastic model (Case #2) with c_3=0.00005 N s/m

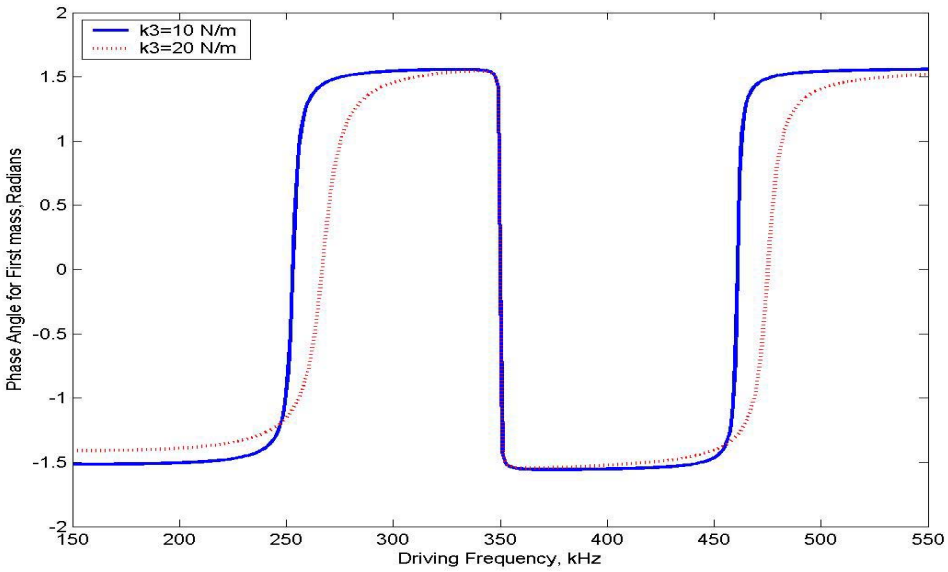

Figure 72: Phase angle of first mass in maxwell visco-elastic model (Case #2) with c_3=0.00005 N s/m

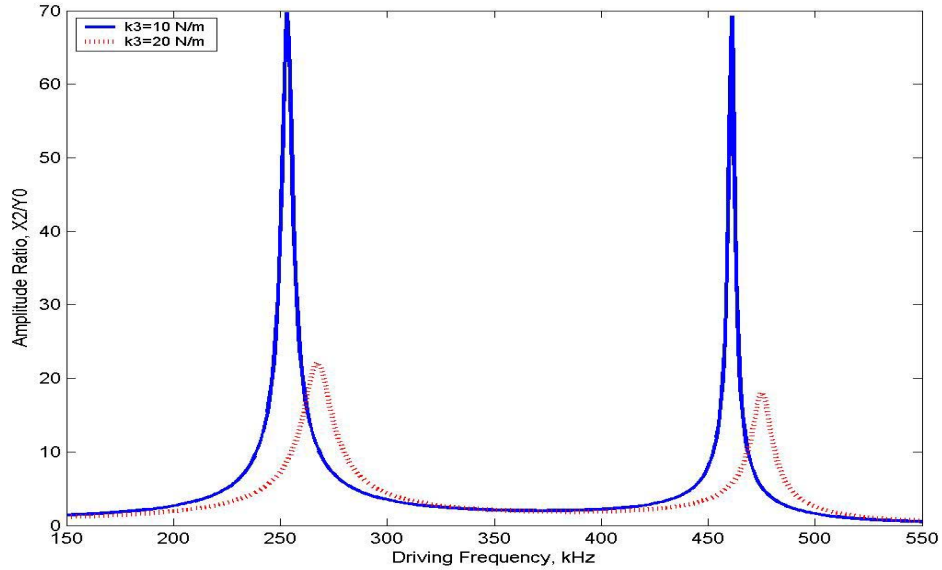

Figure 73: Frequency response of second mass in maxwell visco-elastic model (Case #2) with c_3=0.00005 N s/m

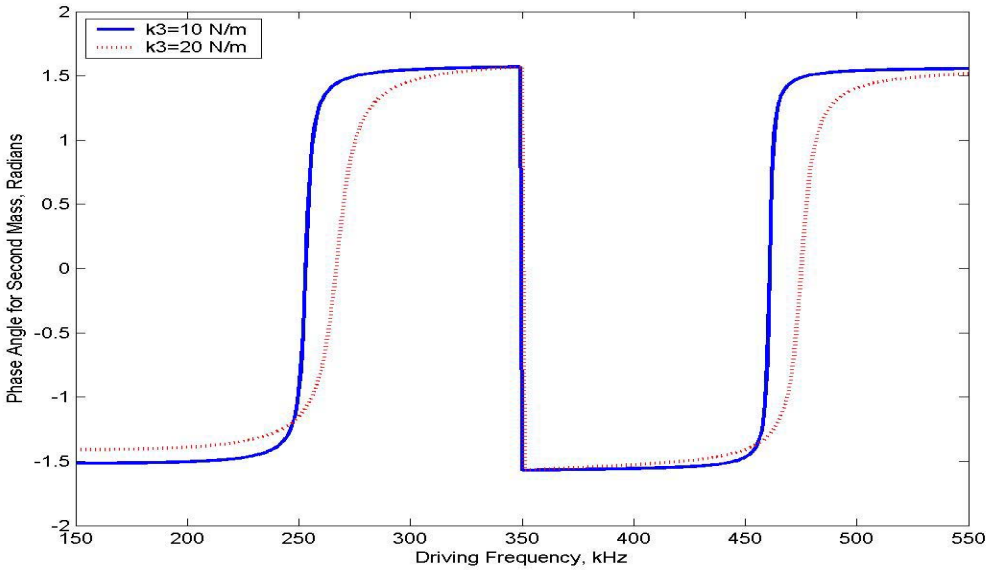

Figure 74: Phase angle of second mass in maxwell visco-elastic model (Case #2) with c_3=0.00005 N s/m

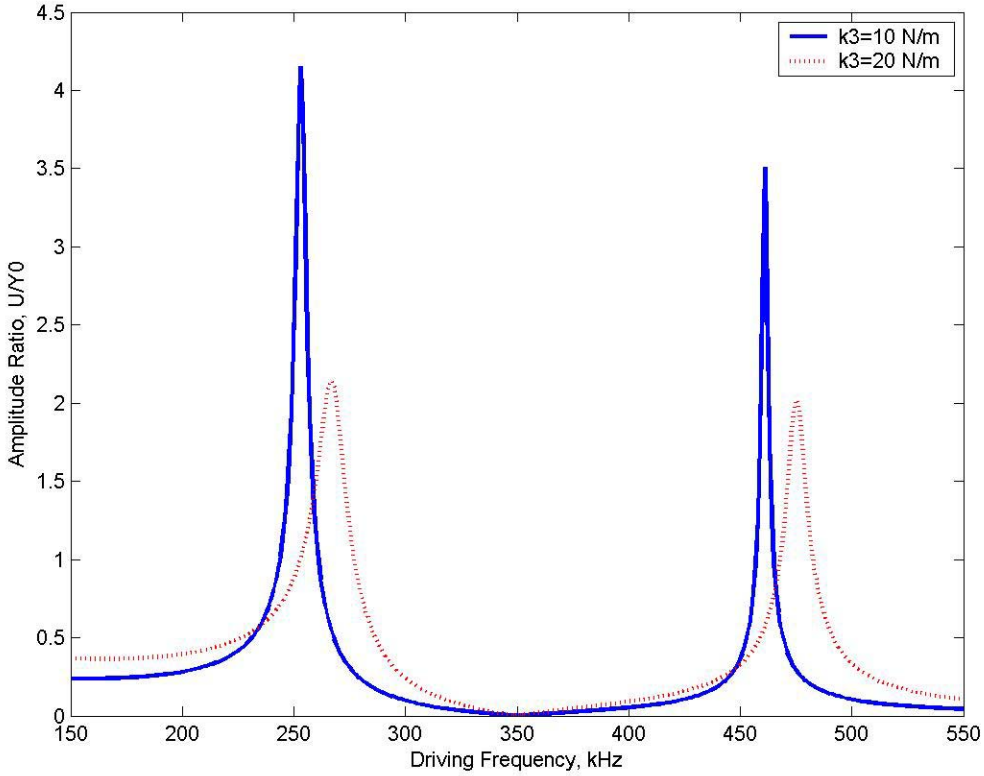

Figure 75: Frequency response of damper in maxwell visco-elastic model (Case #2) with c_3=0.00005 N s/m

spring constant. This signature can be used to determine some of the physical properties of the particle. In the same way, the frequency response can be determined by varying the lower damper constants. Figures 76,78,80, represents the frequency response of the first mass, second mass and the damper respectively. In all these three figures, each one is compared with different lower damper values to see how the amplitude ratio varies. When the lower damper constant c_3 increases, the amplitude ratio is decreases. Phase shift for the change in damper value is shown in Figure 77 and Figure 79. Here also there is a definite phase shift, which will be useful to determine some of the physical properties of the particle.

When the lower damper constant $c_3 = 0.5$ N s/m, then the damper is very rigid. In this case, the Maxwell model will behave like the elastic model, where the spring alone is connected to the tip of the dual cantilever. The natural frequencies obtained from this model can be compared with the natural frequencies obtained from the elastic model for same value of k_3. When the lower damper constant $c_3 = 0$, then the lower spring k_3 connected in series with the lower damper will be hanging free. The natural frequencies obtained for this case will be equal to the natural frequencies of the baseline model. The amount of shift in natural frequencies depends on the damping and same way the amount of change in the amplitude ratio depends on the amount of stiffness.

4.5 VISCO-ELASTIC MODEL #3- SPRING IN SERIES WITH SPRING/DAMPER IN PARALLEL (STANDARD SOLID MODEL)

Visco-elastic model #3 is shown in Figure 44. In Figure 44, a spring k_3 is connected in series to a spring k_4 and a damper c_3, which are connected in parallel. The mathematical model is built in 3.6.1 section. In this section, we are going to discuss how

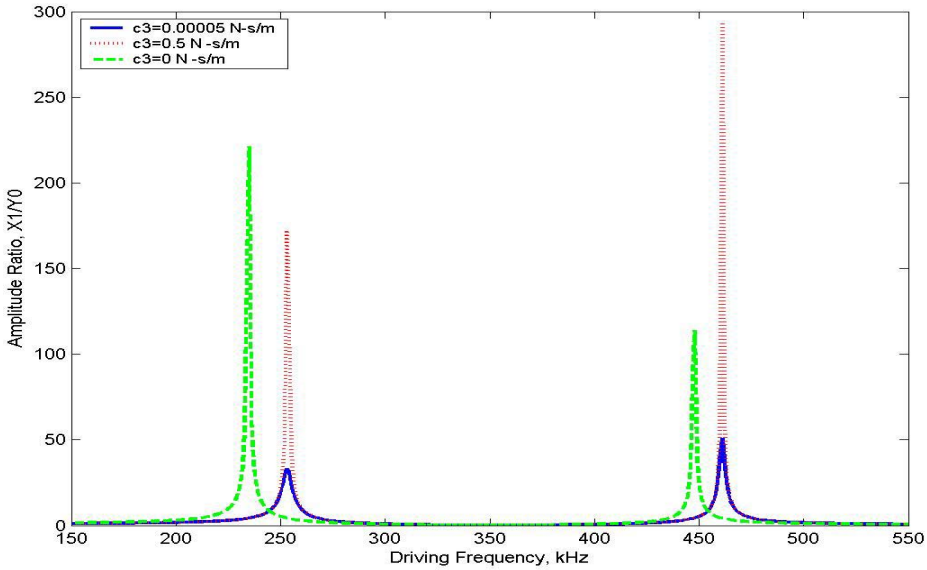

Figure 76: Frequency response of first mass in maxwell visco-elastic model (Case #2) with k_3=10 N/m

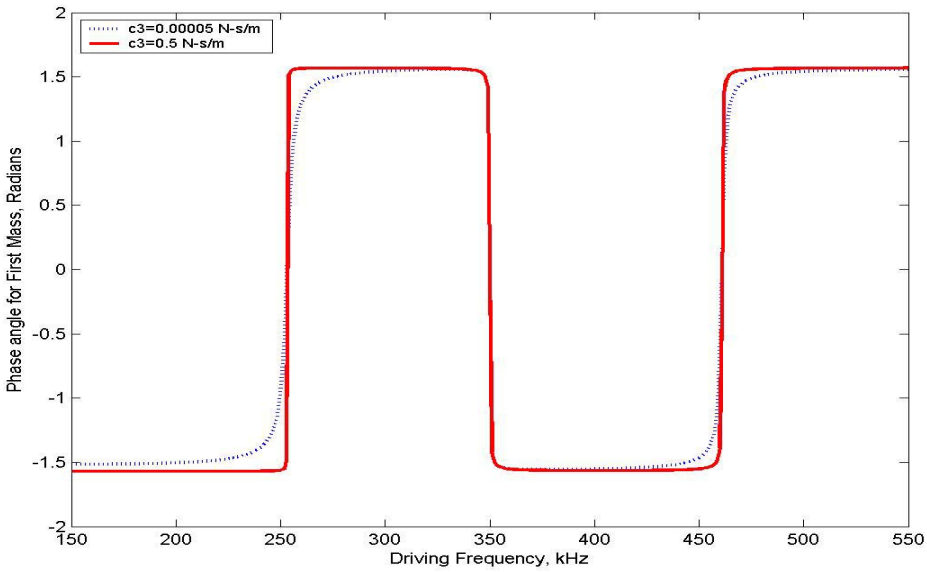

Figure 77: Phase angle of first mass in maxwell visco-elastic model (Case #2) with k_3=10 N/m

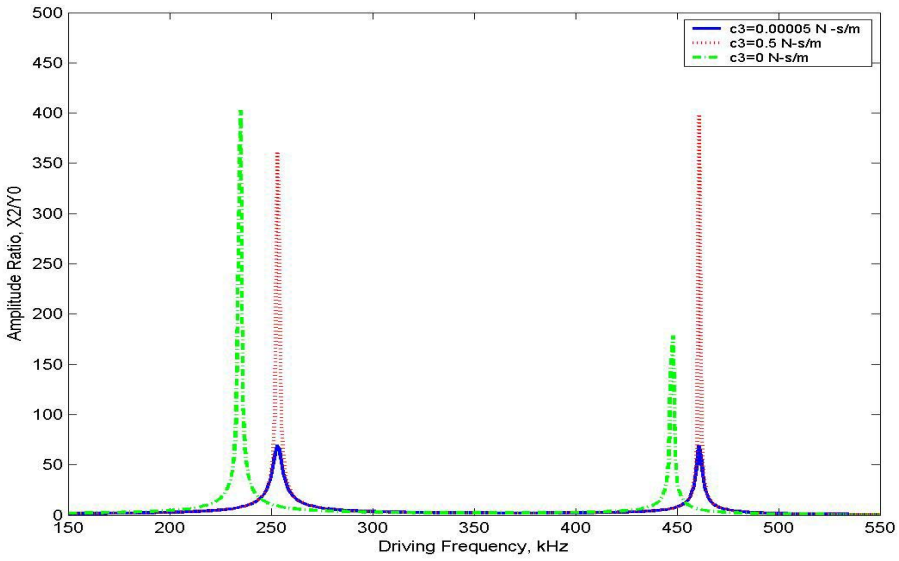

Figure 78: Frequency response of second mass in maxwell visco-elastic model (Case#2) with k_3=10 N/m

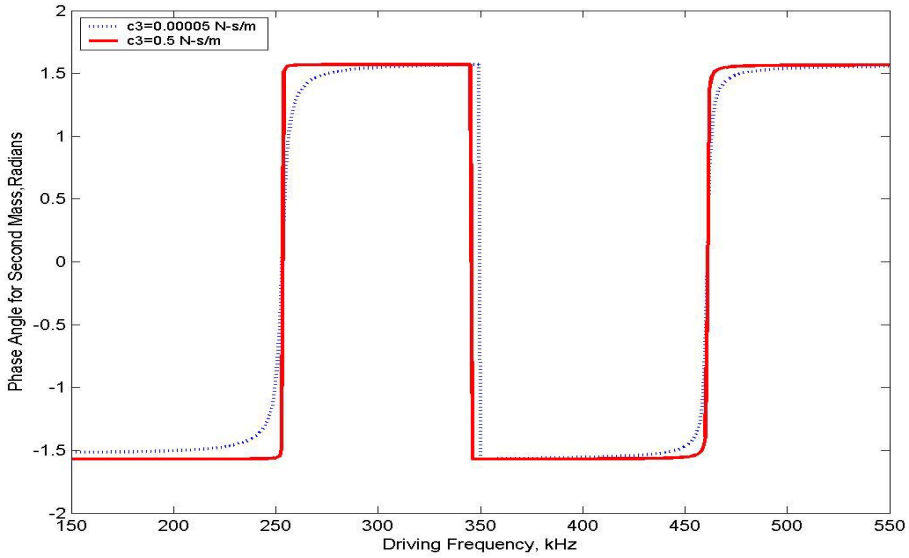

Figure 79: Phase angle of first mass in maxwell visco-elastic model (Case #2) with k_3=10 N/m

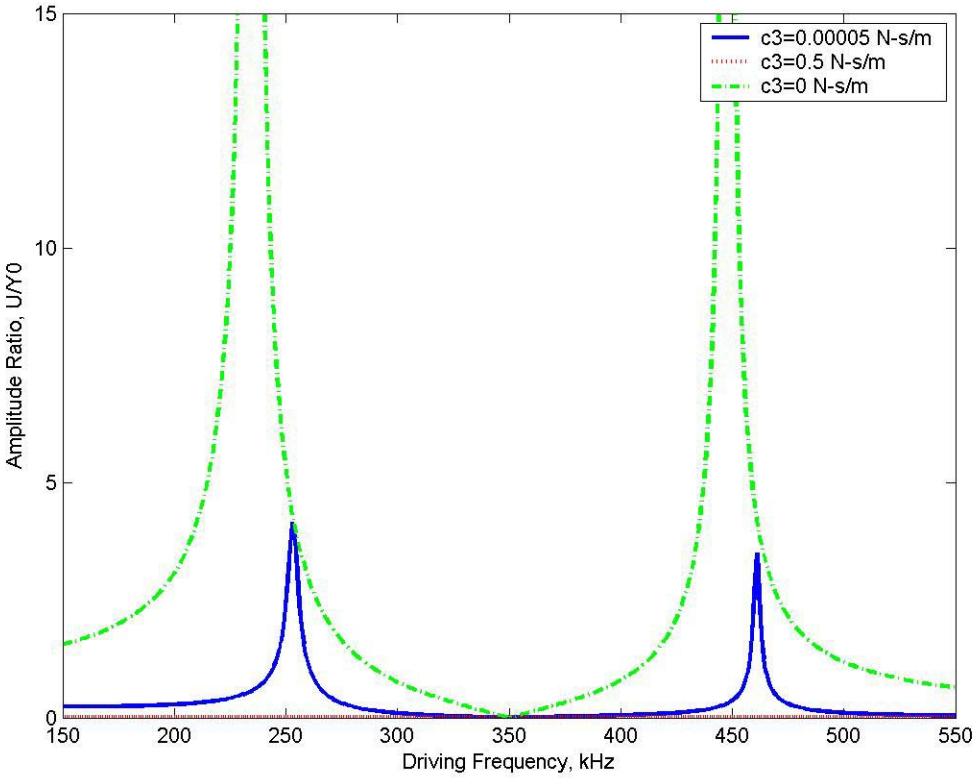

Figure 80: Frequency response of damper for maxwell visco elastic model (Case #2) with k_3=10 N/m

the value of lower springs and lower dashpot affects the frequency response of this standard solid model. Some of the particles that can be identified from this model are silk, nylon, rayon, certain plastics etc., This analysis is similar to a parameter study as we seen in the case of the elastic and viscous models. Same set of example values are taken in this model too (i.e., example values taken for Visco-elastic #2).

First we are going to vary the lower spring constant k_3 and obtaining the frequency response. Figures 81, 83 and 85 represents the frequency response of the first mass, second mass and the damper. From the above three figures we can infer that as the lower spring constant k_3 increases, the natural frequencies also increases. This is the signature we expect form this model. The amount of shift in natural frequencies depends on the amount of damping the system has. In this case also the phase angle is plotted to see whether there is any change in phase angle. This is shown in figures 83 and 84, as wee see it has a definite phase shift for both first as well as for second mass.

Second, we are going to vary the lower spring constant k_4 to see how it affects the frequency response of the model. Figures 86, 88, 90 represent the frequency response of the first mass, second mass and the damper respectively. From the figure we can see that there is not much difference in either the natural frequencies or the amplitude ratio for various spring constant values. This is because the damper, which is connected in parallel to this spring, dominates. Similarly there is not much change in phase angle for the first and second mass (shown in Figures 87 and 89).

Lastly, we are going to vary the lower damper constant and see how it affects the frequency response of the system. Figures 91, 93 and 95 represent the frequency response of the first mass, second mass and the damper respectively. Figures 92 and 94 are the

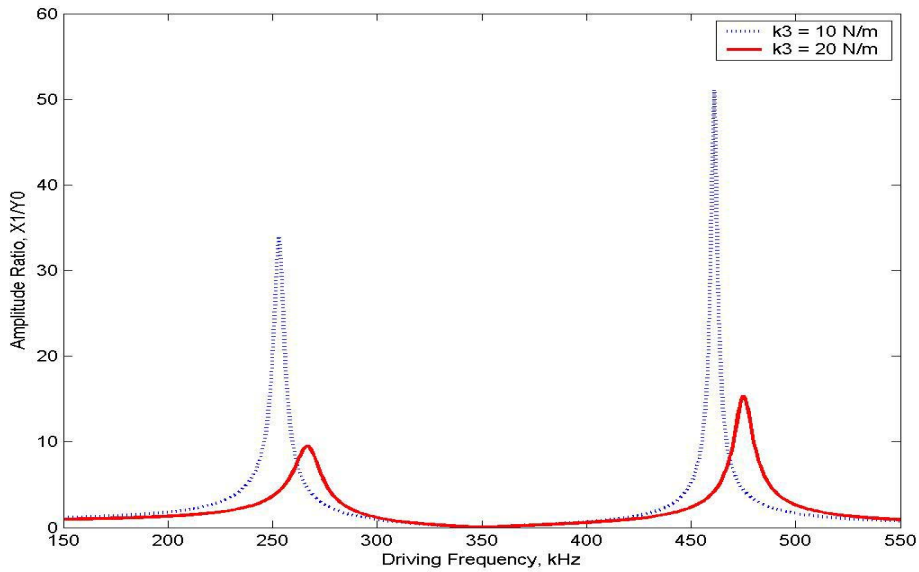

Figure 81: Frequency response of first mass in standard solid visco-elastic model (Case #3) with c_3=0.00005 N s/m and k_4=5 N/m

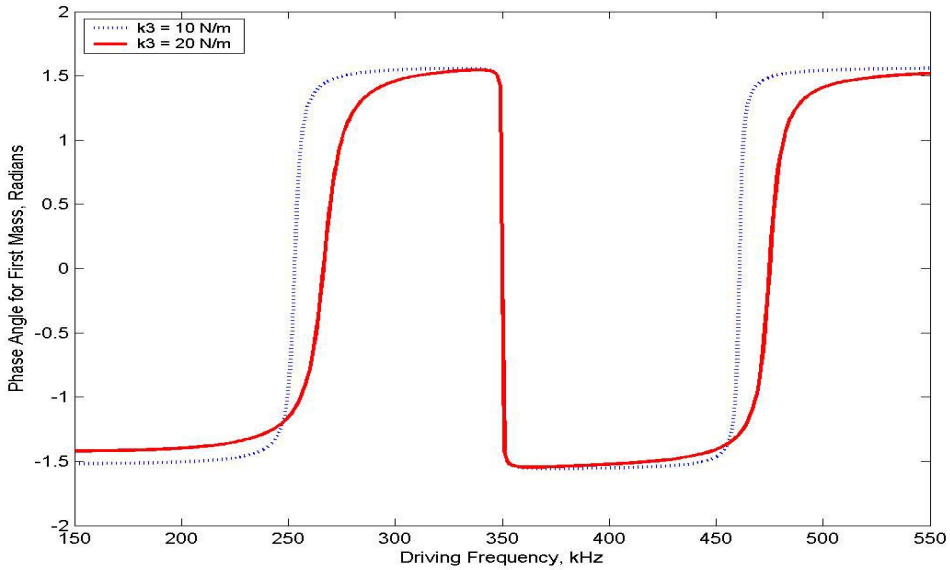

Figure 82: Phase angle of first mass of standard solid visco-elastic model (Case #3) with c_3=0.00005 N s/m and k_4=5 N/m

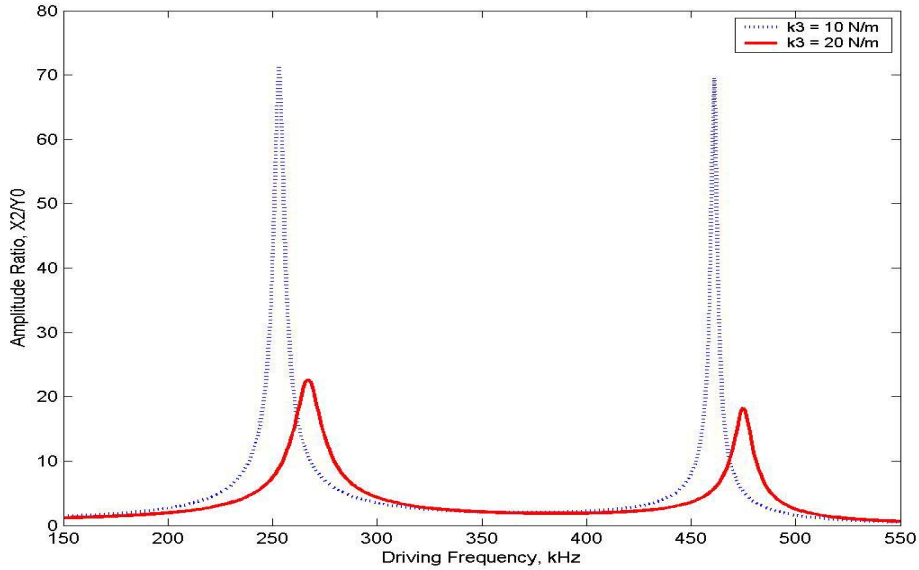

Figure 83: Frequency response of second mass in standard solid visco-elastic model (Case #3) with c_3=0.00005 N s/m and k_4=5 N/m

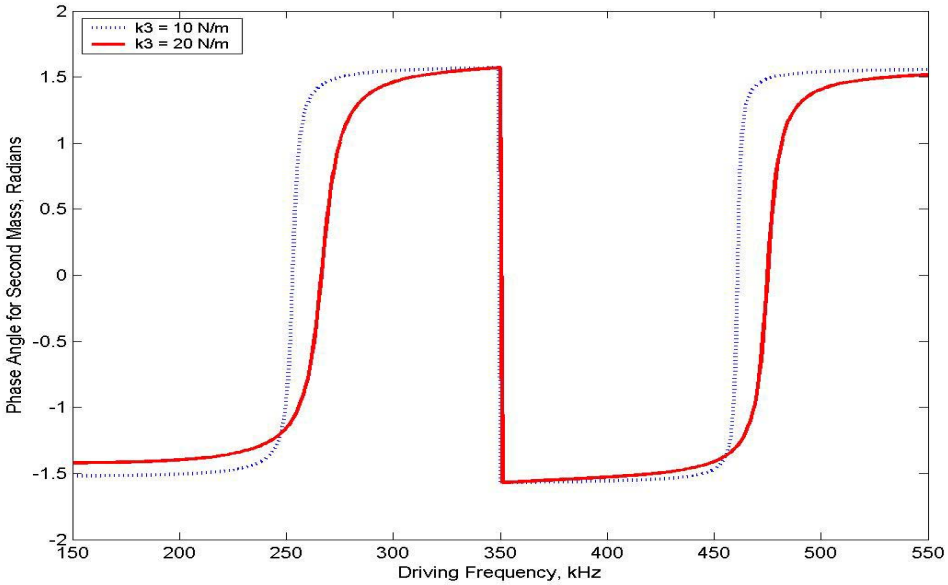

Figure 84: Phase angle of second mass of standard solid visco-elastic model (Case #3) with c_3=0.00005 N s/m and k_4=5 N/m

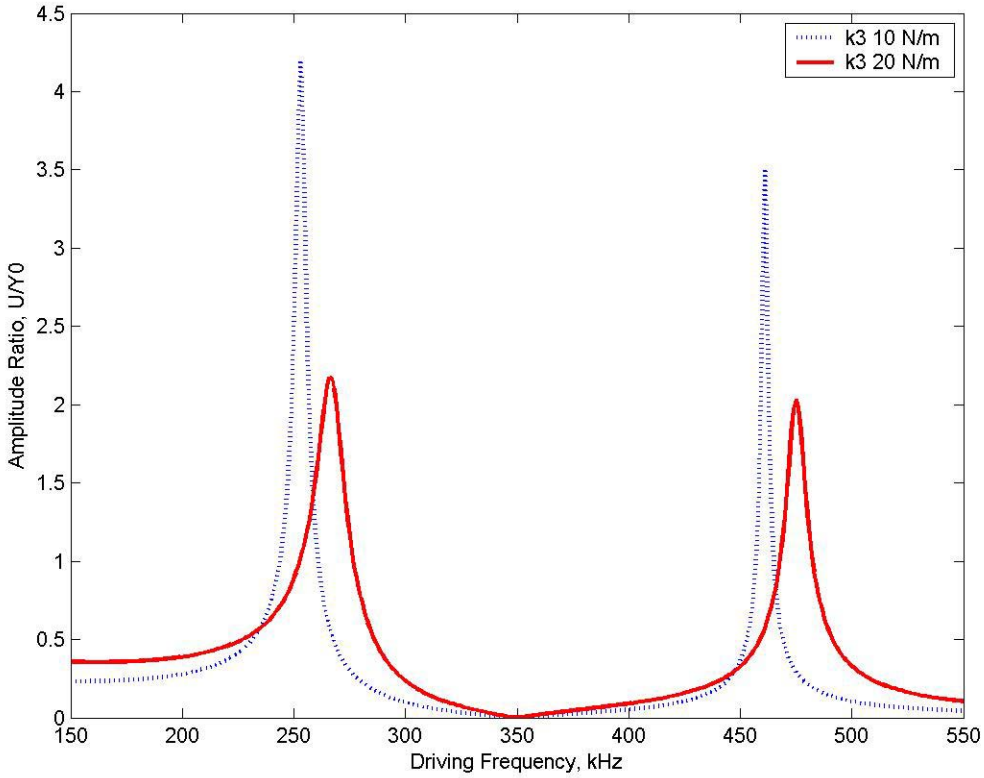

Figure 85: Frequency response of damper in standard solid visco-elastic model (Case #3) with c_3=0.00005 N s/m and k_4=5 N/m

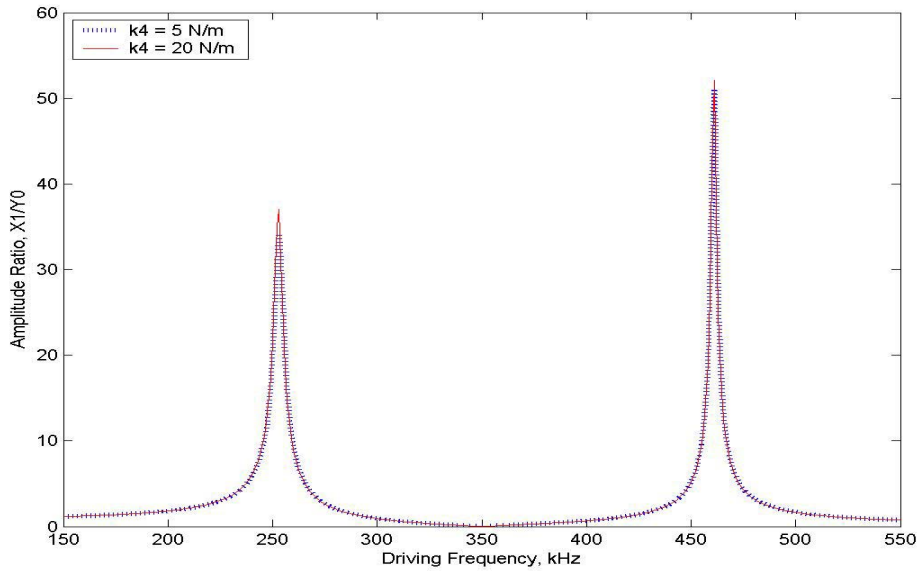

Figure 86: Frequency response of first mass in standard solid visco-elastic model (Case # 3) with k_3=10 N/m and c_3=0.00005 N s/m

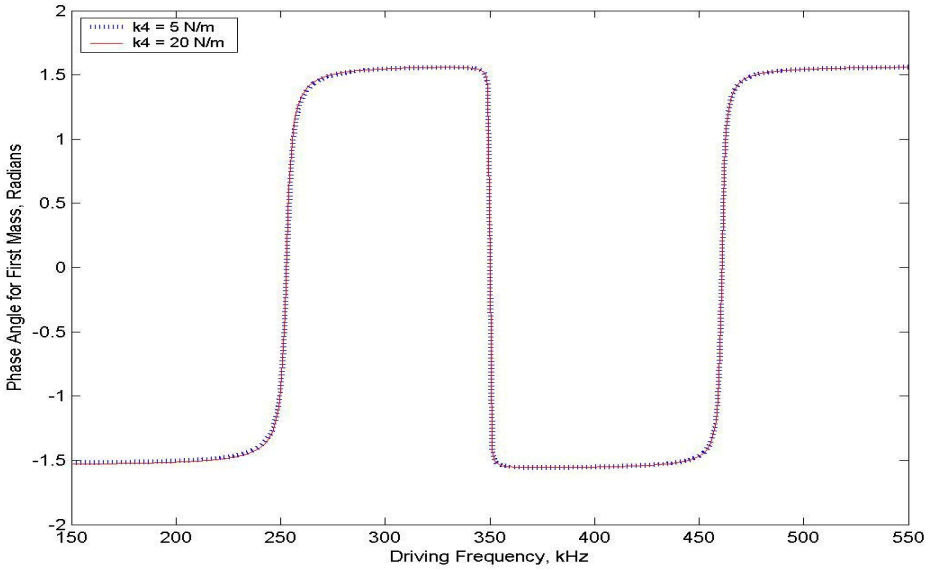

Figure 87: Phase angle of first mass in standard solid visco-elastic model (Case # 3) with k_3=10 N/m and c_3=0.00005 N s/m

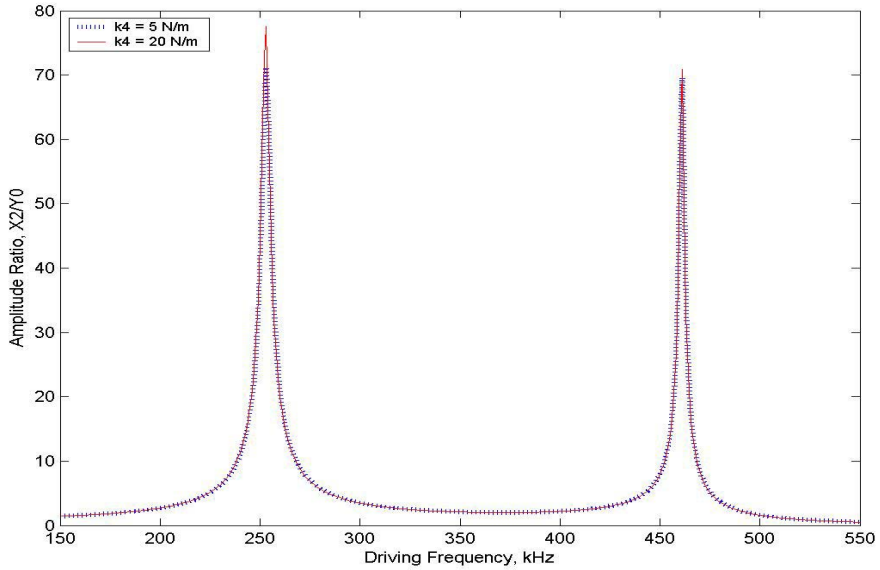

Figure 88: Frequency response of second mass in standard solid visco-elastic model (Case # 3) with k_3=10 N/m and c_3=0.00005 N s/m

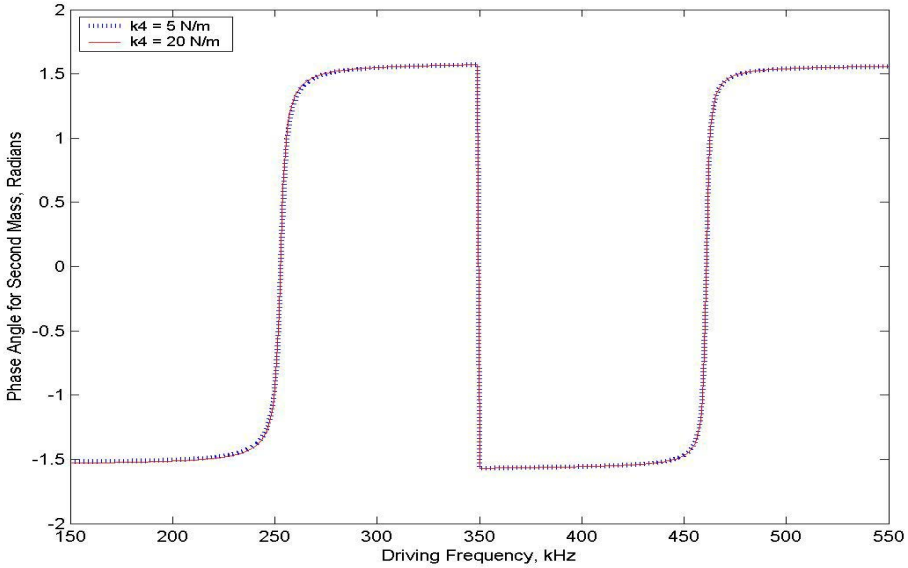

Figure 89: Phase angle of second mass in standard solid visco-elastic model (Case # 3) with k_3=10 N/m and c_3=0.00005 N s/m

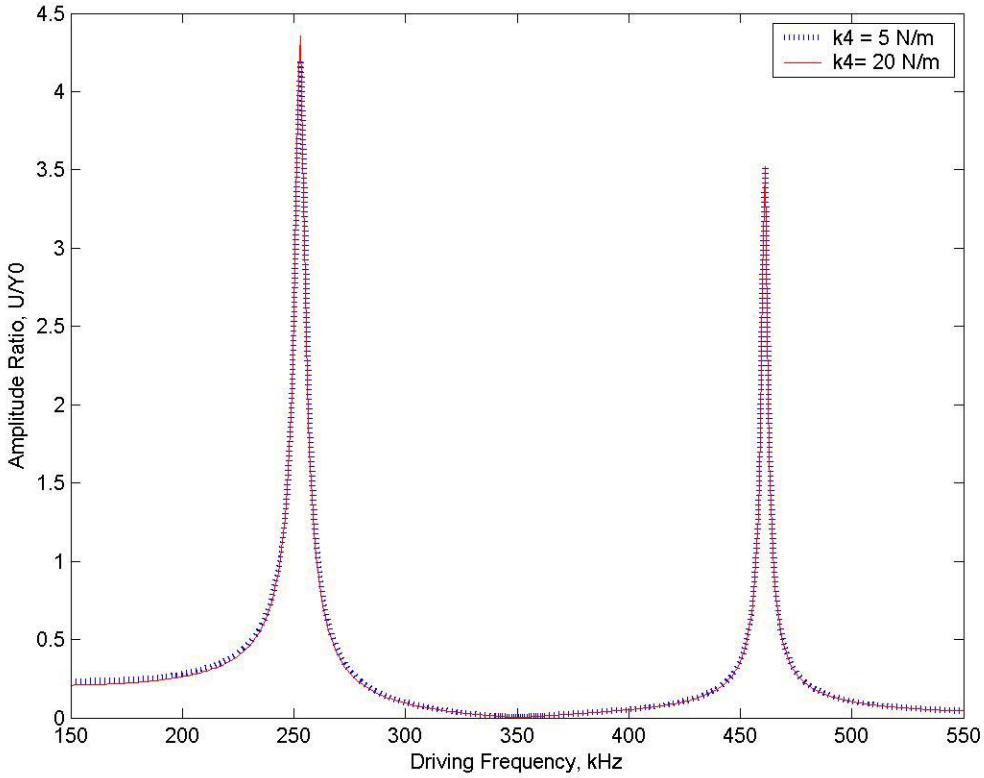

Figure 90: Frequency response of damper in standard solid visco-elastic model (Case # 3) with k_3=10 N/m and c_3=0.00005 N s/m

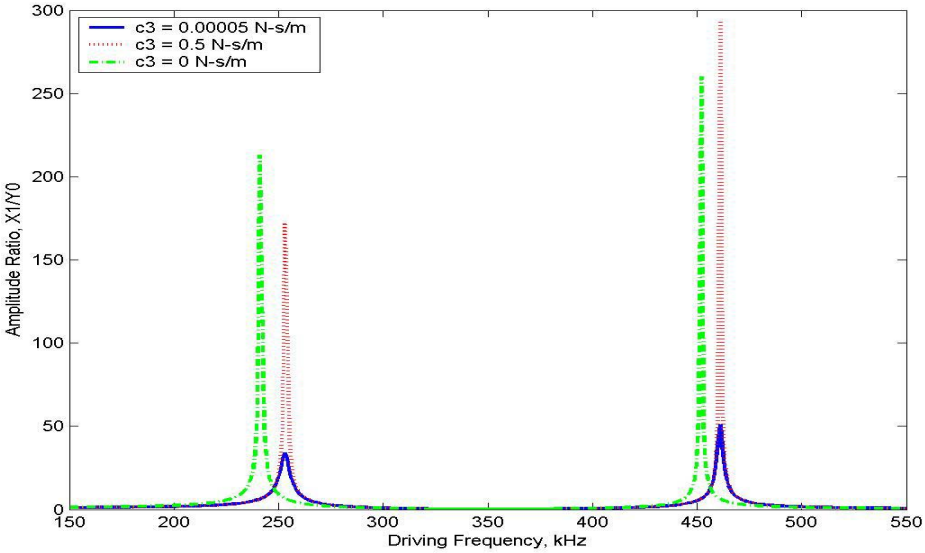

Figure 91: Frequency response of first mass in standard solid visco-elastic model (Case # 3) with k_3=10 N/m and k_4=5 N/m

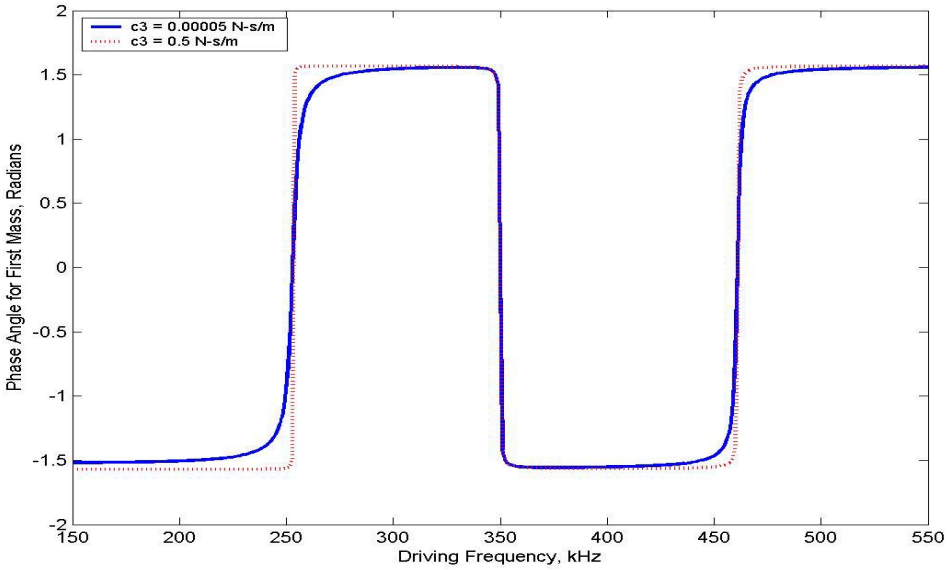

Figure 92: Phase angle of first mass in standard solid visco-elastic model (Case # 3) with k_3=10 N/m and k_4=5 N/m

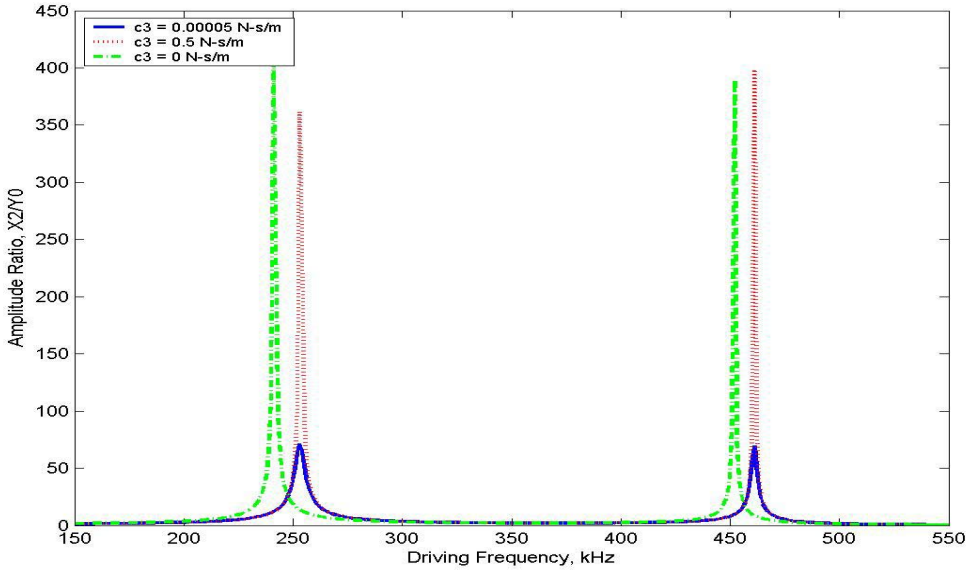

Figure 93: Frequency response of second mass in standard solid visco-elastic model (Case #3) with k_3=10 N/m and k_4=5 N/m

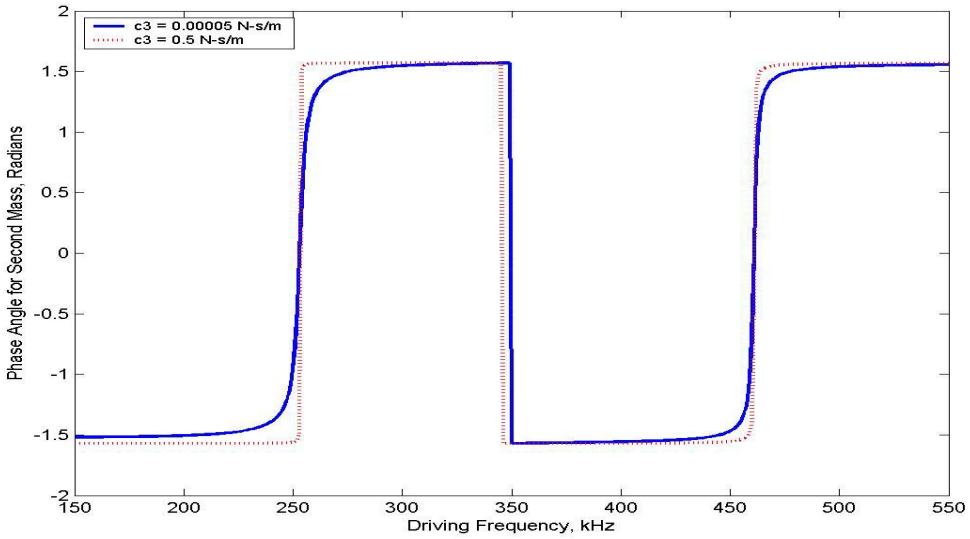

Figure 94: Phase angle of second mass in standard solid visco-elastic model (Case # 3) with k_3=10 N/m and k_4=5 N/m

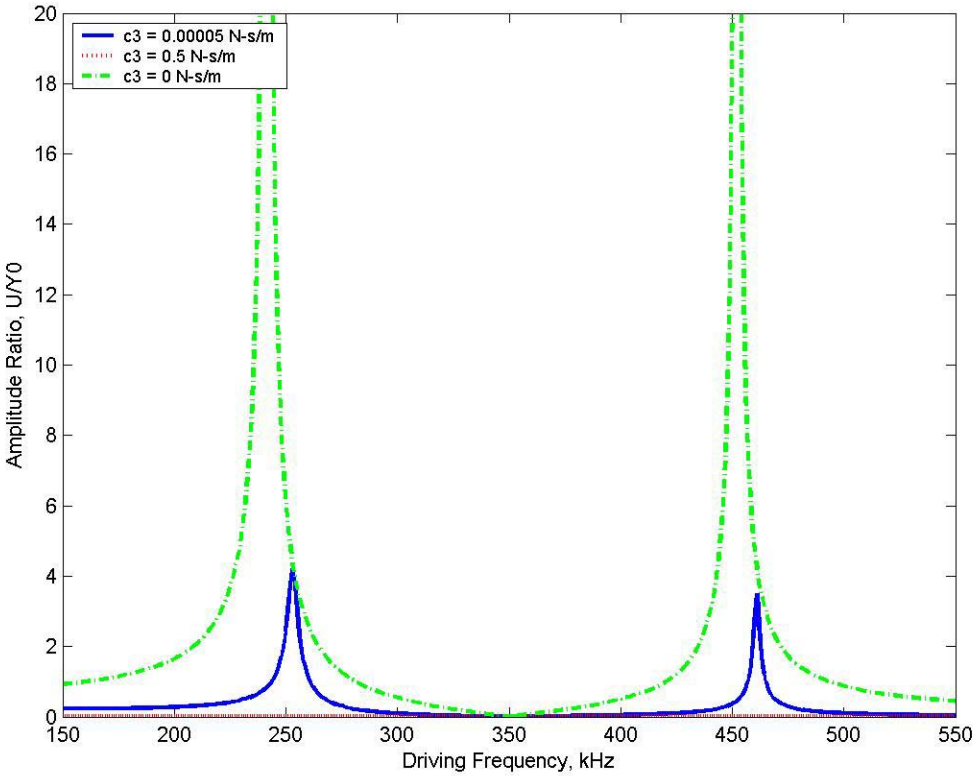

Figure 95: Frequency response of damper in standard solid visco-elastic model (Case #3) with k_3=10 N/m and k_4=5 N/m

phase angle plot for the first mass and the second mass. From these figures, we can infer that as the lower damper constant increases, the amplitude ratio decreases. Also it can be seen that the natural frequency also increases for lower damper constant values. This is because as the lower damper constant value decreases, the lower spring k_4 dominates and it increases the natural frequency. Also there is a significant change in phase angle as wee seen in Figures 92 and 94 for the first mass and the second mass respectively.

When the lower damper constant $c_3 = 0$, then the two springs k_3 and k_4 are in series. This case will be similar to the elastic model where the spring is connected to the tip of the dual cantilever. Since the springs are connected in series, the effective stiffness can be determined. If the effective stiffness calculated above is substituted in the elastic model then, the natural frequency obtained from the elastic model will be closer to the natural frequency determined from this model. When k_4 is zero, then this model becomes similar to visco elastic model #2 where a spring is connected in series with a damper.

There is increasing need for quantitative measurements of materials properties with nano-meter-scale resolution. Applications include materials characterization [1,2], microelectromechanical systems and tribology[3-7], and biological systems[8].Mechanical properties such as modulus, yield strength and work of adhesion are extracted from the SFM date using continuum mechanics models from the field of contact mechanics[14,15].

CHAPTER 5

CONCLUSION

Dual cantilevers provide a realistic means for identifying the physical characteristics of various types of particle that might be attached to a surface. The deflection of the added or the second cantilever gives additional information not normally recovered in typical AFM tests. Classical vibration analyses show that cantilever amplitudes of the contacting tip and free end give signatures that are unique to different particle types. It was not the goal here to quantify physical properties of particles but to qualify the general type of particle under question.

Five different models were used to represent behavior of the particles: 1) spring, 2) damper, 3) spring/damper in parallel, 4) spring/damper in series and 5) spring in series with a parallel spring and damper. Distinct response signatures of each of the particle models are summarized below.

1) Spring: Increase in natural frequency of both the fundamental and the second modes of vibration. The degree of hardness of the particle is manifested by a higher shift in both natural frequencies. The second cantilever can act as a dynamic absorber by completely suppressing the dynamic amplitude of the cantilever tip. In this case, only the second cantilever responds.
2) Damper: Particle damping greatly affects the dynamic response amplitude of the tip but has a much lesser effect on the dynamic amplitude of the second cantilever.

3) Spring/damper in parallel: This model reflects a change in both natural frequencies (1^{st} and 2^{nd} modes) as well as a reduction in vibration amplitudes.
4) Spring/damper in series: This model also reflects in both natural frequencies as well as a reduction in vibration amplitudes. This model has the advantages of both elastic model and viscous model. Properties of the particulates can be manifested by the amount of shift in natural frequencies and change in amplitude.
5) Spring in series with a parallel spring and damper: In this model the amount of shift in natural frequencies depends on the magnitude of damping and the same way change in the amplitude ratio depends on the amount of stiffness.

A basic assumption made in this study is that the tip remains in contact with the surface particle long enough for steady state vibrations to occur. In reality, the tip may become disengaged and reattach itself during the contact encounter. This scenario is much more involved and represents a challenge for further research on this topic. These mechanical models do not quantitatively describe actual polymers. However, they do capture the major features of the polymer response and therefore provide simple models that are useful for semi-quantitative analysis of data and for the design and interpretation of experiments.

LIST OF REFERENCES

List of references

1) G.Bining, C.F.Quate, CH.Gerber, Phys.Rev.lett.56, 930 (1986).
2) Daniel Rugar and Paul Hansma., " Atomic Force Microscopy" American Institute of Physics, October 1990, pp 25 and 29.
3) D.Sarid, Scanning Force Microscopy with Application to Electric, Magnetic, and Atomic forces, Oxford University Press, New York, 1991.
4) T.R.Albrecht and C.F.Quate, J.Appl.Phys. 62, 2599 (1987)
5) Salmeron.M, D.F. Ogletree, C.Ocal,[a)] H.C. Wang, G.Neubauer, and W.kolb[b)] and G.Meyers., "Tip-surface forces during imaging by scanning tunneling microscopy", J.Vac.Sci.Technol, B9(2), Mar/Apr 1991 ,p.1347.
6) Nancy A.Burnham and Richard J.Colton., "Measuring the nanomechanical properties and surface forces of materials using and atomic force microscope", J.Vac.Sci.Technol, A7(4), Jul/Aug 1989, pp 2906 and 2907.
7) James De Yoreo and Terry Land., " The Secrets of Crystal Growth" ., Science& Technology Review November 1996.
8) Jeffrey L.Hutter and John Bechhoefer., "Measurement and manipulation of van der Waals forces in atomic-force microscopy", J.Vac.Sci.Technol, B 12(3), May/Jun 1994, pp2252 and 2252.
9) http://stm2.nrl.navy.mil/how-afm/how-afm.html
10) G.Meyer and N.M Amer, Appl.Phys.lett.53, 1045 (1988).

11) R.J.Warmack, X.Y.Zhang, T.Thundat, and D.P Allison, Rev.Sci.Instrum 65, 394 (1994).

12) http://spm.phy.bris.ac.uk/techniques/AFM/

13) R.Weisendanger, H.J.Guntherodt, Eds., Scanning Tunneling Microscopy II, vol.28, Springer-Verlag, 1992.

14) D.R.Baselt, J.D Baldeschwieler, J.Vac Sci.Technol. B10, 2316(1992)

15) C.J.Chen, Introduction to Scanning Tunneling Microscopy, Oxford Press, 1993.

16) C.J.Chen, J.Phys. Cond.Matt.3, 1227(1991).

17) J.Israelachville, Intermolecular and Surface force, 2nd Ed. Academic press, London, 1991.

18) C.A.J.Putman, K.O Van der Werf, B.G De Grooth, N.F. Van Hulst and J.Greve, Biophys.J.67, 1749(1994).

19) C.A.J.Putman, K.O.Van der Werf, B.G De Grooth, N.F Van Hulst and J.Greve, Appl.Phys.lett. 64, 2454(1994).

20) Chen G.Y, R.J Warmack, A.Huang and T.Thundat., "Harmonic response of near-contact scanning force microscopy", J.Appl.Phys.78(3), 1 August 1995 ,p.1465 – 1469.

21) F.O.Goodman and N.Garcia, Phys.Rev.B.43, 4728(1991)

22) P.K. Hansama, J.P.Cleverland, M.Radmacher, D.A Walters, P.Hillner, M.Bezanilla, M.Fritz, D.Vie, H.G.Hansama, C.B Prater, J.Massie, L.Fukunaga, J.Gurley and V.Elings, Appl.Phys.lett. 64.28 (1994).

23) G.Y.Chen, R.J Warmack, T.Thundat, D.P Allison, and A.Huang, Rev.Sci.Instru. 65, 2532 (1994).

24) Ahmet Oral,[a),b)] , Ralph A.grimble, H.Ozgur Ozer [a)] Peter H.Hoffmann, and John B.Pethica., "Quantitative atom-resolved force gradient imaging using noncontact atomic force microscopy" Applied Physics Letters, Volume 79, Number 12, 17th September 2001.

25) Nancy A.Burnham, Dawn D.Dominguez, Robert L.Mowery, and Richard J.Colton., "Probing the Surface Forces of Monolayer Films with and Atomic-Force Microscope", Physical Review Letters, Volume 64, Number 16, 16th April 1990, pp1931 and 1932.

26) Nancy A.Burnham [a)] and Richard J.Colton., "Interpretation issues in force microscopy", J.Vac.Sci.Technol, A9(4), Jul/Aug 1991 pp2553.

27) Burnham.N.A, O.P Behrend, F.Oulevey, G.Gremaud, P-J gallo, D.Gourdon, E Dupas, A J Kulik, H M Pollock and G A D Briggs., "How does a tip tap?", Nanotechnology 8 (1997) pp67-75.

28) http://www.che.utoledo.edu/nadarajah/webpages/whatsafm.html

29) http://www.physics.ucsb.edu/~hhansma/afm-acs_news.htm

30) Kelly., Fundamentals of Mechanical Vibrations 2nd Edition ., McGraw Hill Publications

31) Bharath Bhushan., Tribology and Mechanics of Magnetic Storage Devices., Springer-Verlag New York, Inc.1996, p136

32) Parter C.B, P.G. Maivald, K.J.Kjoller and M.G.Heaton., "Probing Nano-scale Forces with Atomic force microscope".

33) Bharath Bhushan., Hand Book of Micro/Nano Tribology 2nd Edition., CRC press.

34) Lieng-Haung Lee., Adhesion Science and Technology ., Polymer Science and Technology Volume 9B., Xerox Corporation Rochester, New York, Plenum Press.

35) Microlevers, Park Scientific Instruments, Sunnyvale, CA.

36) D.J.Barber and R.Loudon, An introduction to the properties of condensed matter, Cambridge University Press, New York, 1989.

37) G.Meyer and N.M.Amer, appl.phys.Lett.53, 2400(1988).

38) S.Alexander, L.Hellemans, O.Marti, J.Gurley, J.appl.phys.65, 164 (1989).

39) G.Y.Chen, R.J.Warmack, A.Huang and T.Thundat, J.Appl.Phys.78, (1995) (in press).

40) T.Thundat, X.Y Czheng, G.Y. Chen, S.L Sharp and R.J Warmack, Appl.Phys.lett. 63, 2150(1993)

41) Don.W.Dareing, Thomas G.Thundat, Investigation of the Dynamics of a Microcantilever in the proximity of a surface.

42) Anatolii D.Zimon., Adhesion of Dust and Powder., Second Edition, Consultants Bureau. New York and London

VITA

Ramanathan Narayanan was born in Tamil nadu, India on March 2nd 1977. His parents, Mr. and Mrs. Narayanan, and his sister, Rajeswari, resides in Tamil nadu, India. The author graduated from the Department of Mechanical Engineering at Annamalai University with a Bachelor of Engineering degree, in 1998. After working as senior engineer in Orient Components Private Limited for two years, he came to United States. In, August 2001, he enrolled in the Department of Mechanical Engineering where he was awarded the Master of Science degree in Mechanical Engineering in December 2003, after completing his thesis entitled "Investigation of Compound Micro Cantilever for Imaging and Identifying Micro/Nano Particulates". He held a Graduate assistantship during most of his graduate studies.